


Search for bottom-type vectorlike quark pair production in dileptonic and fully hadronic final states in proton-proton collisions at $\sqrt{s} = 13$ TeV

A. Hayrapetyan *et al.*^{*}
(CMS Collaboration)

 (Received 21 February 2024; accepted 22 July 2024; published 17 September 2024)

A search is described for the production of a pair of bottom-type vectorlike quarks (B VLQs) with mass greater than 1000 GeV. Each B VLQ decays into a b quark and a Higgs boson, a b quark and a Z boson, or a t quark and a W boson. This analysis considers both fully hadronic final states and those containing a charged lepton pair from a Z boson decay. The products of the $H \rightarrow bb$ boson decay and of the hadronic Z or W boson decays can be resolved as two distinct jets or merged into a single jet, so the final states are classified by the number of reconstructed jets. The analysis uses data corresponding to an integrated luminosity of 138 fb^{-1} collected in proton-proton collisions at $\sqrt{s} = 13$ TeV with the CMS detector at the LHC from 2016 to 2018. No excess over the expected background is observed. Lower limits are set on the B VLQ mass at the 95% confidence level. These depend on the B VLQ branching fractions and are 1570 and 1540 GeV for 100% $B \rightarrow bH$ and 100% $B \rightarrow bZ$, respectively. In most cases, the mass limits obtained exceed previous limits by at least 100 GeV.

DOI: [10.1103/PhysRevD.110.052004](https://doi.org/10.1103/PhysRevD.110.052004)

I. INTRODUCTION

A puzzle in elementary particle physics is the fact that the electroweak scale is so much lower than the Planck scale, which is connected to the stability of the Higgs boson (H) mass, m_H [1]. In the standard model (SM), the Higgs boson is a fundamental particle, first observed by the ATLAS and CMS Collaborations in 2012 [2–4] at the CERN LHC. In contrast to the leptons, quarks, and vector gauge bosons of the SM, the SM Higgs boson is a fundamental scalar particle with higher-order contributions to its mass due to vacuum fluctuations that diverge quadratically with the length scale. This results in m_H being driven to the cutoff value of these fluctuations. If there is no new physics below the Planck scale, this cutoff value would be about 10^{19} GeV, which predicts m_H to be many orders of magnitude greater than the observed value of 125 GeV [5,6].

Several theories have been proposed to solve this problem, including supersymmetry [7,8], composite-Higgs models [9,10] (where the Higgs boson is made up of smaller constituents bound by a new type of gauge interaction), and little-Higgs models [11,12] (where the Higgs boson is a pseudo-Nambu–Goldstone boson arising

from spontaneous breaking of a global symmetry at the TeV energy scale). In the composite-Higgs case, the mass divergence does not arise since the UV cutoff is the scale set by the composite size, while, in the case of little-Higgs models, the Higgs boson is “naturally” light because of the collective breaking of the global symmetry via two couplings [13].

In both the composite- and little-Higgs models, a new type of particle arises [14]: a vectorlike fermion that couples to the weak gauge bosons through purely vector current couplings. The strongly interacting vectorlike fermions are referred to as vectorlike quarks (VLQs). Unlike heavy fourth-generation sequential chiral quarks, these are not excluded by the measured H production cross section [15,16] because the nonchirality of the VLQs allows for gauge-invariant mass terms in the Lagrangian and thus does not require Yukawa couplings.

There are four types of VLQs with renormalizable couplings to SM quarks. These are defined by their electrical charge: $-1/3$ (B), $+2/3$ (T), $+5/3$ (X), or $-4/3$ (Y) [17]. The B VLQ mixes with the chiral down-type quarks, and similarly, the T VLQ mixes with the chiral up-type quarks. Precision measurements that constrain additional couplings of the first- and second-generation SM quarks [18–20] indicate that the primary couplings of the T and B VLQs are to third-generation SM quarks. The values of the T and B VLQ branching fractions are determined by unknown parameters in the theory: the VLQ multiplet configuration, the VLQ mass, and the coupling of the VLQ to chiral quarks [21]. The possible decays of the B VLQ are $B \rightarrow bH$, $B \rightarrow bZ$, and $B \rightarrow tW$, so the branching

^{*}Full author list given at the end of the article.

Published by the American Physical Society under the terms of the [Creative Commons Attribution 4.0 International license](https://creativecommons.org/licenses/by/4.0/). Further distribution of this work must maintain attribution to the author(s) and the published article’s title, journal citation, and DOI. Funded by SCOAP³.

fractions of these three modes sum to 100%. In TB doublet models, the branching fractions $\mathcal{B}(B \rightarrow bH)$ and $\mathcal{B}(B \rightarrow bZ)$ are approximately equal with values determined by the relative mixing of the T and B VLQs with SM quarks [17]. They range from 50% each for the case of no Tt mixing to 0% each for the case of no Bb mixing. In XTB triplet models, $\mathcal{B}(B \rightarrow bZ)$ and $\mathcal{B}(B \rightarrow bH)$ are each approximately 50% for B VLQ masses above 2 TeV, while in TBY triplet models and B singlet models $\mathcal{B}(B \rightarrow bZ)$ and $\mathcal{B}(B \rightarrow bH)$, they are each approximately 25% for B VLQ masses above 2 TeV. In this analysis, lower limits on the B VLQ mass are presented over the full range of branching fractions.

Previously, the best B mass limits from the CMS Collaboration for pair-produced B VLQs [22] were obtained by analyzing events with fully hadronic final states using data from proton-proton (pp) collisions at $\sqrt{s} = 13$ TeV, corresponding to an integrated luminosity of 137 fb^{-1} . In that analysis, B masses were excluded at 95% confidence level (CL) up to 1570, 1390, and 1450 GeV in the 100% $B \rightarrow bH$, 100% $B \rightarrow bZ$, and TB doublet with no Tt mixing (50% $B \rightarrow bH$ and 50% $B \rightarrow bZ$) models, respectively. The best B mass limits from the ATLAS Collaboration in pair-produced B events using pp collisions at $\sqrt{s} = 13$ TeV at 95% CL are 1030 GeV (based on 36.1 fb^{-1}) for the 100% $B \rightarrow bH$ case [23] and 1420 and 1320 GeV (based on 136 fb^{-1}) [24] for the 100% $B \rightarrow bZ$ and TB doublet with no Tt mixing models, respectively.

The analysis presented here combines the fully hadronic and leptonic categories and improves upon the previous CMS analysis in two ways. First, the fully hadronic category is extended by including two additional modes in which one of the VLQs in an event decays to t and W so that, in addition to the $bHbH$, $bHbZ$, and $bZbZ$ decay modes considered in [22], the $bHtW$ and $bZtW$ decay modes are also included. Second, dileptonic events in which a Z boson in either the $bHbZ$ or $bZbZ$ mode decays to a pair of opposite-sign electrons or muons are included. Because the dileptonic branching fraction of the Z boson is an order of magnitude smaller than its hadronic branching fraction, the number of events in these channels is significantly less than in the fully hadronic ones. However, this is offset by the substantially lower background in these channels and results in significantly improved sensitivity to events in which a VLQ decays to bZ , leading to improved sensitivity for large $\mathcal{B}(B \rightarrow bZ)$.

II. ANALYSIS OVERVIEW

In this analysis, we search for events featuring the production of a pair of bottom-type VLQs, B , with mass greater than 1000 GeV, in data collected with the CMS detector from pp collisions at $\sqrt{s} = 13$ TeV at the LHC in 2016–2018, corresponding to an integrated

luminosity of 138 fb^{-1} [25–27]. We consider three possible decays of the B : a b quark and a Higgs boson ($B \rightarrow bH$), a b quark and a Z boson ($B \rightarrow bZ$), and a t quark and a W boson ($B \rightarrow tW$). Events are classified into different channels depending on three properties. The first is whether the event falls into the “fully hadronic” category, in which all of the bosons in an event decay into hadronic jets, or the “leptonic” category, where an event contains a $B \rightarrow bZ$ decay in which the Z boson decays into a pair of leptons, either electrons (ee) or muons ($\mu\mu$). Since an essential element of the analysis is the categorization of events based on their kinematical reconstruction, events with leptonic W boson decays are not considered. Figures 1 and 2 show the representative Feynman diagrams for the different decay modes in the fully hadronic and leptonic categories, respectively.

The second property determining the event classification is the reconstructed decay mode, which is determined by the decays of the two B VLQs. The leptonic category includes only $bHbZ$ and $bZbZ$ decay modes (i.e., events with one $B \rightarrow bH$ and one $B \rightarrow bZ$ decay, and events with two $B \rightarrow bZ$ decays, respectively), while the fully hadronic category includes, in addition, $bHbH$, $bHtW$, and $bZtW$ decay modes. The $tWtW$ mode is not considered since its high jet multiplicity results in a large number of possible jet combinations.

The third property determining the event classification is the number of reconstructed jets. Because the bosons produced in the B VLQ decay often have a significant Lorentz boost, the two jets produced in the hadronic decay of a W , Z , or Higgs boson can merge and be reconstructed as a single merged jet. In the tW case, the t quark decay into bW can produce three jets (one from the b quark and two from the W boson), two jets (one from the b quark and a merged jet from the W boson), or one fully merged jet. As a result, the final state can have a different jet multiplicity, depending on the number of merged jets. In the leptonic category, we also include events where an additional jet is produced from initial- or final-state radiation (ISR or FSR). Events containing ISR and FSR are not included in the hadronic category due to the large number of possible jet combinations resulting from the higher jet multiplicities.

The reconstruction of events and assignment of jets to parent particles is performed using a modified χ^2 metric, χ_{mod}^2 , which uses as input the mass differences between the two reconstructed bosons and the Higgs, Z , or W boson, normalized by their resolutions, and the fractional mass difference of the two reconstructed VLQs. The value of $\chi_{\text{mod}}^2/\text{ndf}$, where ndf is the number of degrees of freedom, is calculated for each possible reconstructed decay mode and jet assignment, and the mode with the lowest value is selected as the reconstructed mode. Thus, each event is assigned to exactly one reconstructed mode. In the leptonic case, the $\chi_{\text{mod}}^2/\text{ndf}$ value is also used to identify extra jets that are likely to be from ISR and FSR.

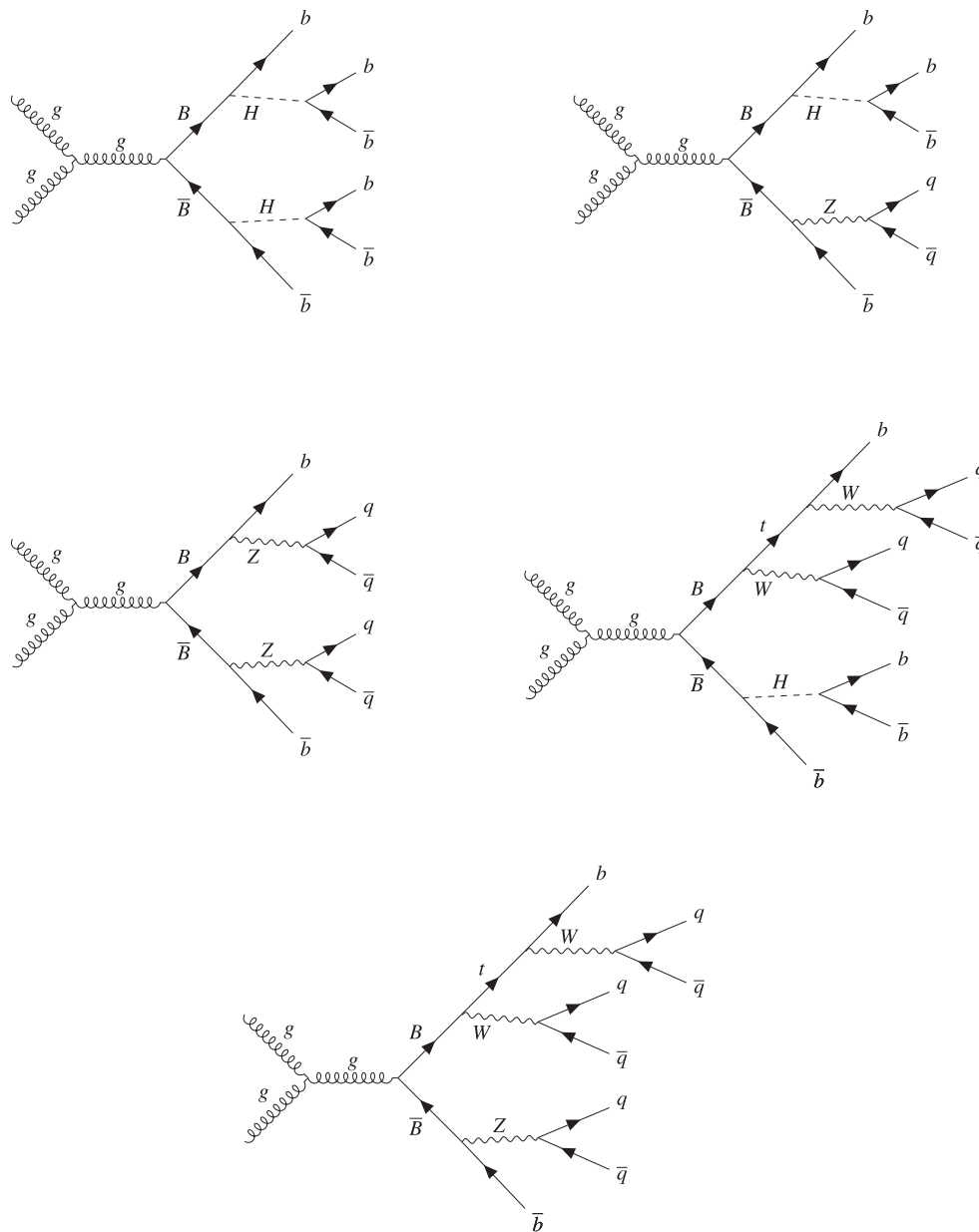


FIG. 1. Feynman diagrams for the pair production of bottom-type VLQs that decay into a b or t quark or antiquark and either a Higgs, Z , or W boson with fully hadronic final states. Upper row: $bHbH$ and $bHbZ$; middle row: $bZbZ$ and $bHtW$; lower row: $bZtW$. Modes with decays to $tWtW$ (not shown) are also possible but not considered in this analysis. The B and \bar{B} can be exchanged in the decays.

The signature in the leptonic category consists of three or four final-state jets and a pair of oppositely charged, same-flavor electrons or muons with an invariant mass consistent with the Z boson mass. In the fully hadronic category, the signature consists of four, five, or six final-state jets. Table I summarizes the final event classification, showing the set of “channels” defined by the event category, decay mode, and jet multiplicity.

The main background in the leptonic category consists of Drell-Yan (DY) dilepton production in association with jets, while in the fully hadronic category, the background is

predominantly from SM events composed uniquely of jets produced through the strong interaction, referred to as quantum chromodynamics (QCD) multijet events.

The χ^2_{mod} requirement also aids in separating potential signal events from background by ensuring that the jets are kinematically consistent with production from a Higgs, Z , or W boson and that the reconstructed VLQs have masses consistent with each other. Further signal separation is achieved by requiring that some of the jets are tagged as originating from b quarks, either using tagging of individual jets or tagging of $b\bar{b}$ pairs in merged jets from $H \rightarrow b\bar{b}$

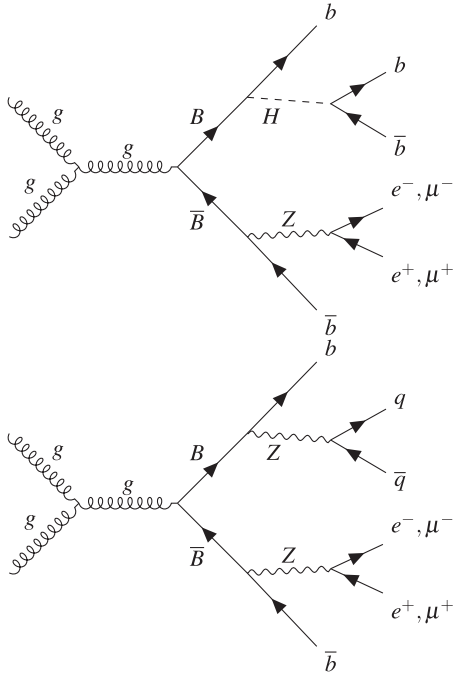


FIG. 2. Feynman diagrams of the pair production of bottom-type VLQ quarks that decay into a b quark or antiquark and either a Higgs or Z boson with a dilepton final state: $bHbZ$ mode (upper) and $bZbZ$ mode (lower). The B and \bar{B} can be exchanged in the decays.

decays. In addition, in the dileptonic case, the two leptons are also required to be kinematically consistent with the decay of a Z boson.

III. CMS DETECTOR

The central feature of the CMS apparatus is a superconducting solenoid of 6 m internal diameter, providing a magnetic field of 3.8 T. Within the solenoid volume are a silicon pixel and strip tracker, a lead tungstate crystal electromagnetic calorimeter (ECAL), and a brass and

TABLE I. Summary of channels considered for each category and jet multiplicity. Although events with a jet from ISR or FSR are included in the leptonic category, for these events the extra jet is not included in the categorization of the jet multiplicity of the event.

Jet multiplicity	Leptonic category	Fully hadronic category
3	$bHbZ, bZbZ$...
4	$bHbZ, bZbZ$	$bHbH, bHbZ, bZbZ$
5	...	$bHbH, bHbZ, bZbZ, bHtW, bZtW$
6	...	$bHbH, bHbZ, bZbZ, bHtW, bZtW$

scintillator hadron calorimeter (HCAL), each composed of a barrel and two end-cap sections. Forward calorimeters extend the pseudorapidity (η) coverage provided by the barrel and end-cap detectors. Muons are measured in gaseous detectors embedded in the steel flux-return yoke outside the solenoid.

The ECAL consists of 75 848 lead tungstate crystals, which provide coverage in $|\eta| < 1.48$ in a barrel region and $1.48 < |\eta| < 3.0$ in two end-cap regions. In the region $|\eta| < 1.74$, the HCAL cells have widths of 0.087 in η and 0.087 in azimuth (ϕ). For $|\eta| < 1.48$, the HCAL cells map in the η - ϕ plane onto 5×5 arrays of ECAL crystals to form calorimeter towers projecting radially outwards from close to the nominal interaction point. For $|\eta| > 1.74$, the coverage of the towers increases progressively to a maximum of 0.174 in $\Delta\eta$ and $\Delta\phi$. Within each tower, the energy deposits in ECAL and HCAL cells are summed to define the calorimeter tower energies, which are subsequently used to provide the energies and directions of hadronic jets. When combining information from the entire detector, the jet energy resolution typically amounts to 15%–20% at 30 GeV, 10% at 100 GeV, and 5% at 1 TeV. The electron momentum is estimated by combining the energy measurement in the ECAL with the momentum measurement in the tracker. The momentum resolution for electrons with $p_T \approx 45$ GeV from $Z \rightarrow ee$ decays ranges from 1.6% to 5%. It is generally better in the barrel region than in the end caps and also depends on the bremsstrahlung energy emitted by the electron as it traverses the material in front of the ECAL [28,29].

Muons are measured in the pseudorapidity range $|\eta| < 2.4$, with detection planes made using three technologies: drift tubes, cathode strip chambers, and resistive-plate chambers. The single muon trigger efficiency exceeds 90% over the full η range, and the efficiency to reconstruct and identify muons is greater than 96%. Matching muons to tracks measured in the silicon tracker results in a relative transverse momentum (p_T) resolution, for muons with p_T up to 100 GeV, of 1% in the barrel and 3% in the end caps. The p_T resolution in the barrel is better than 7% for muons with p_T up to 1 TeV [30].

Events of interest are selected using a two-tiered trigger system. The first level, composed of custom hardware processors, uses information from the calorimeters and muon detectors to select events at a rate of around 100 kHz within a fixed latency of about 4 μ s [31]. The second level, known as the high-level trigger, consists of a farm of processors running a version of the full event reconstruction software optimized for fast processing, and it reduces the event rate to around 1 kHz before data storage [32].

A more detailed description of the CMS detector, together with a definition of the coordinate system used and the relevant kinematic variables, can be found in Ref. [33].

IV. DATA AND SIMULATED EVENTS

Signal events with pair production of VLQs were simulated using the Monte Carlo generator MADGRAPH5_aMC@NLO [34]. For samples corresponding to 2016 data, version v2.3.3 was used with NNPDF3.0 next-to-leading order (NLO) parton distribution functions (PDFs) [35]; for samples corresponding to 2017–2018 data, v2.4.2 was used with NNPDF3.1 next-to-NLO PDFs [36]. The generated VLQ masses m_B cover the range 1000–1800 GeV in steps of 100 GeV. Hadronization of the underlying partons was simulated using PYTHIA v8.212 [37] with the CUETP8M1 tune [38] for samples corresponding to 2016 data, and with the CP5 tune [39] for samples corresponding to 2017 and 2018 data. Corrections to the cross sections to next-to-NLO and next-to-next-to-leading logarithmic soft-gluon resummation were obtained using TOP++ 2.0 [40–42] with the MSTW2008NNLO68CL PDF set from the LHAPDF 5.9.0 library [43–45].

Although the background estimate is derived purely from data, simulated background samples are used for cross-checks of the data distributions. The background processes considered include DY + jets, QCD multijet, W + jets, Z + jets, and $t\bar{t}$ + jets. The DY + jets process is simulated with MADGRAPH5_aMC@NLO v2.6.0 at NLO, using the FxFx prescription [46] for jet merging, while the other four backgrounds are simulated using MADGRAPH5_aMC@NLO v2.4.2 at leading order with the MLM prescription [47] for jet merging. The hadronization is simulated in the same way as for the signal samples.

In order to simulate the effect of additional pp interactions within the same or nearby bunch crossings (“pileup”), PYTHIA v8.226 with a total inelastic pp cross section of 69.2 mb [48] was used to simulate minimum bias events to overlay on the hard scattering process. Following event generation, the GEANT4 package [49,50] was used to simulate the CMS detector response. Scale factors corresponding to jet energy corrections, jet energy resolutions [51], QCD renormalization and factorization scales, pileup, and jet tagging [52,53] were applied to the simulated signal events so that the corresponding distributions would agree with those in the data.

V. LEPTON AND JET RECONSTRUCTION AND JET TAGGING

The particle-flow algorithm [54] aims to reconstruct and identify each individual particle in an event, with an optimized combination of information from the various elements of the CMS detector. The primary vertex is taken to be the vertex corresponding to the hardest scattering in the event, evaluated using tracking information alone, as described in Sec. 9.4.1 of Ref. [55]. The energy of photons is obtained from the ECAL measurement. The energy of electrons is determined from a combination of the electron momentum from the track, the energy of the corresponding

ECAL cluster, and the energy sum of all bremsstrahlung photons spatially compatible with originating from the electron track. The energy of muons is obtained from the curvature of the corresponding track. The energy of charged hadrons is determined from a combination of their momentum measured in the tracker and the matching ECAL and HCAL energy deposits, corrected for the response function of the calorimeters to hadronic showers. Finally, the energy of neutral hadrons is obtained from the corresponding corrected ECAL and HCAL energies.

For each event, hadronic jets are clustered from these reconstructed particles using the infrared and collinear safe anti- k_T algorithm via FASTJET [56,57]. To account for the difference between merged and resolved jets, two separate clusterings are performed on the input particles, one using a distance parameter of 0.4 (“AK4 jets”) and the other using a distance parameter of 0.8 (“AK8 jets”). Jet momentum is determined as the vectorial sum of all particle momenta in the jet, and from simulation it is found to be, on average, within 5% to 10% of the true momentum over the entire p_T spectrum and detector acceptance. Pileup can contribute additional tracks and calorimetric energy depositions to the jet momentum. The pileup-per-particle identification algorithm (PUPPI) [58,59] is used to mitigate the effect of pileup at the reconstructed-particle level, making use of local shape information, event pileup properties, and tracking information. A local shape variable is defined, which distinguishes between collinear and soft diffuse distributions of other particles surrounding the particle under consideration. The former is attributed to particles originating from the hard scatter and the latter to particles originating from pileup interactions. Charged particles identified to be originating from pileup vertices are discarded. For each neutral particle, a local shape variable is computed using the surrounding charged particles compatible with the primary vertex within the tracker acceptance ($|\eta| < 2.5$) and using both charged and neutral particles in the region outside of the tracker coverage. The momenta of the neutral particles are then rescaled according to their probability to originate from the primary interaction vertex deduced from the local shape variable, superseding the need for jet-based pileup corrections [58].

Jet energy corrections are derived from simulation studies so that the average measured energy of jets becomes identical to that of particle-level jets. *In situ* measurements of the momentum balance in dijet, photon + jet, Z + jet, and multijet events are used to account for any residual differences in the jet energy scale between data and simulation [51]. Additional selection criteria are applied to each jet to remove jets potentially dominated by anomalous contributions from various subdetector components or reconstruction failures.

We require AK4 jets to have $p_T > 50$ GeV and AK8 jets to have $p_T > 200$ GeV, with $|\eta| < 2.4$ in both cases. The event jet multiplicity is determined by the number of AK4

jets in the event passing these requirements. For the AK8 jets, a grooming algorithm is applied. In this algorithm, the constituents of the AK8 jets are reclustered using the Cambridge-Aachen algorithm [60,61]. The “modified mass drop tagger” algorithm [62,63], also known as the “soft-drop” (SD) algorithm, with angular exponent $\beta = 0$, soft cutoff threshold $z_{\text{cut}} < 0.1$, and characteristic radius $R_0 = 0.8$ [64], is applied to remove soft, wide-angle radiation from the jet. The resulting “soft-drop mass” provides a more accurate estimate of the mass of the parent Higgs, Z , or W boson in the case of merged jets and so is used in these cases.

The final state is expected to contain two b jets from the decays of the VLQs and may contain additional $b\bar{b}$ pairs from $H \rightarrow b\bar{b}$ or $Z \rightarrow b\bar{b}$ decays. Consequently, identification of these b jets provides an effective way to discriminate signal events from SM background. For individual jets, the DEEPJET b discriminant [52,53,65] is applied to AK4 jets to obtain single b tags, while for merged jets containing $b\bar{b}$ pairs, an algorithm developed for $H \rightarrow b\bar{b}$ tagging [53] is applied to AK8 jets to obtain double- b tags.

In the leptonic category, electrons or muons are selected with $p_T > 50$ GeV and $|\eta| < 2.4$. Electrons and muons are required to pass a loose set of identification requirements, and muons are additionally required to pass a loose isolation requirement to reject muons within jets from, e.g., semileptonic decays of b quarks [28,30]. Studies of the dileptonic mass distributions in simulation showed that this additional loose isolation requirement on muons improved the Z boson purity, while a similar loose isolation requirement on electrons was not needed.

VI. EVENT SELECTION, RECONSTRUCTION, AND CATEGORIZATION

In this section, the selection and categorization of events is described. This consists of the online selection of events by selected triggers; the off-line requirements on jets, leptons, and b -tagged jets; and the reconstruction of the VLQ candidates and selection of the event category.

A. Online event selection

Events are selected online with the following high-level trigger requirements:

- (i) For the fully hadronic category, the trigger requires the scalar sum of the measured jet p_T values to be greater than 900 (1050) GeV in the 2016 (2017–2018) data set.
- (ii) For leptonic events containing muons, the trigger requires a muon with $p_T > 50$ GeV. For 2017–2018 data, a trigger that accepts muons with $p_T > 100$ GeV identified from their signature in the tracker is also used as a backup to the primary trigger for consistency with other analyses [66].

- (iii) For leptonic events containing electrons, a set of triggers is used to increase the efficiency, selecting any of the following: an electron passing a tight set of identification criteria with $p_T > 27, 35, \text{ or } 32$ GeV in 2016, 2017, or 2018, respectively; an electron with $p_T > 115$ GeV; a photon with $p_T > 200$ GeV (175 GeV in 2016); a pair of isolated electrons with $p_T > 23$ (12) GeV for the leading (subleading) electron; a pair of electrons with $p_T > 33$ GeV; or a pair of photons with $p_T > 70$ GeV (60 GeV in 2016).

The trigger efficiencies are measured using data sets collected by triggers independent of those used in the analysis. For the fully hadronic category, the trigger efficiencies are parametrized by H_T , defined as the scalar sum of the p_T of all off-line AK4 jets satisfying the above p_T and η requirements. The efficiency exceeds 99% for values of H_T greater than 1350 GeV. For the leptonic category, the trigger efficiencies are parametrized by the highest p_T lepton. Both the electron and muon trigger efficiencies exceed 98% for values of the highest lepton p_T greater than 50 GeV.

B. Off-line requirements on jets, leptons, and b -tagged jets

Off-line selection requirements are then applied. For the leptonic category, the event is required to have at least three and no more than five AK4 jets with $p_T > 50$ GeV and $|\eta| < 2.4$, and to have at least one pair of opposite-sign, same-flavor leptons with an invariant mass in the range $80 < m_{\ell\ell} < 102$ GeV, consistent with the Z boson mass. If there are two such pairs each with invariant mass within the Z boson mass window, the pair with the mass closest to that of the Z boson is used. For the fully hadronic category, there must be at least four and no more than six AK4 jets with $p_T > 50$ GeV and $|\eta| < 2.4$, and the event must have $H_T > 1350$ GeV. In addition, to ensure orthogonality with both the leptonic analysis and with other B VLQ searches using a single lepton, any event with an isolated electron or muon with $p_T > 50$ GeV, or at least one lepton pair meeting the criteria for the leptonic category, is rejected.

A requirement is also placed on the minimum number of jets tagged as originating from a b quark. For the fully hadronic category, the number of tagged b jets and the working points (WPs) for the taggers are optimized for discovery of a 1400 GeV VLQ signal. The WPs used for the single- b tagger, “loose,” “medium,” and “tight,” correspond to an identification efficiency of approximately 93%, 82%, and 65%, respectively, for b jets with $p_T > 30$ GeV in simulated $t\bar{t}$ events, with a probability of 10%, 1%, and 0.1%, respectively, for light-quark (u, d, s) and gluon jets to be misidentified as b jets [52]. For the $b\bar{b}$ tagger, two WPs, “loose” and “medium 2,” are used, corresponding to an identification efficiency of approximately 75% and 45%, respectively, with a misidentification

TABLE II. Required minimum number of single (N_b) and double ($N_{b\bar{b}}$) b tags, and WPs used for each category, decay mode, jet multiplicity (N_j), and number of merged jets (N_{AK8}). The working points are described in the text. For a given event mode, there can be several jet multiplicities depending on the number of merged jets.

Decay mode	N_j	N_{AK8}	Min N_b	b tagger WP	Min $N_{b\bar{b}}$	$b\bar{b}$ tagger WP
Fully hadronic $bHbH$	4	2	2	Medium	1	Loose
Fully hadronic $bHbH$	5	1	3	Medium	1	Loose
Fully hadronic $bHbH$	6	0	4	Medium
Fully hadronic $bHbZ$	4	2	2	Loose	1	Medium 2
Fully hadronic $bHbZ$	5	1	3	Medium	0	Loose
Fully hadronic $bHbZ$	6	0	4	Medium
Fully hadronic $bZbZ$	4	2	2	Medium	0	Loose
Fully hadronic $bZbZ$	5	1	2	Medium	0	Loose
Fully hadronic $bZbZ$	6	0	2	Tight
Fully hadronic $bHtW$	5	3	2	Medium	0	Loose
Fully hadronic $bHtW$	6	2	3	Medium	0	Loose
Fully hadronic $bZtW$	5	3	2	Medium	0	Loose
Fully hadronic $bZtW$	6	2	2	Tight	0	Loose
Leptonic $bHbZ$	3	1	1	Medium
Leptonic $bHbZ$	4	0	1	Medium
Leptonic $bZbZ$	3	1	1	Medium
Leptonic $bZbZ$	4	0	1	Medium

probability of 11% and 3%, respectively [53]. For the leptonic category, the medium WP is used for the single b tagger in all channels. Table II summarizes the final requirements.

C. Event reconstruction and categorization

We define a “preselection” sample, which consists of events that pass all of the selection requirements except for the b tagging. Before the b -tagging requirements are applied, the event sample is dominated by SM backgrounds, primarily QCD multijet and $t\bar{t}$ processes, and any potential contribution from the signal is negligible. Using the “preselection” events, candidate bosons (Higgs, Z , or W) and VLQs are reconstructed. A candidate boson is formed from either two AK4 jets or a single AK8 jet, with the mass taken as the invariant mass of the two jets in the former case and the soft-drop mass of the jet in the latter case. We only use AK8 jets that have a soft-drop mass greater than 50 GeV and match to an AK4 jet within $\Delta R = \sqrt{(\Delta\eta)^2 + (\Delta\phi)^2} < 0.3$. In order to avoid overlap with another AK4 jet which could affect the AK8 jet mass, the AK8 jet is discarded if there is another AK4 jet that matches to it within $\Delta R < 0.6$.

A VLQ candidate decaying to bH or bZ is then formed by combining an additional jet with a boson candidate, with its reconstructed mass m_{VLQ} taken to be the invariant mass of this combination. In the tW case, a t quark candidate can be reconstructed either from a single AK8 jet, with the mass taken to be the soft-drop mass of the jet, or from two or

three AK4 jets, with the mass taken to be the invariant mass of these jets.

The decay mode, as well as the assignment of reconstructed jets to their parent particles, is determined using the modified χ^2 parameter, χ_{mod}^2 , evaluated for all possible decay modes and jet assignments. Because the inputs to χ_{mod}^2 are not necessarily distributed as Gaussian variables, the resulting expression does not follow a true χ^2 distribution, and thus χ_{mod}^2 is used to denote it. However, since χ_{mod}^2 is used for the event selection to choose the channel and jet configuration as well as provide a discriminant, this difference does not affect the outcome of the analysis.

The general form of χ_{mod}^2 is as follows in the fully hadronic category:

$$\chi_{\text{mod}}^2 = \frac{(\Delta m_{VLQ} - \overline{\Delta m_{VLQ}})^2}{\sigma_{\Delta m_{VLQ}}^2} + \frac{(m_1 - \overline{m}_1)^2}{\sigma_{m_1}^2} + \frac{(m_2 - \overline{m}_2)^2}{\sigma_{m_2}^2}, \quad (1)$$

where Δm_{VLQ} is the fractional mass difference of the two reconstructed VLQ candidates in the event, given by $\Delta m_{VLQ} = 2(m_{VLQ1} - m_{VLQ2}) / (m_{VLQ1} + m_{VLQ2})$; $m_{1,2}$ are the masses of the two reconstructed bosons; $\overline{m}_{1,2}$ and $\overline{\Delta m_{VLQ}}$ are the average masses of the bosons and Δm_{VLQ} , respectively; and σ are the standard deviations. The values of \overline{m}_i , σ_{m_i} , $\overline{\Delta m_{VLQ}}$, and $\sigma_{\Delta m_{VLQ}}$ are computed by using simulated signal samples with $m_B = 1400$ GeV and

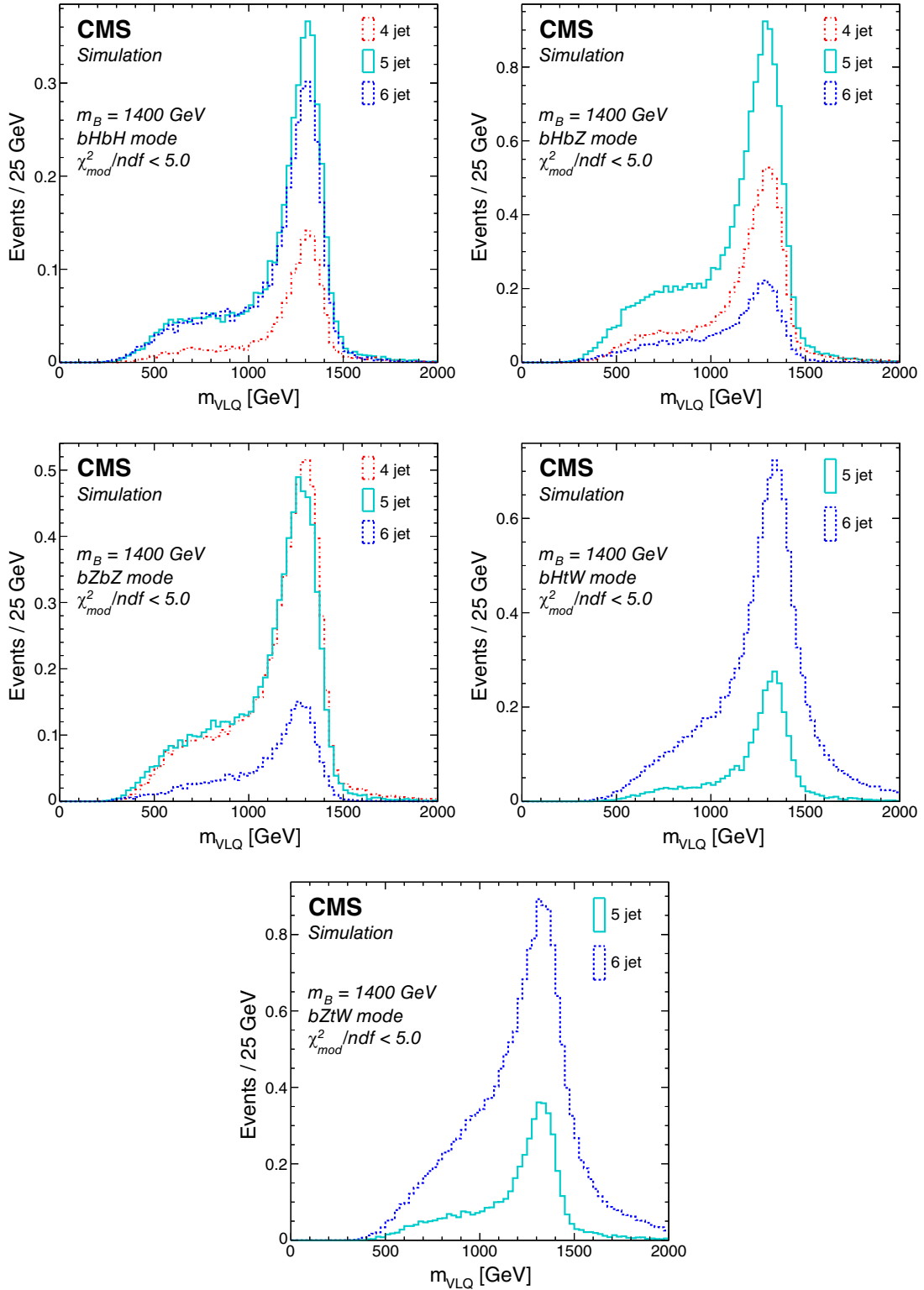


FIG. 3. Reconstructed VLQ mass distributions for simulated events for the channels in the fully hadronic category with $m_B = 1400$ GeV. Upper row: channels in the $bHbH$ (left) and $bHbZ$ (right) decay modes. Middle row: channels in the $bZbZ$ (left) and $bHtW$ (right) decay modes. Lower row: channels in the $bZtW$ decay mode. The different colors indicate the different jet multiplicities. A selection of $\chi^2_{\text{mod}}/\text{ndf} < 5$ has been applied. The values represent the expected number of events over the background in the 2016–2018 data sample.

selecting events where the jets are closely matched to the generated partons in simulation.

In the case where the decay mode contains a $B \rightarrow tW$ decay, another term is added to the χ^2_{mod} expression for each reconstructed t quark: $(m_t - \bar{m}_t)/\sigma_{m_t}^2$, where m_t is the reconstructed t quark mass, and \bar{m}_t and σ_{m_t} are the average and standard deviation of the t quark mass in simulation. This term is added to aid in distinguishing such events from events where one of the B VLQs decays to bZ . Because of the missing momentum in events with a leptonic W boson decay, the m_W term and, subsequently, the Δm_{VLQ} term used in the χ^2_{mod} calculation would not be accurate enough to allow adequate categorization of the event. As a result, events with leptonic W boson decays are not considered in this analysis.

In the leptonic category, only the mass of the hadronically decaying boson is included in χ^2_{mod} , so the expression is simply

$$\chi^2_{\text{mod}} = \frac{(\Delta m_{\text{VLQ}} - \overline{\Delta m_{\text{VLQ}}})^2}{\sigma_{\Delta m_{\text{VLQ}}}^2} + \frac{(m_1 - \bar{m}_1)^2}{\sigma_{m_1}^2}, \quad (2)$$

where m_1 is the mass of the hadronically decaying Higgs or Z boson.

Mass distributions for the parent Z , W , H , or t are obtained and then fitted with a bifurcated Gaussian (i.e., a Gaussian that has a different σ parameter above and below the mean). Consequently, when the χ^2_{mod} value is computed, the appropriate σ value is used depending on whether the reconstructed mass is above or below \bar{m} . These distributions are computed separately depending on whether the final state is reconstructed as two resolved jets or one merged jet, and also separately for each jet multiplicity. The values for $\sigma_{\Delta m_{\text{VLQ}}}$ are typically around 0.1, while the values for σ_{m_i} are roughly 10–20 GeV.

Once the χ^2_{mod} value has been computed for all channels within an event category, the channel with the smallest $\chi^2_{\text{mod}}/\text{ndf}$ is selected. The value of ndf is 2 for the leptonic channels; 3 for the fully hadronic modes $bHbH$, $bHbZ$, and $bZbZ$; and 4 for the fully hadronic modes $bHtW$ and $bZtW$. This method was found to have good accuracy, as determined by tests with the signal simulations. Although the mode of some events is not correctly identified, these events are not rejected but are included as part of the signal under a different mode, while the selection based on χ^2_{mod} still provides good background rejection.

The performance of the χ^2_{mod} -based reconstruction is indicated by the average of the two reconstructed VLQ masses, referred to as m_{VLQ} , which is shown for simulated signal samples with $m_B = 1400$ GeV in Fig. 3 (channels in the fully hadronic category) and Fig. 4 (channels in the dileptonic category). The mass is well reconstructed for events near the peak; the low-mass tail corresponds to events in which the selected jet permutation is incorrect.

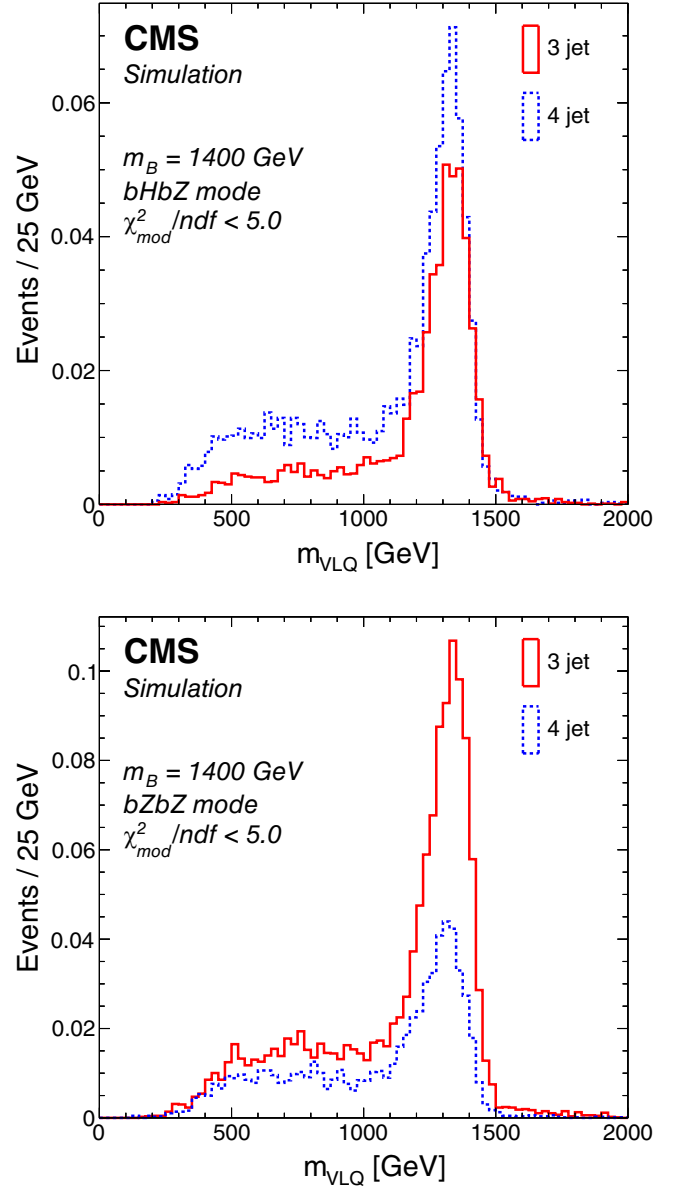


FIG. 4. Reconstructed VLQ mass distributions for simulated events passing the b -tag requirement for the channels in the dileptonic category with $m_B = 1400$ GeV in the $bHbZ$ (upper) and $bZbZ$ (lower) event modes. A selection of $\chi^2_{\text{mod}}/\text{ndf} < 5$ has been applied. The values represent the expected number of events over the background in the 2016–2018 data sample.

Tests on simulated signal samples with different B VLQ masses showed similar performance.

In the leptonic category, in order to account for a possible jet due to ISR or FSR, an extra jet reconstructed by the method described in Sec. V but not originating from VLQ pair production is allowed. Specifically, for events that contain five reconstructed jets, the $\chi^2_{\text{mod}}/\text{ndf}$ is evaluated for all possible assignments of four jets with one jet discarded, and the event is then treated as a four-jet event using the four jets that resulted in the best $\chi^2_{\text{mod}}/\text{ndf}$. For events that

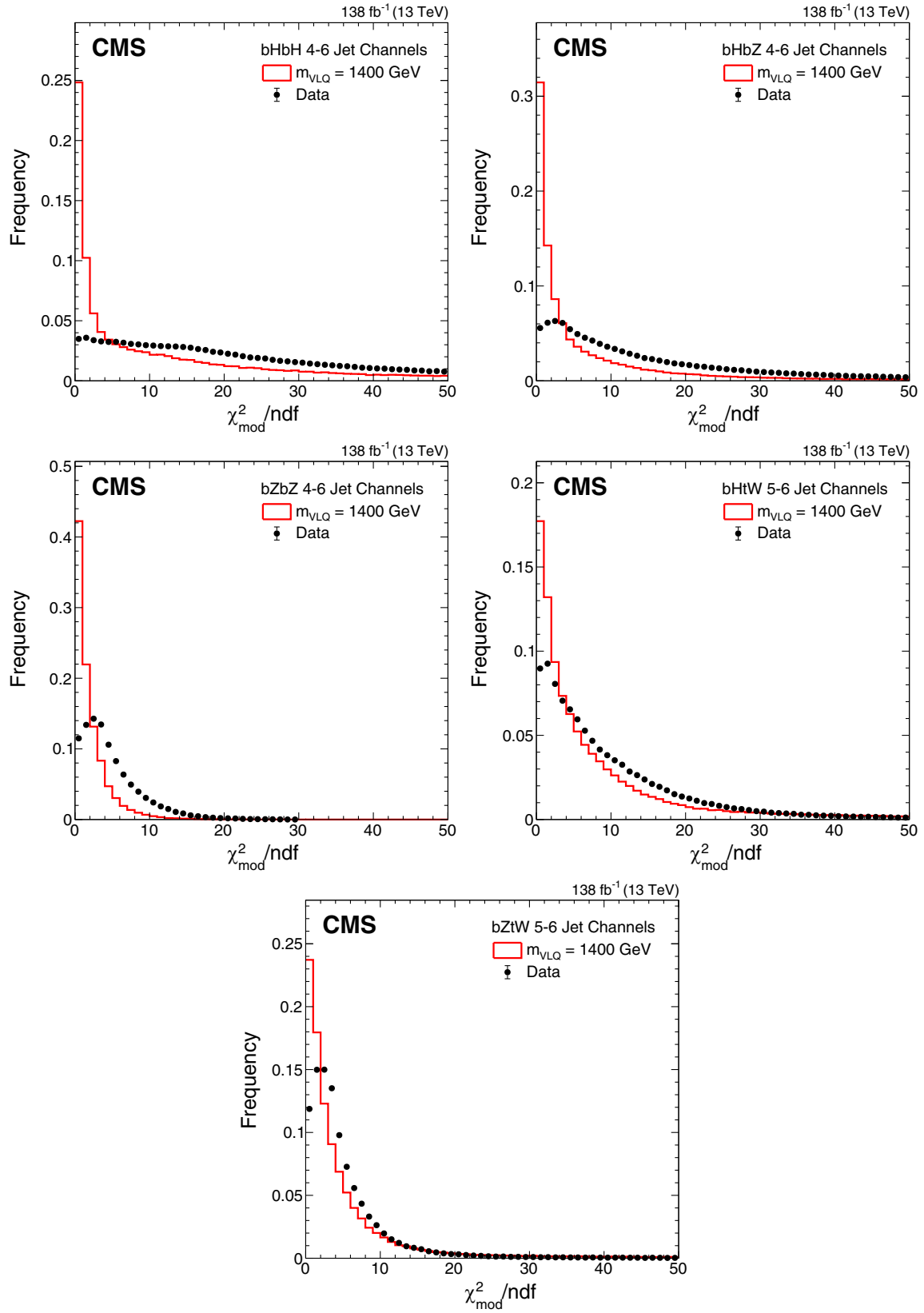


FIG. 5. Normalized distributions of the value of the least $\chi^2_{\text{mod}}/\text{ndf}$ for simulated signal events and data events in the fully hadronic category before any b -tagging requirements are applied in the fully hadronic category. Upper row: $bHbH$ (left), $bHbZ$ (center), and $bZbZ$ (right) decay modes. Lower row: $bHtW$ (left) and $bZtW$ (right) decay modes. A signal mass of $m_B = 1400$ GeV is used and compared against all three years of data. All jet multiplicities have been combined together.

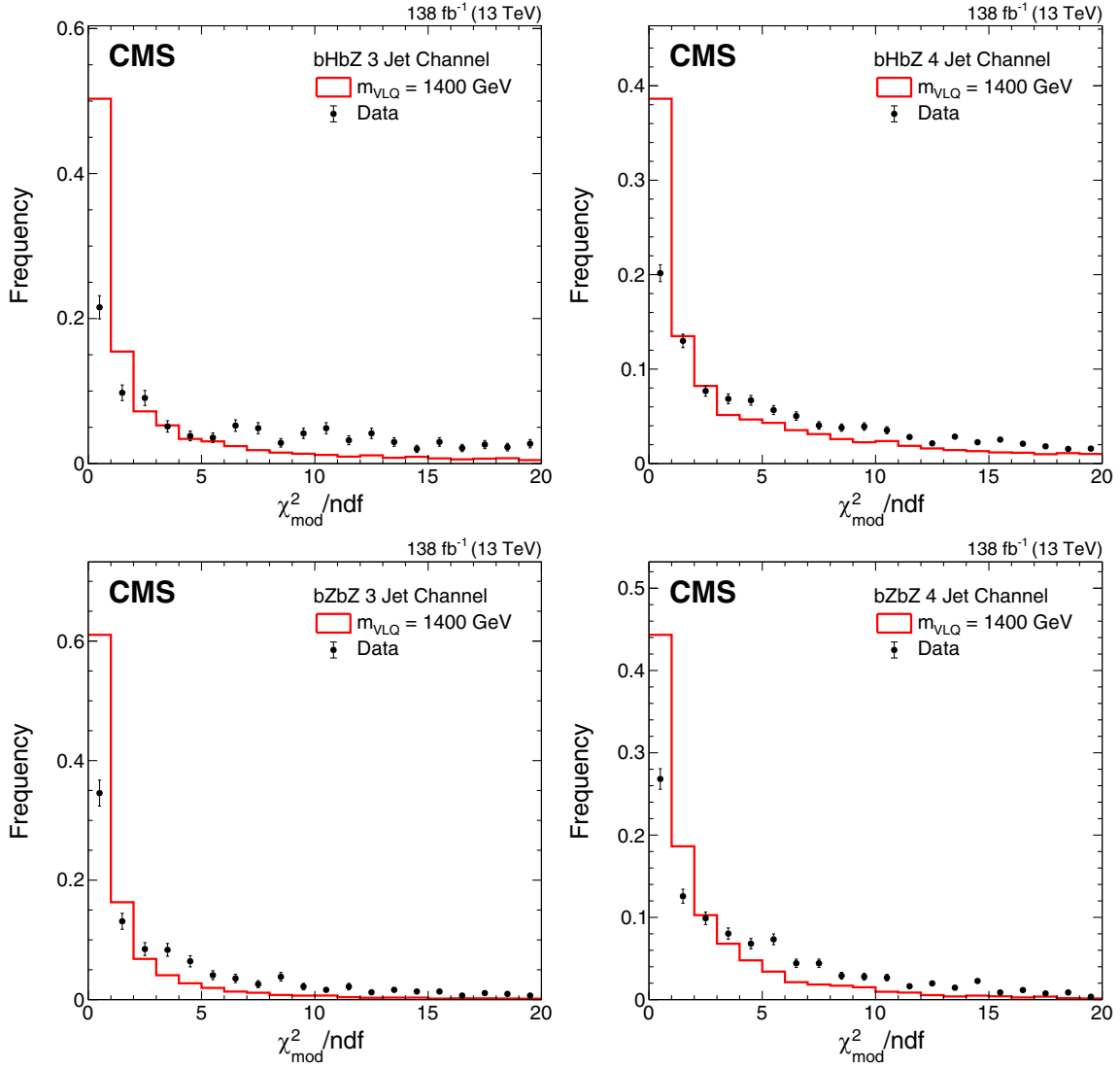


FIG. 6. Normalized distributions of the value of the least $\chi^2_{\text{mod}}/\text{ndf}$ for simulated signal events and data events in the leptonic category before any b -tagging requirements are applied. Upper row: $bHbZ$ decay mode, three-jet (left) and four-jet (right) events. Lower row: $bZbZ$ decay mode, three-jet (left) and four-jet (right) events. A signal mass of $m_B = 1400$ GeV is used and compared against all three years of data.

contain four reconstructed jets, the $\chi^2_{\text{mod}}/\text{ndf}$ is calculated for these four jets, and then also for each possible jet assignment for a three-jet event. If the four-jet $\chi^2_{\text{mod}}/\text{ndf}$ is less than each of the three-jet $\chi^2_{\text{mod}}/\text{ndf}$ values, then it is treated as a four-jet event. Otherwise, it is treated as a three-jet event using those three jets.

Figures 5 and 6 show the resulting distributions in the fully hadronic and leptonic categories, respectively, of the value of the least $\chi^2_{\text{mod}}/\text{ndf}$ for simulated signal events compared to the distributions for data events before any b -tagging requirements are applied. In these plots, the two distributions are normalized to the same area.

Since the $\chi^2_{\text{mod}}/\text{ndf}$ values tend to be lower for signal events than for background events, an upper bound is set on the least $\chi^2_{\text{mod}}/\text{ndf}$ in order to provide background rejection.

This limit is optimized for signal sensitivity separately for each category and channel, using a B mass of 1400 GeV. For the fully hadronic category, equal branching fractions for $B \rightarrow bH$, $B \rightarrow bZ$, and $B \rightarrow tW$ are assumed, and for the leptonic category, branching fractions of $\mathcal{B}(B \rightarrow bH) = 30\%$ and $\mathcal{B}(B \rightarrow bZ) = 70\%$ are used. Table III shows the optimized $\chi^2_{\text{mod}}/\text{ndf}$ limits obtained for each category. These values do not depend significantly on the B mass assumed in the optimization since the $\chi^2_{\text{mod}}/\text{ndf}$ measure in Eqs. (1) and (2) depends on the mass difference between the two reconstructed VLQ candidates and not the VLQ mass itself. As a cross-check, the optimization was performed with other B masses, resulting in only small changes in the optimal $\chi^2_{\text{mod}}/\text{ndf}$ limit values. These optimized $\chi^2_{\text{mod}}/\text{ndf}$ limits are then used in conjunction

TABLE III. Optimized upper bound values of the $\chi^2_{\text{mod}}/\text{ndf}$ selection as a function of jet multiplicity and decay mode.

Decay mode	Jet multiplicity			
	3	4	5	6
Fully hadronic $bHbH$...	1.5	2.75	1.0
Fully hadronic $bHbZ$...	2.0	1.25	1.25
Fully hadronic $bZbZ$...	0.75	1.25	1.75
Fully hadronic $bHtW$	2.5	5.0
Fully hadronic $bZtW$	1.5	6.0
Leptonic $bHbZ$	2.9	2.5
Leptonic $bZbZ$	2.0	2.6

with b tagging to provide signal discrimination in the reconstructed m_{VLQ} spectrum, which is used to obtain the background estimate described in the next section.

VII. BACKGROUND ESTIMATION

As the QCD multijet background is difficult to precisely model in simulation, the background estimation is based exclusively on control samples in data. Since the composition and behavior of the background are different between the fully hadronic and dileptonic categories, separate methods are used for each category.

A. Background estimation in the fully hadronic category

The background estimation for the fully hadronic category generally follows the procedure described in Ref. [22]. Using the preselection sample defined in Sec. VIC, the expected distribution of the number of events as a function of the VLQ candidate mass is obtained and then fit with the function

$$n(x) = p_0 \exp[-(p_1 x + \theta(-x)p_2 x^2)] \quad (3)$$

in the range $m_{\text{VLQ}} > 800$ GeV, where $x \equiv m/\text{GeV} - 1200$ and $\theta(x)$ is the Heaviside step function. The second-order term is applied only for mass values less than 1200 GeV to account for the shape change of the distribution in the low-mass region compared to a traditional exponential function caused by the trigger turn on. This is also the reason the fit only includes $m_{\text{VLQ}} > 800$ GeV. Smoothness at the $m_{\text{VLQ}} = 1200$ GeV interface is enforced by employing the same parameter p_1 for both $m_{\text{VLQ}} < 1200$ GeV and $m_{\text{VLQ}} > 1200$ GeV. Figure 7 shows the resulting fit results for six representative fully hadronic channels.

The second step is to estimate the reduction in background that results from applying the jet b -tagging requirements. This factor is called the background jet-tagged fraction (BJTF). It is obtained by using events in a sideband region defined by the mass range $500 < m_{\text{VLQ}} < 800$ GeV. This mass range is chosen to ensure that the sideband region

is free of any potential signal, as this range is below the current lower exclusion limits on the VLQ mass [22,67,68]. Table IV summarizes the values of the BJTF derived from this sideband region, denoted ϵ_0 in Eq. (4), for the different channels considered.

We allow for a dependence of the BJTF factor on m_{VLQ} that could occur, for example, because the jet tagging efficiency depends on the p_T of the jet, and VLQs with higher mass will generally produce jets with higher p_T . For this, we define a control region as events with $\chi^2_{\text{mod}}/\text{ndf}$ in the range $12 < \chi^2_{\text{mod}}/\text{ndf} < 48$. The dependence of the BJTF on m_{VLQ} in this control region is then fit with a first-order polynomial, denoted $\epsilon(m) = p_0 + p_1 m$. Checks with F -tests indicate that the first-order polynomial fit is preferred over higher-order fits. Figure 8 shows the BJTF distribution in the control regions along with the first-order polynomial fits for a few representative fully hadronic channels.

The estimate of the number of background events in the signal region, n_{bkg} , as a function of m_{VLQ} is then given by the following expression:

$$n_{\text{bkg}}(m_{\text{VLQ}}) = n(m_{\text{VLQ}}) \epsilon_0 \frac{\epsilon(m_{\text{VLQ}})}{\left(\int_{500 \text{ GeV}}^{800 \text{ GeV}} \epsilon(m') dm' \right) / (300 \text{ GeV})}, \quad (4)$$

where $n(m_{\text{VLQ}})$ is the number of candidates as a function of m_{VLQ} in the preselected sample, as shown in Fig. 7, ϵ_0 is the BJTF determined from the sideband with low VLQ mass, as shown in Table IV, and the last factor is the correction for the dependence of the BJTF on m_{VLQ} , as shown in Fig. 8.

B. Background estimation in the leptonic category

The background estimation for the leptonic category is based on a procedure similar to that for the fully hadronic category, but with different definitions of the signal and control regions. In particular, the use of b tagging is different for the two categories. For the leptonic category, the BJTF factor described above is not used. Instead, for the leptonic category, the signal region is defined to be events with $\chi^2_{\text{mod}}/\text{ndf} < 5$ for which at least one of the jets directly originating from the B VLQ candidate (i.e., not associated with an H or a Z boson decay) is b tagged (called b -tag events). The control region is defined to be events with the same $\chi^2_{\text{mod}}/\text{ndf} < 5$ requirement but where neither of the jets directly originating from a B VLQ candidate is b tagged (called b -veto events). Notably, these requirements are both independent of the hadronically decaying H or Z boson.

First, the VLQ mass distribution in the control region is fit with an exponential function over the mass range $800 < m_{\text{VLQ}} < 2000$ GeV. Figure 9 shows the resulting distributions and the exponential fits for each of the four leptonic channels. Then, this distribution is normalized to

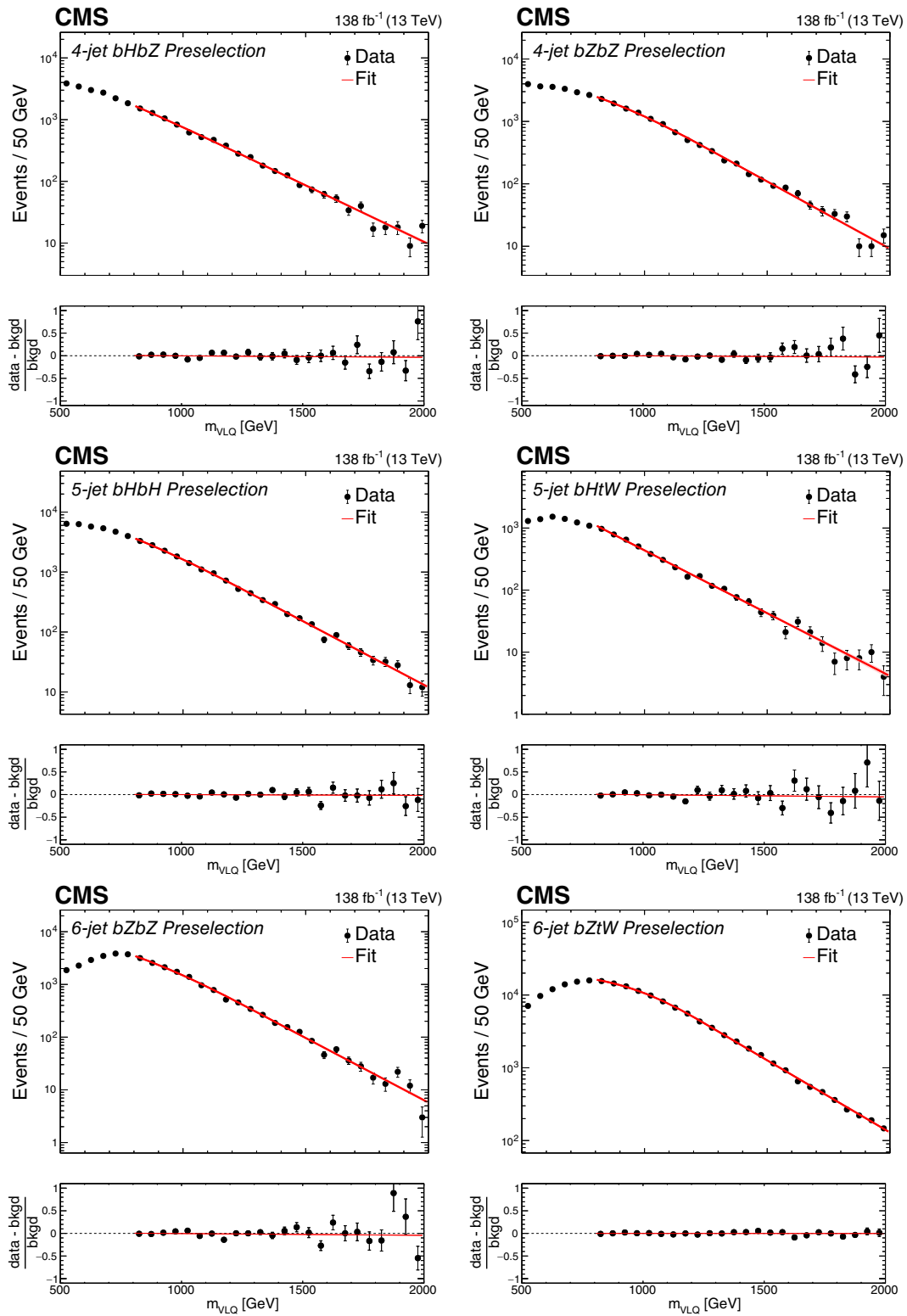


FIG. 7. Distributions of m_{VLQ} for the preselected data sample in the fully hadronic category for some selected channels. Upper row: four-jet $bHbZ$ (left) and four-jet $bZbZ$ (right) modes. Middle row: five-jet $bHbH$ (left) and five-jet $bHtW$ (right) modes. Lower row: six-jet $bZbZ$ (left) and six-jet $bZtW$ (right) modes. The fit to the data (shown by the black points) is given by the red line, and the bottom panel displays the fractional difference between the data and fit, $(data-fit)/fit$.

TABLE IV. Values of the BJTF for data events in the control region with $500 < m_{\text{VLQ}} < 800$ GeV for each of the fully hadronic channels considered. The uncertainties shown are statistical.

	$bHbH$	$bHbZ$	$bZbZ$	$bHtW$	$bZtW$
Four jets	0.0010 ± 0.0007	0.0032 ± 0.0005	0.0075 ± 0.0016
Five jets	0.0009 ± 0.0002	0.0040 ± 0.0004	0.0492 ± 0.0020	0.0243 ± 0.0019	0.0223 ± 0.0019
Six jets	0.0020 ± 0.0003	0.0018 ± 0.0003	0.0368 ± 0.0018	0.0089 ± 0.0003	0.0311 ± 0.0005

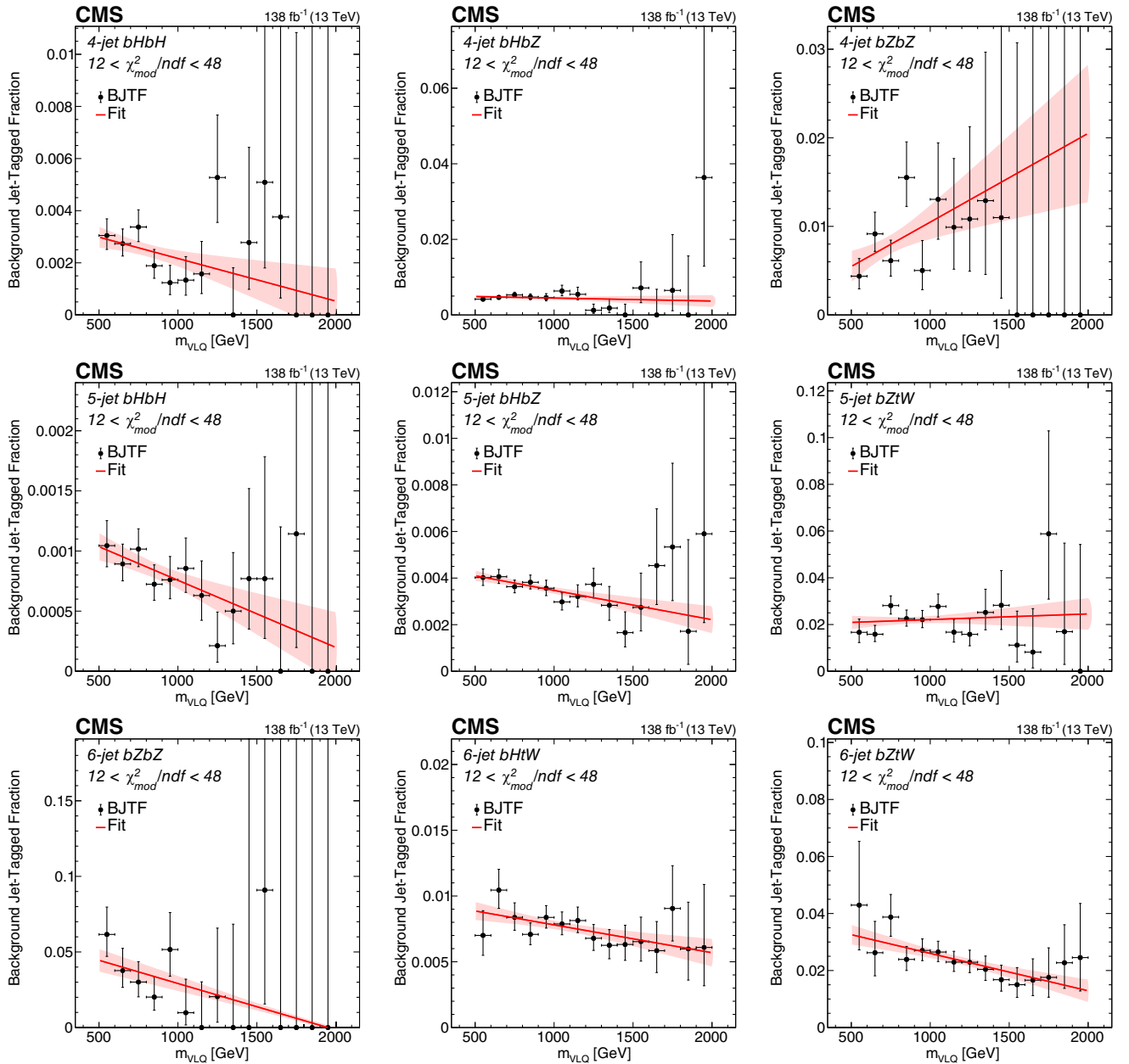


FIG. 8. Value of BJTF as a function of m_{VLQ} in the control region with $12 < \chi^2_{\text{mod}}/\text{ndf} < 48$ for some selected fully hadronic channels. Upper row: four-jet events in the $bHbH$ (left), $bHbZ$ (center), and $bZbZ$ (right) modes. Middle row: five-jet events in the $bHbH$ (left), $bHbZ$ (center), and $bZtW$ (right) modes. Lower row: six-jet events in the $bZbZ$ (left), $bHtW$ (center), and $bZtW$ (right) modes. The linear fit is shown by the red line, and the associated uncertainty in the fit is shown by the shaded band.

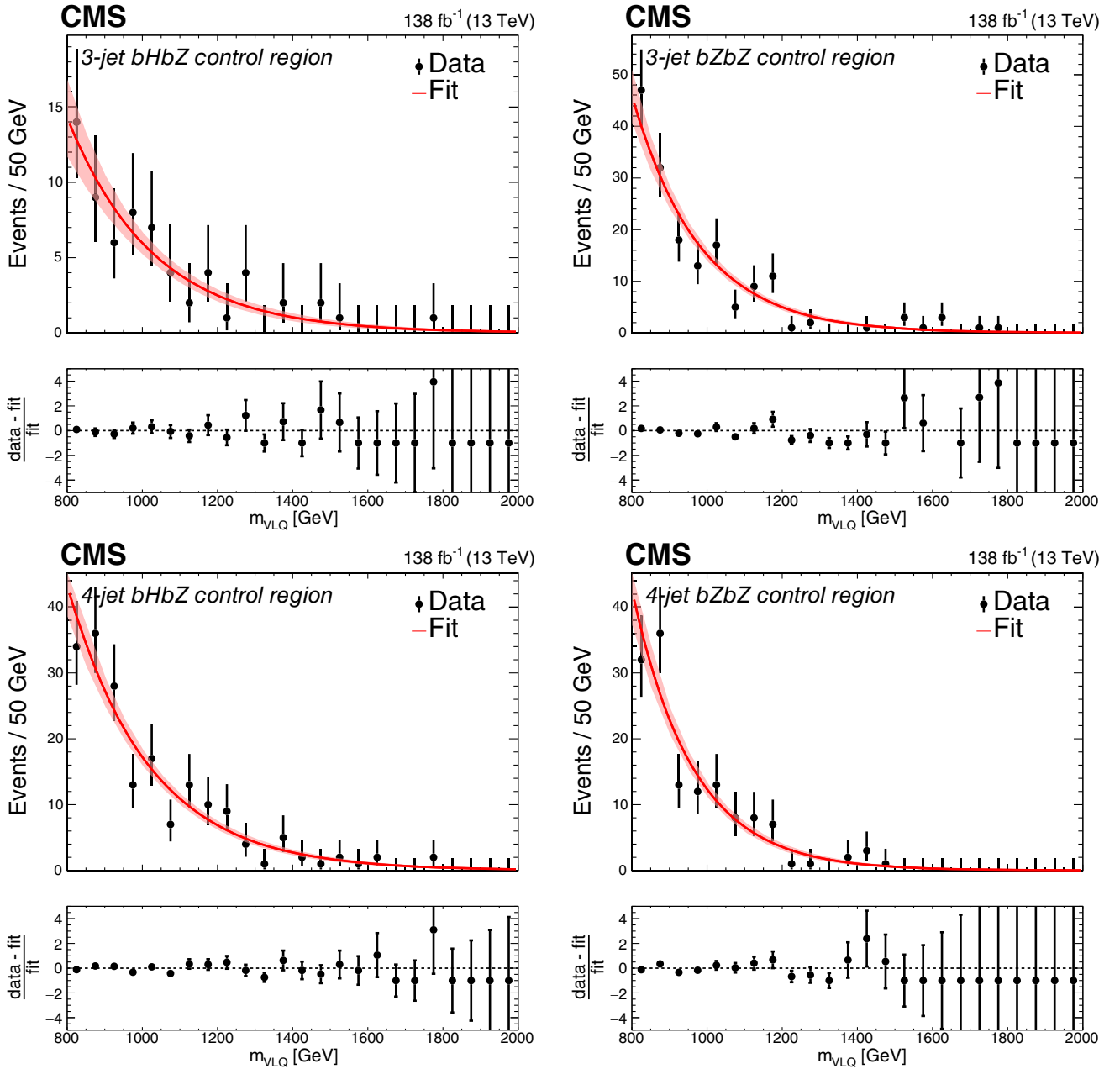


FIG. 9. Distributions of m_{VLQ} for events in the control region for the channels in the leptonic category. Upper row: three-jet events in the $bHbZ$ (left) and $bZbZ$ (right) modes. Lower row: four-jet events in the $bHbZ$ (left) and $bZbZ$ (right) modes. The exponential fit and its uncertainty are shown by the red line and the light red shaded band, respectively. The bottom panel shows the fractional difference between the data and fit, $(\text{data}-\text{fit})/\text{fit}$.

TABLE V. Values of the b -tag to b -veto ratio for events in the mass range $450 < m_{VLQ} < 900$ GeV with $\chi^2_{\text{mod}}/\text{ndf} < 5$, for each of the dileptonic channels. The uncertainties shown are statistical only.

	$bHbZ$	$bZbZ$
Three jets	0.101 ± 0.010	0.130 ± 0.006
Four jets	0.127 ± 0.009	0.125 ± 0.074

the expected distribution in the signal region by multiplying by a normalization factor, the ratio of b -tag events to b -veto events in the low-mass range of $450 < m_{VLQ} < 900$ GeV. Table V shows the resulting normalization factors for the four channels.

Next, events with $\chi^2_{\text{mod}}/\text{ndf}$ in the range $5 < \chi^2_{\text{mod}}/\text{ndf} < 20$ are used to check for possible dependence of the normalization factors on the VLQ candidate mass. Figure 10 shows the b -tag to b -veto ratio as a function

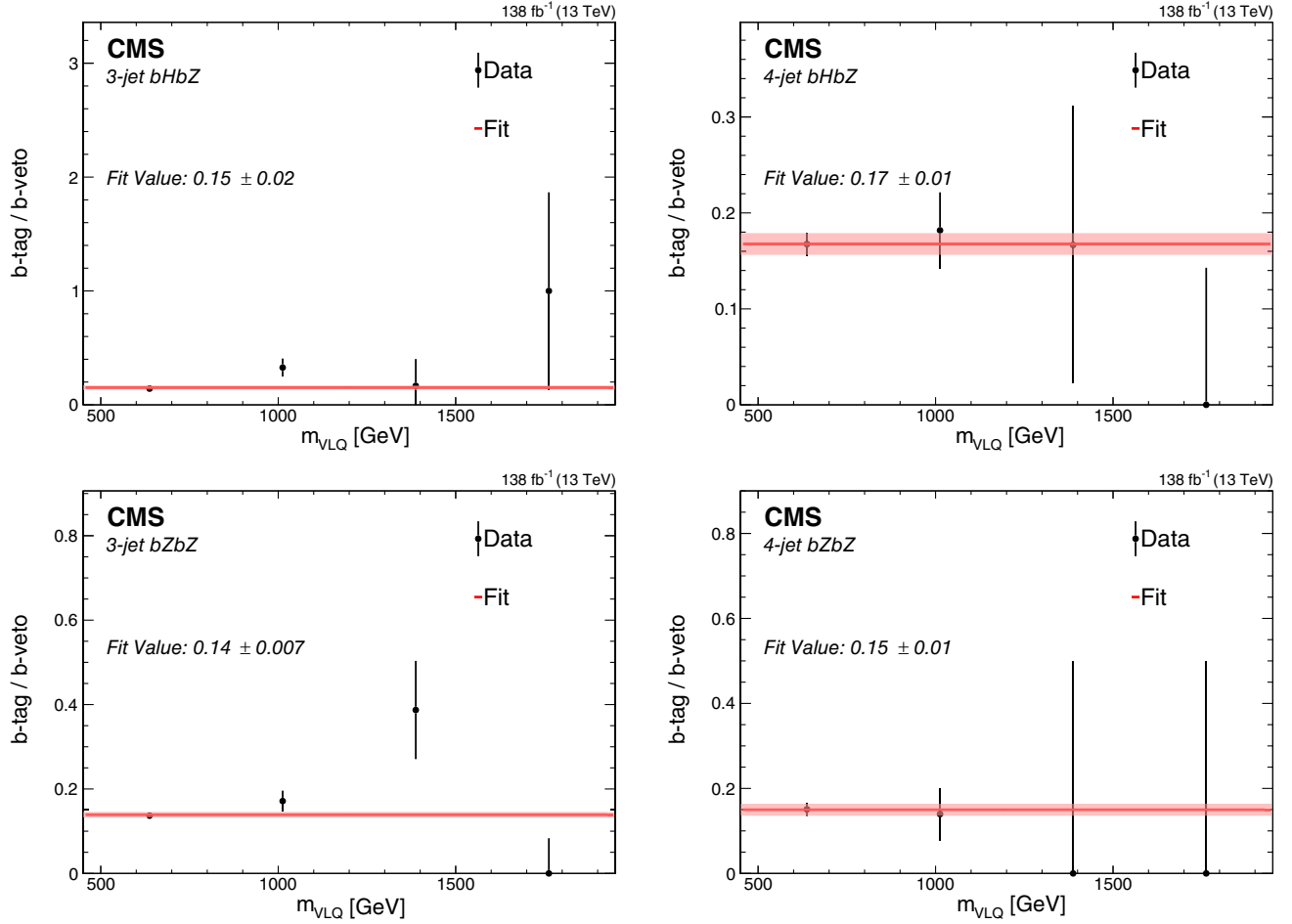


FIG. 10. Normalization factor as a function of m_{VLQ} for leptonic events in the $5 < \chi_{\text{mod}}^2/\text{ndf} < 20$ region. Upper row: $bHbZ$ events in the three-jet (left) and four-jet (right) channels. Lower row: $bZbZ$ events in the three-jet (left) and four-jet (right) channels. The fit to a constant value and its uncertainty are shown by the red line and the light red shaded band, respectively.

of m_{VLQ} for events in the range $5 < \chi_{\text{mod}}^2/\text{ndf} < 20$ for all four leptonic channels. As a cross-check, the dependence of the b -tag to b -veto ratio as a function of m_{VLQ} for simulated Drell-Yan events, which constitute the dominant background, is shown in Fig. 11 over the full mass range, which verifies that the normalization factors do not have a significant dependence on the VLQ mass.

We next check that the b -tag to b -veto ratio in the range $5 < \chi_{\text{mod}}^2/\text{ndf} < 20$ correctly represents the ratio in the range $\chi_{\text{mod}}^2/\text{ndf} < 5$ by plotting the ratio as a function of $\chi_{\text{mod}}^2/\text{ndf}$, shown in Fig. 12. No significant dependence over the $\chi_{\text{mod}}^2/\text{ndf}$ region is observed.

The fit to a constant value is therefore sufficient for all channels, as there is no statistically significant evidence for a mass dependence of the b -tag to b -veto ratio. The normalization factor is thereby set to be the ratio of b -tag events to b -veto events in the 450 to 900 GeV mass range using events with $\chi_{\text{mod}}^2/\text{ndf} < 5$, that is, the ratio of low-mass signal region events to low-mass control region events. Although there is no statistically significant

evidence of a normalization factor mass dependence, steps are taken to estimate the uncertainty that such a dependence may create in this factor. For this, we compare the ratio of b -tag events to b -veto events in the low-mass range to the ratio of b -tag to b -veto events in the high-mass range, using events in the $\chi_{\text{mod}}^2/\text{ndf}$ range of $5 < \chi_{\text{mod}}^2/\text{ndf} < 20$. Figure 13 (left) shows that the low-mass and high-mass ratios are consistent for all four channels. As a check on this procedure, the same comparison is performed for simulated Drell-Yan events using the optimally tuned $\chi_{\text{mod}}^2/\text{ndf}$. The results, displayed in Fig. 13 (right), show that the low-mass and high-mass ratios are consistent, even after an upper bound is applied on the value of $\chi_{\text{mod}}^2/\text{ndf}$.

The estimate of the number of background events in the signal region, n_{bkg} , as a function of m_{VLQ} is given by the following expression:

$$n_{\text{bkg}}(m_{\text{VLQ}}) = f(m_{\text{VLQ}}) \frac{\int_{450 \text{ GeV}}^{900 \text{ GeV}} n_{\text{signal}}(m') dm'}{\int_{450 \text{ GeV}}^{900 \text{ GeV}} n_{\text{control}}(m') dm'}, \quad (5)$$

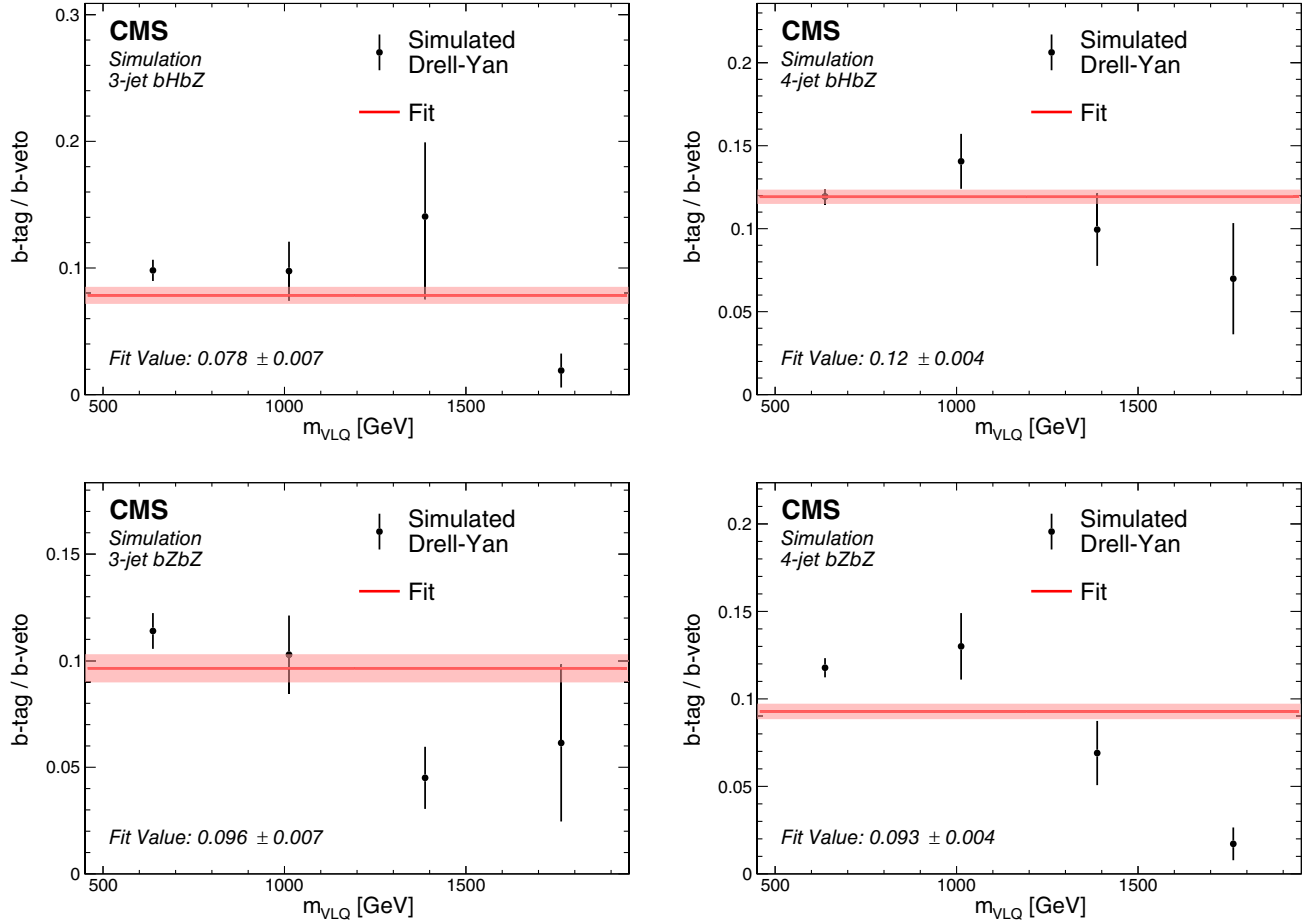


FIG. 11. Normalization factor in the leptonic category as a function of m_{VLQ} for simulated Drell-Yan events with $\chi^2_{\text{mod}}/\text{ndf} < 5$. Upper row: $bHbZ$ events in the three-jet (left) and four-jet (right) channels. Lower row: $bZbZ$ events in the three-jet (left) and four-jet (right) channels. The fit to a constant value and its uncertainty are shown by the red line and the light red shaded band, respectively.

where $f(m_{VLQ})$ is the fitted function for the number of candidates as a function of m_{VLQ} in the control region, as shown in Fig. 9, and the second term is the normalization factor, as determined by the ratio of the number of events in the signal region to the control region with $450 < m_{VLQ} < 900$ GeV. For the final evaluation of the number of events in the sideband region, the $\chi^2_{\text{mod}}/\text{ndf}$ requirement for each particular channel is applied.

VIII. SYSTEMATIC UNCERTAINTIES

The systematic uncertainties are listed in Tables VI and VII. They include the following:

- (i) Integrated luminosity: The integrated luminosities for the 2016–2018 data-taking years have 1.2%–2.5% individual uncertainties [25–27], while the overall uncertainty for the 2016–2018 period is 1.6%.
- (ii) Trigger: The uncertainties in the trigger efficiencies are determined from the uncertainties in the fitting parameters from fits of the trigger efficiencies with respect to H_T , using constant functions for channels

in the hadronic category and logistic functions for channels in the leptonic category. For 2016, 2017, and 2018, they are 2.0%, 0.05%, and 0.01%, respectively, for the jet triggers used; 0.3%, 0.2%, and 0.2% for the muon triggers; and 0.2%, 0.3%, and 0.2% for the electron triggers.

- (iii) Dilepton Z boson efficiency: The total dimuon and dielectron efficiencies are determined using simulated signal events. The net efficiency is calculated by multiplying the efficiencies for each step in the dilepton Z boson selection process: exactly two leptons, both leptons pass the identification and isolation requirements, and the dilepton Z boson invariant mass is between 80 and 102 GeV. The uncertainty in the total efficiency is found to be 0.3% for both the dimuon and dielectron cases.
- (iv) Scale factors: Scale factors for jet energy, jet energy resolution, b -tagging efficiency, and lepton efficiency (including isolation, identification, and reconstruction for individual leptons) are needed to correct the distributions in simulation to match those in data. The resulting uncertainty in the

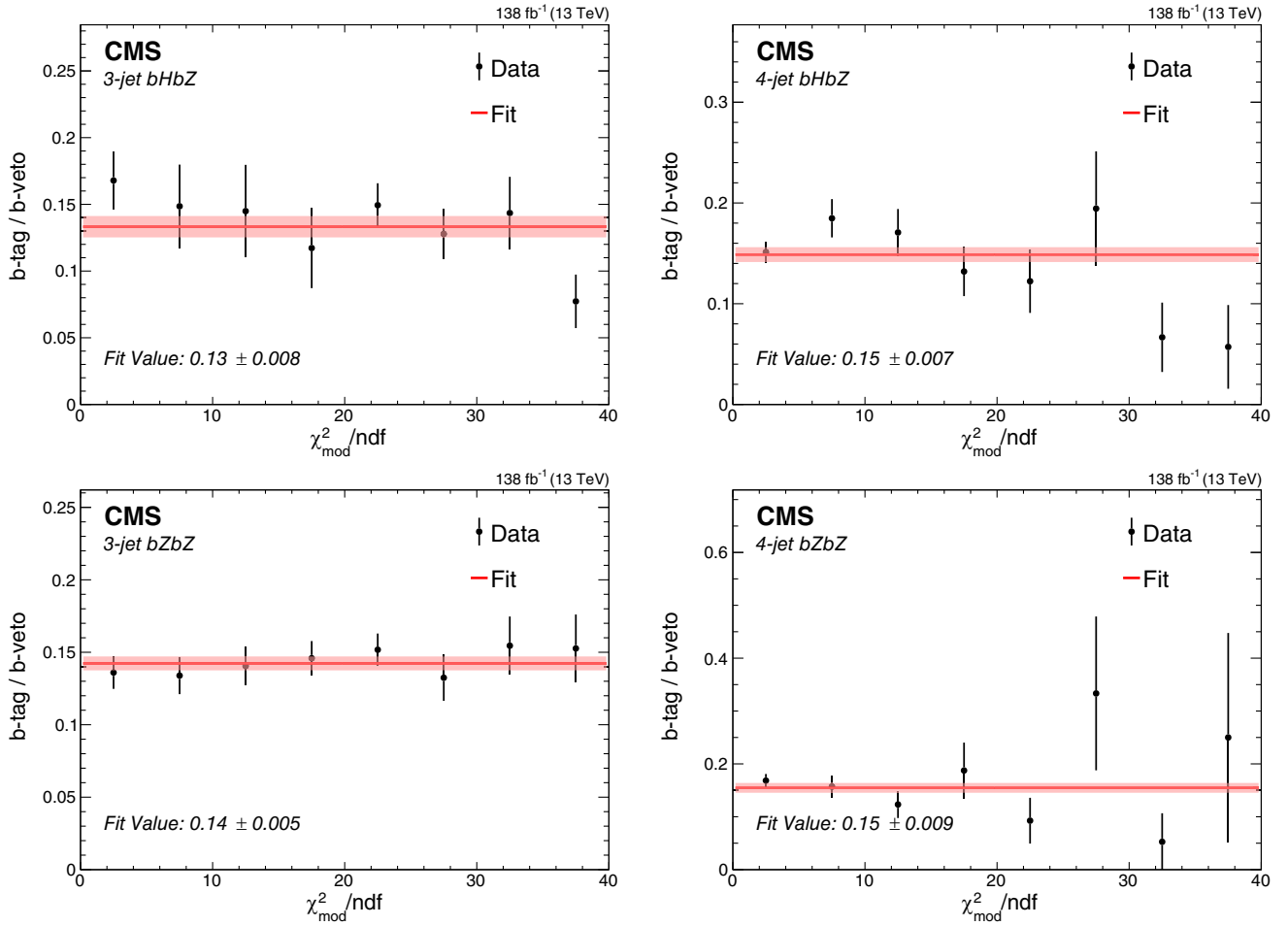


FIG. 12. Normalization factor in the leptonic category as a function of $\chi^2_{\text{mod}}/\text{ndf}$. Upper row: three-jet events in the $bHbZ$ (left) and $bZbZ$ (right) decay modes. Lower row: four-jet events in the $bHbZ$ (left) and $bZbZ$ (right) decay modes. The fit to a constant value and its uncertainty are shown by the red line and the light red shaded band, respectively.

simulated signal efficiency is determined by varying each scale factor up and down by 1 standard deviation. The uncertainties over each year are treated as uncorrelated. The uncertainties depend upon the event channel. Typical values are as follows: 0.5%–4.0% for jet energy, 0.5%–2.5% for jet resolution, 5.0%–12% for b tagging, and 10%–12% for the overall lepton efficiency (where the larger value is due to the combination of isolation, identification, and reconstruction scale factors for the individual leptons).

- (v) Background estimation in the fully hadronic category: There are two sources of uncertainty in the background estimate as a function of the average mass of the two VLQ candidates, $n_{\text{bkg}}(m_{\text{VLQ}})$ in Eq. (4). The first is from the fit for $n(m_{\text{VLQ}})$, and it is determined from the uncertainties in the fit parameters p_0 , p_1 , and p_2 . The second is the uncertainty in the mass dependence of the BJTF factor, which is similarly determined from the uncertainties in the

first-order polynomial fit parameters, p_0 and p_1 , shown in the definition of $\varepsilon(m)$. For each of the fits, the nuisance parameters are determined by decorrelating the fit parameters using the covariance matrix of the fit. Additionally, we include an uncertainty to account for our choice of fit function (referred to as “BJTF fit form” in Table VI).

- (vi) Background estimation in the dileptonic category: Similarly, there are two sources of uncertainty in the background estimate as a function of the average mass of the two VLQ candidates, $n_{\text{bkg}}(m_{\text{VLQ}})$ in Eq. (5). The first arises from the fit for $f(m_{\text{VLQ}})$, and it is determined from the uncertainties in the exponential fit parameters. The second is the uncertainty in the mass dependence of the normalization factor, the b -tag to b -veto ratio, which is assigned to be one-half of the absolute value of the difference between this ratio in the low- and high-mass ranges, as shown in Fig. 13 (left).

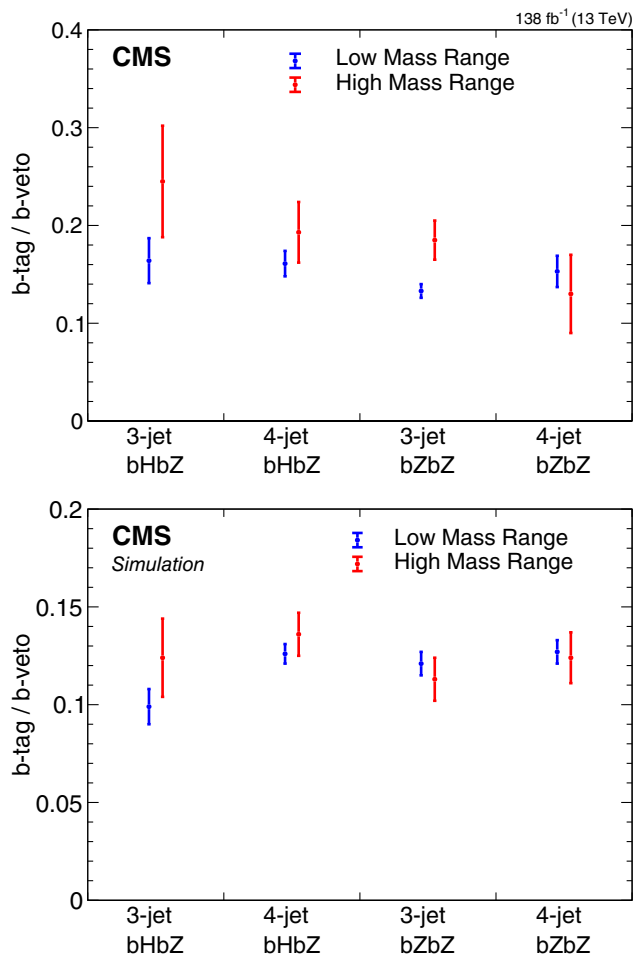


FIG. 13. Normalization factor in the low-mass region (450 to 900 GeV) and the high-mass region (800 to 2000 GeV) for events with $5 < \chi^2_{\text{mod}}/\text{ndf} < 20$ in data (upper) and simulated Drell-Yan events with $\chi^2_{\text{mod}}/\text{ndf} < 5$ (lower).

- (vii) PDFs: The uncertainty associated with the choice of PDF set is calculated by following the PDF4LHC procedure to generate a set of weights for each uncertainty in the NNPDF3.0 distribution [69]. The uncertainty in the signal acceptance is then determined from the standard deviation of the distribution of the signal acceptance for each weight.
- (viii) QCD scale: The systematic uncertainty on the QCD scale is estimated by independently multiplying the default values of the renormalization and factorization scales, μ_R and μ_F , by factors of 2.0 and 0.5, and assigning the systematic error to be half of the resulting range of cross sections. In this procedure, following the results from [70], the cases of varying one scale by 2.0 and the other by 0.5 are excluded since these correspond to unjustified values of $\log(\mu_R/\mu_F)$. The range over the remaining seven combinations is then used.
- (ix) Pileup: The uncertainty due to the number of pileup events in the simulated events is evaluated by

varying the pp inelastic cross section [48] by ± 1 standard deviation and determining the resulting change in the event selection efficiency.

- (x) Trigger prefiring: Because of detector effects, ECAL and muon triggers can appear in the bunch crossing preceding the actual collision. This effect is not accounted for in simulation, so corrections are applied to obtain the correct trigger efficiency. The uncertainties in these corrections are propagated to the event efficiency to obtain the resulting uncertainty.

Tables VI and VII summarize these uncertainties for the case of 40% $\mathcal{B}(B \rightarrow bH)$, 40% $\mathcal{B}(B \rightarrow bZ)$, and 20% $\mathcal{B}(B \rightarrow tW)$ branching fractions and a VLQ mass of 1400 GeV. For each uncertainty, it is noted whether it affects the signal efficiency or the background estimate and whether it affects the shape of the mass distribution or only the overall rate.

In general, the statistical uncertainty has the most significant impact on the results, in part because it also increases the systematic uncertainties related to the background fit functions. These uncertainties tend to be largest for the four-jet channels since these have the fewest events.

In addition, an uncertainty of 6% is assigned to account for uncertainties in the VLQ pair production cross section [45]. This uncertainty is separate from the others described above, and it is used only for the error band on the theory curve shown in the exclusion limit plots in Fig. 18.

IX. RESULTS

The data distributions in each channel are fit as a function of the reconstructed VLQ mass using COMBINE [71], including the relevant systematic uncertainties listed in Tables VI and VII as uncorrelated nuisance parameters. Figures 14–16 show, for the hadronic category, the comparison of the distribution of the reconstructed VLQ mass, after the final optimized selection requirements have been applied, for data, expected background, and simulated signal events with VLQ masses of 1000, 1200, 1400, 1600, and 1800 GeV. Figure 17 shows the same comparison for selected channels in the leptonic category. Branching fractions of $\mathcal{B}(B \rightarrow bH) = 50\%$ and $\mathcal{B}(B \rightarrow bZ) = 50\%$ are assumed. The data in Figs. 14–20 are available in tabular form in the HEPData record for this analysis [72].

No statistically significant excess of data over the background expectation is observed in this mass range. We set exclusion limits on the VLQ mass as a function of the branching fractions $\mathcal{B}(B \rightarrow bH)$, $\mathcal{B}(B \rightarrow bZ)$, and $\mathcal{B}(B \rightarrow tW)$. The results for the fully hadronic and leptonic categories, and for all jet multiplicities and event modes, are combined to set the limits. The signal extraction procedure is based on a binned maximum likelihood fit, where each systematic uncertainty is incorporated as a nuisance parameter into the fit, with the effect of the systematic uncertainty included as a log-normal probability distribution per bin.

TABLE VI. Table of systematic uncertainties for the fully hadronic channels for a simulated signal mass of 1400 GeV and branching fractions of $\mathcal{B}(B \rightarrow bH) = 40\%$, $\mathcal{B}(B \rightarrow bZ) = 40\%$, and $\mathcal{B}(B \rightarrow tW) = 20\%$. The only parameters in the fits that have significant uncertainties ($> 0.01\%$) are the scaling parameters (denoted by p_0).

Systematic	Signal/Background	Rate/Shape	Four jets	Five jets	Six jets
Jet trigger efficiency	Signal	Rate	0.6%	0.6%	0.6%
Luminosity	Signal	Rate	1.6%	1.6%	1.6%
PDFs	Signal	Rate	1.5%	1.5%	1.5%
QCD μ_R and μ_F scales	Signal	Rate	14.0%	14.0%	14.0%
<i>Fully hadronic bHbH event mode</i>					
Low-mass BJTF	Background	Rate	70.7%	18.9%	13.5%
Background fit p_0	Background	Shape	9.7%	9.6%	9.6%
BJTF fit form	Background	Rate	5.6%	21.4%	0.1%
BJTF fit p_0	Background	Shape	9.7%	9.6%	9.6%
Jet tag scale factors	Signal	Shape	4.6%	5.8%	7.1%
Jet energy resolution	Signal	Shape	0.3%	1.4%	2.0%
Jet energy scale	Signal	Shape	1.3%	2.1%	3.4%
Pileup	Signal	Shape	0.3%	0.3%	1.5%
<i>Fully hadronic bHbZ event mode</i>					
Low-mass BJTF	Background	Rate	17.2%	8.2%	14.6%
Background fit p_0	Background	Shape	9.7%	9.6%	9.4%
BJTF fit form	Background	Rate	0.7%	1.5%	1.3%
BJTF fit p_0	Background	Shape	9.7%	9.6%	9.4%
Jet tag scale factors	Signal	Shape	4.8%	5.7%	7.2%
Jet energy resolution	Signal	Shape	0.2%	1.0%	1.6%
Jet energy scale	Signal	Shape	1.2%	0.3%	1.4%
Pileup	Signal	Shape	0.1%	0.0%	1.1%
<i>Fully hadronic bZbZ event mode</i>					
Low-mass BJTF	Background	Rate	20.9%	3.8%	4.5%
Background fit p_0	Background	Shape	9.8%	9.8%	9.5%
BJTF fit form	Background	Rate	10.4%	0.0%	34.3%
BJTF fit p_0	Background	Shape	9.8%	9.8%	9.5%
Jet tag scale factors	Signal	Shape	5.0%	5.0%	4.9%
Jet energy resolution	Signal	Shape	0.3%	0.5%	1.0%
Jet energy scale	Signal	Shape	1.0%	2.8%	3.9%
Pileup	Signal	Shape	0.4%	0.1%	0.2%
<i>Fully hadronic bHtW event mode</i>					
Low-mass BJTF	Background	Rate	...	7.4%	3.2%
Background fit p_0	Background	Shape	...	9.4%	10.2%
BJTF fit form	Background	Rate	...	0.3%	0.6%
BJTF fit p_0	Background	Shape	...	9.4%	10.2%
Jet tag scale factors	Signal	Shape	...	4.1%	5.6%
Jet energy resolution	Signal	Shape	...	0.7%	0.4%
Jet energy scale	Signal	Shape	...	0.3%	1.5%
Pileup	Signal	Shape	...	0.1%	0.7%
<i>Fully hadronic bZtW event mode</i>					
Low-mass BJTF	Background	Rate	...	8.0%	1.6%
Background fit p_0	Background	Shape	...	9.7%	10.6%
BJTF fit form	Background	Rate	...	0.6%	1.9%
BJTF fit p_0	Background	Shape	...	9.7%	10.6%
Jet tag scale factors	Signal	Shape	...	3.6%	4.1%
Jet energy resolution	Signal	Shape	...	1.0%	0.4%
Jet energy scale	Signal	Shape	...	0.5%	1.4%
Pileup	Signal	Shape	...	0.0%	0.6%

TABLE VII. Table of systematic uncertainties for the dileptonic $bHbZ$ and $bZbZ$ channels for a simulated signal mass of 1400 GeV and branching fractions of $\mathcal{B}(B \rightarrow bH) = 40\%$, $\mathcal{B}(B \rightarrow bZ) = 40\%$, and $\mathcal{B}(B \rightarrow tW) = 20\%$.

Systematic	Signal/Background	Rate/Shape	3 jets	4 jets
$Z \rightarrow ee$ efficiency	Signal	Rate	0.8%	0.8%
$Z \rightarrow \mu\mu$ efficiency	Signal	Rate	0.6%	0.6%
Electron trigger efficiency	Signal	Rate	0.4%	0.4%
Muon trigger efficiency	Signal	Rate	0.1%	0.1%
Luminosity	Signal	Rate	1.6%	1.6%
PDFs	Signal	Rate	2.0%	2.0%
QCD μ_R and μ_F scales	Signal	Rate	15.1%	15.1%
<i>Dileptonic $bHbZ$ event mode</i>				
Background exponential fit	Background	Shape	24.4%	16.1%
Jet tag scale factors	Signal	Shape	6.9%	7.8%
Normalization factor mass dependence	Background	Rate	55.9%	7.1%
Normalization factor (b -tag/ b -veto)	Background	Rate	14.4%	8.2%
Jet energy resolution	Signal	Shape	0.4%	1.3%
Jet energy scale	Signal	Shape	0.5%	2.5%
Lepton scale factors	Signal	Shape	12.4%	11.4%
Pileup	Signal	Shape	0.5%	1.1%
Trigger prefireing	Signal	Shape	0.3%	0.3%
<i>Dileptonic $bZbZ$ event mode</i>				
Background exponential fit	Background	Shape	26.0%	20.1%
Jet tag scale factors	Signal	Shape	7.1%	8.0%
Normalization factor mass dependence	Background	Rate	4.6%	10.6%
Normalization factor (b -tag/ b -veto)	Background	Rate	14.6%	9.4%
Jet energy resolution	Signal	Shape	0.4%	0.8%
Jet energy scale	Signal	Shape	0.2%	0.6%
Lepton scale factors	Signal	Shape	11.7%	11.6%
Pileup	Signal	Shape	0.5%	0.4%
Trigger prefireing	Signal	Shape	0.3%	0.3%

The CL_s criterion [73,74] is used to obtain a limit at 95% CL using the profile likelihood test statistic in the asymptotic approximation [75].

The exclusion limit on the VLQ mass is derived from the intersection of the limit curve with the predicted theoretical cross section as a function of the VLQ mass. Figure 18 shows the observed and expected limits at 95% CL on the cross section of VLQ pair production as functions of VLQ mass, for four representative branching fraction hypotheses: $\mathcal{B}(B \rightarrow bH) = 100\%$; $\mathcal{B}(B \rightarrow bZ) = 100\%$; $\mathcal{B}(B \rightarrow bH) = \mathcal{B}(B \rightarrow bZ) = 50\%$, corresponding to the TB doublet model with no Tt mixing and also to the large VLQ mass XTB triplet model; and $\mathcal{B}(B \rightarrow bH) = \mathcal{B}(B \rightarrow bZ) = 25\%$, $\mathcal{B}(B \rightarrow tW) = 50\%$, corresponding to the large VLQ mass TBY triplet and B singlet models.

Figures 19 and 20 show the expected and observed exclusion limits, respectively, on VLQ mass as a function of $\mathcal{B}(B \rightarrow bH)$ and $\mathcal{B}(B \rightarrow tW)$, omitting points for which the exclusion limit is less than 1000 GeV. In the 100% $B \rightarrow bZ$ model, the limits on the B VLQ mass have been improved by 120 GeV compared to the previous best limits, set by ATLAS [24]; in the TB doublet model with no Tt mixing, the limits have been improved by 50 GeV compared to the previous best limits, set by CMS [22].

X. SUMMARY

A search for B VLQs has been presented, using data from proton-proton collisions collected by the CMS detector in 2016–2018 at $\sqrt{s} = 13$ TeV. Results are combined from the fully hadronic category, where each B VLQ decays into either a b quark and a Higgs boson (H), a b quark and a Z boson, or a t quark and a W boson; and the leptonic category, where each B VLQ decays into a b quark and either an H or a Z boson, and at least one decay includes a Z boson that decays into a pair of charged leptons. Since the dileptonic (e and μ) branching fraction of the Z boson is 6.7%, the rate of four-lepton events is an order of magnitude less than that of two-lepton events, which require only one dileptonic Z boson decay. Therefore, including the four-lepton signature would not provide a significant increase in sensitivity at the current integrated luminosity. To account for the fact that the two jets from an H , a Z , or a W boson decay may be reconstructed separately, or may be merged into a single reconstructed jet due to a high Lorentz boost, events are separated into different jet multiplicity categories and reconstructed appropriately. Backgrounds are estimated from data, and limits are set on the VLQ mass at

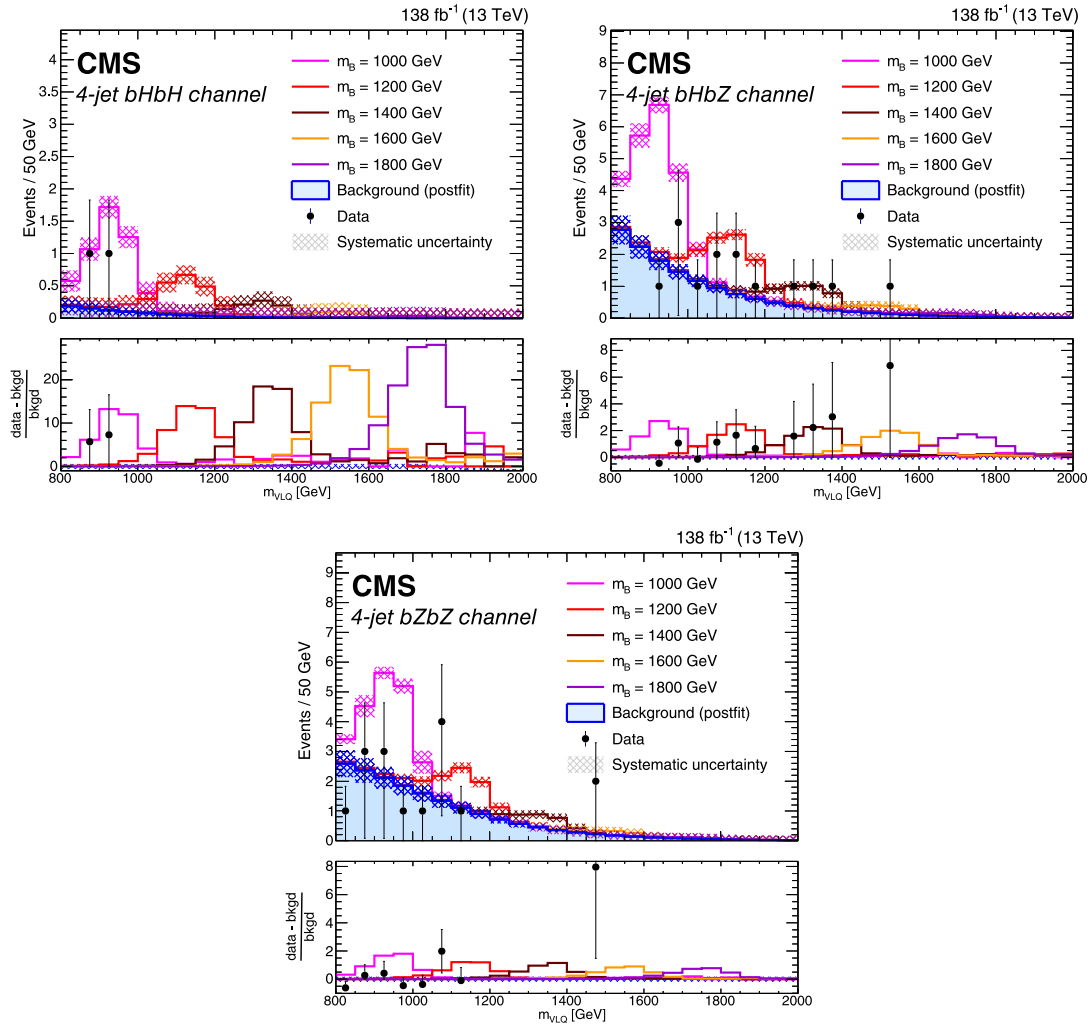


FIG. 14. Distributions of reconstructed VLQ mass for expected postfit background (blue histogram), signal plus background (colored lines), and observed data (black points) for events in the hadronic category. The channels shown are four-jet $bHbH$ (upper left), four-jet $bHbZ$ (upper right), four-jet $bZbZ$ (lower center). Five signal masses are shown: 1000 (magenta), 1200 (red), 1400 (maroon), 1600 (orange), and 1800 GeV (purple). The signal distributions are normalized to the number of events estimated from the expected VLQ production cross section. The assumed branching fractions are $\mathcal{B}(B \rightarrow bH) = \mathcal{B}(B \rightarrow bZ) = 50\%$, $\mathcal{B}(B \rightarrow tW) = 0\%$. The background distribution is independent of the signal branching fractions. The hatched regions indicate the total systematic uncertainties in the background estimate.

95% confidence level as a function of the branching fractions $\mathcal{B}(B \rightarrow bH)$, $\mathcal{B}(B \rightarrow bZ)$, and $\mathcal{B}(B \rightarrow tW)$. The most significant improvement over previous results is an increased sensitivity for scenarios with large $\mathcal{B}(B \rightarrow bZ)$ due to the inclusion of events with leptonic Z boson decays. The current results represent the most stringent limits on B VLQs to date.

ACKNOWLEDGMENTS

We congratulate our colleagues in the CERN accelerator departments for the excellent performance of the LHC and thank the technical and administrative staffs at CERN and at other CMS institutes for their contributions to the success of the CMS effort. In addition, we gratefully acknowledge

the computing centers and personnel of the Worldwide LHC Computing Grid and other centers for delivering so effectively the computing infrastructure essential to our analyses. Finally, we acknowledge the enduring support for the construction and operation of the LHC, the CMS detector, and the supporting computing infrastructure provided by the following funding agencies: SC (Armenia), BMBWF and FWF (Austria); FNRS and FWO (Belgium); CNPq, CAPES, FAPERJ, FAPERGS, and FAPESP (Brazil); MES and BNSF (Bulgaria); CERN; CAS, MoST, and NSFC (China); Minciencias (Colombia); MSES and CSF (Croatia); RIF (Cyprus); SENESCYT (Ecuador); ERC PRG, RVTT3 and MoER TK202 (Estonia); Academy of Finland, MEC, and HIP (Finland); CEA and CNRS/IN2P3 (France); SRNSF

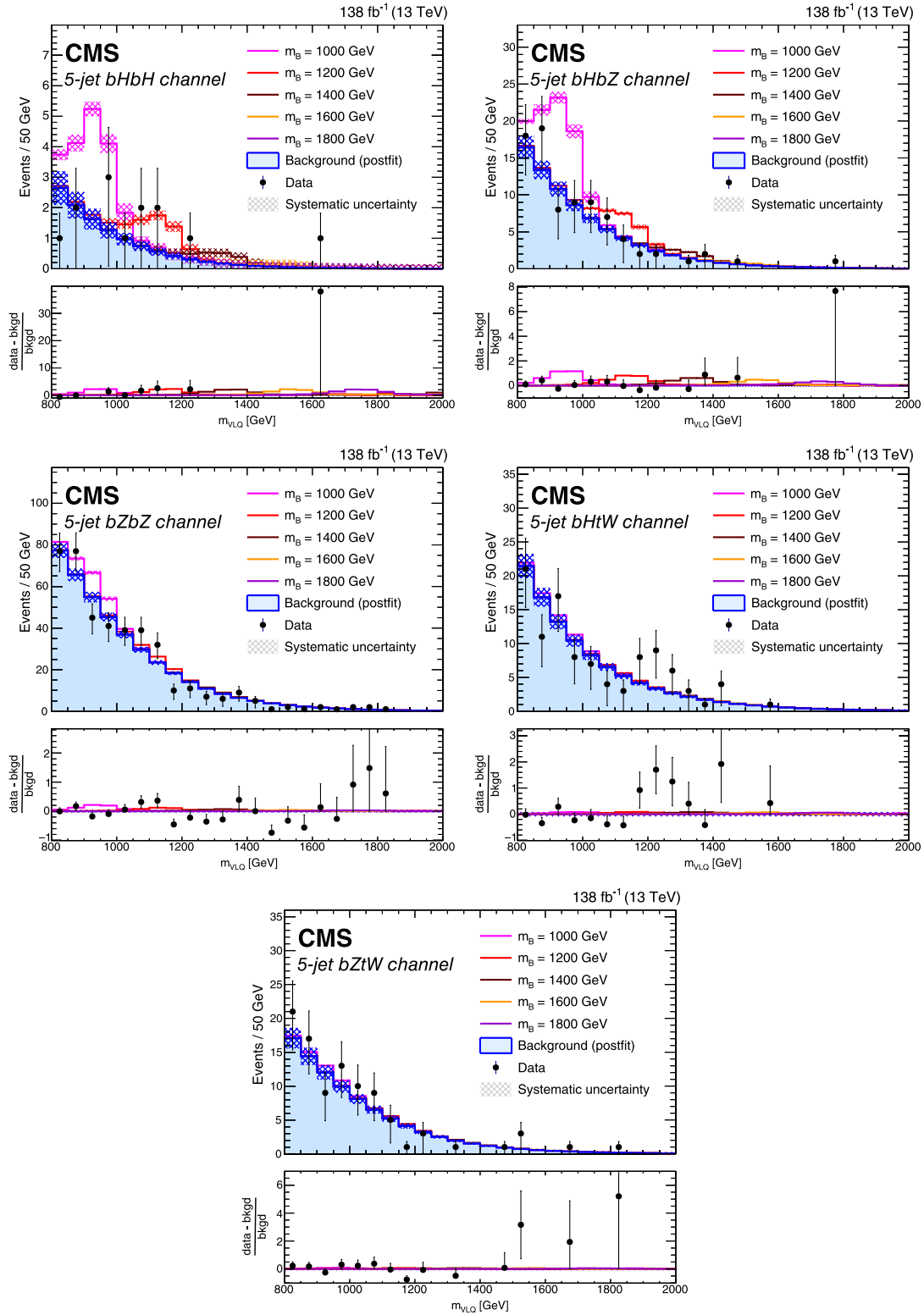


FIG. 15. Distributions of reconstructed VLQ mass for expected postfit background (blue histogram), signal plus background (colored lines), and observed data (black points) for events in the hadronic category. The channels shown are five-jet $bHbH$ (upper left), five-jet $bHbZ$ (upper right), five-jet $bZbZ$ (middle left), five-jet $bHtW$ (middle right), and five-jet $bZtW$ (lower center). Five signal masses are shown: 1000 (magenta), 1200 (red), 1400 (maroon), 1600 (orange), and 1800 GeV (purple). The signal distributions are normalized to the number of events estimated from the expected VLQ production cross section. The assumed branching fractions are $\mathcal{B}(B \rightarrow bH) = \mathcal{B}(B \rightarrow bZ) = 50\%$, $\mathcal{B}(B \rightarrow tW) = 0\%$. The background distribution is independent of the signal branching fractions. The hatched regions indicate the total systematic uncertainties in the background estimate.

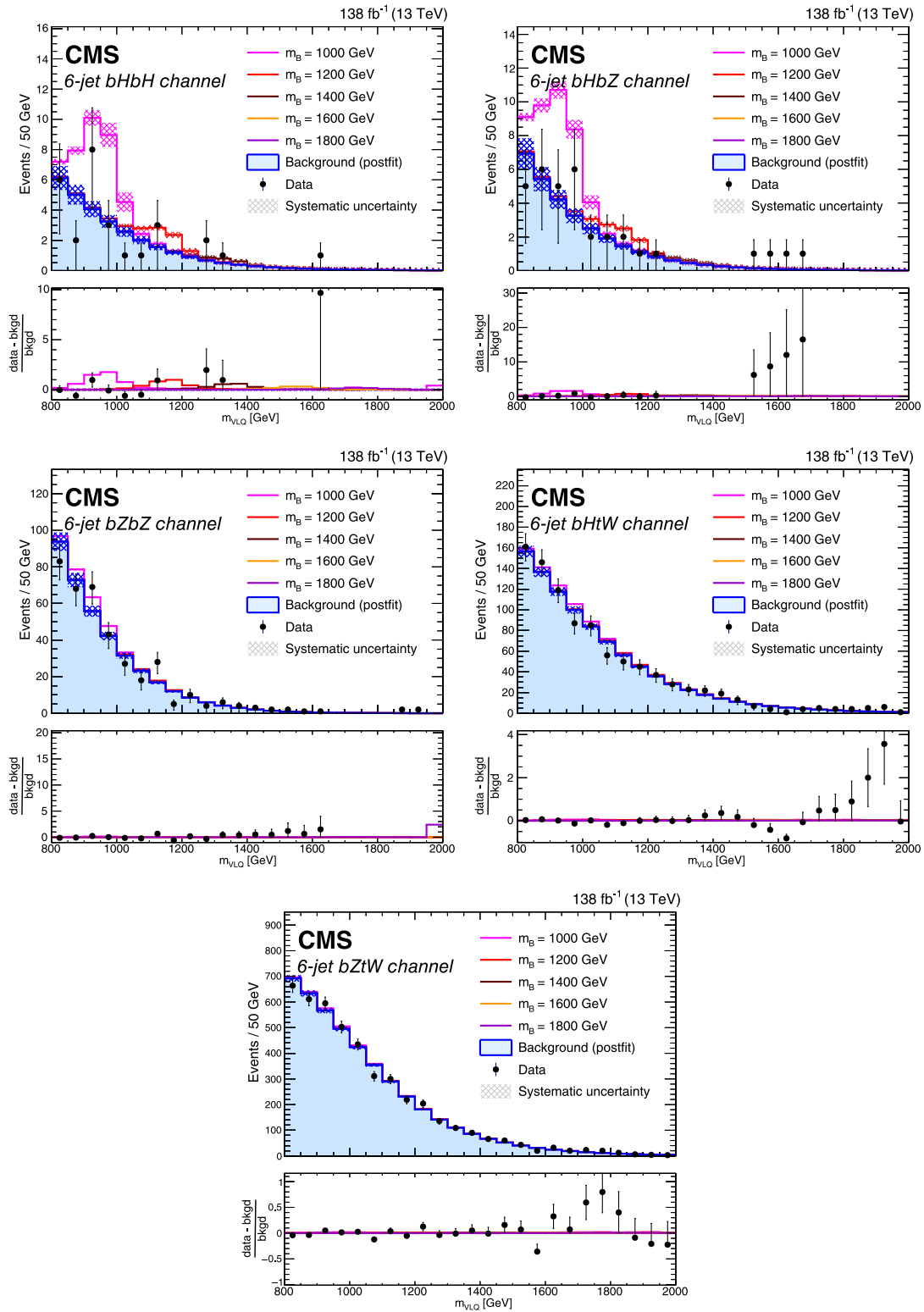


FIG. 16. Distributions of reconstructed VLQ mass for expected postfit background (blue histogram), signal plus background (colored lines), and observed data (black points) for events in the hadronic category. The channels shown are six-jet $bHbH$ (upper left), six-jet $bHbZ$ (upper right), six-jet $bZbZ$ (middle left), six-jet $bHtW$ (middle right), and six-jet $bZtW$ (lower center). Five signal masses are shown: 1000 (magenta), 1200 (red), 1400 (maroon), 1600 (orange), and 1800 GeV (purple). The signal distributions are normalized to the number of events estimated from the expected VLQ production cross section. The assumed branching fractions are $B(B \rightarrow bH) = B(B \rightarrow bZ) = 50\%$, $B(B \rightarrow tW) = 0\%$. The background distribution is independent of the signal branching fractions. The hatched regions indicate the total systematic uncertainties in the background estimate.

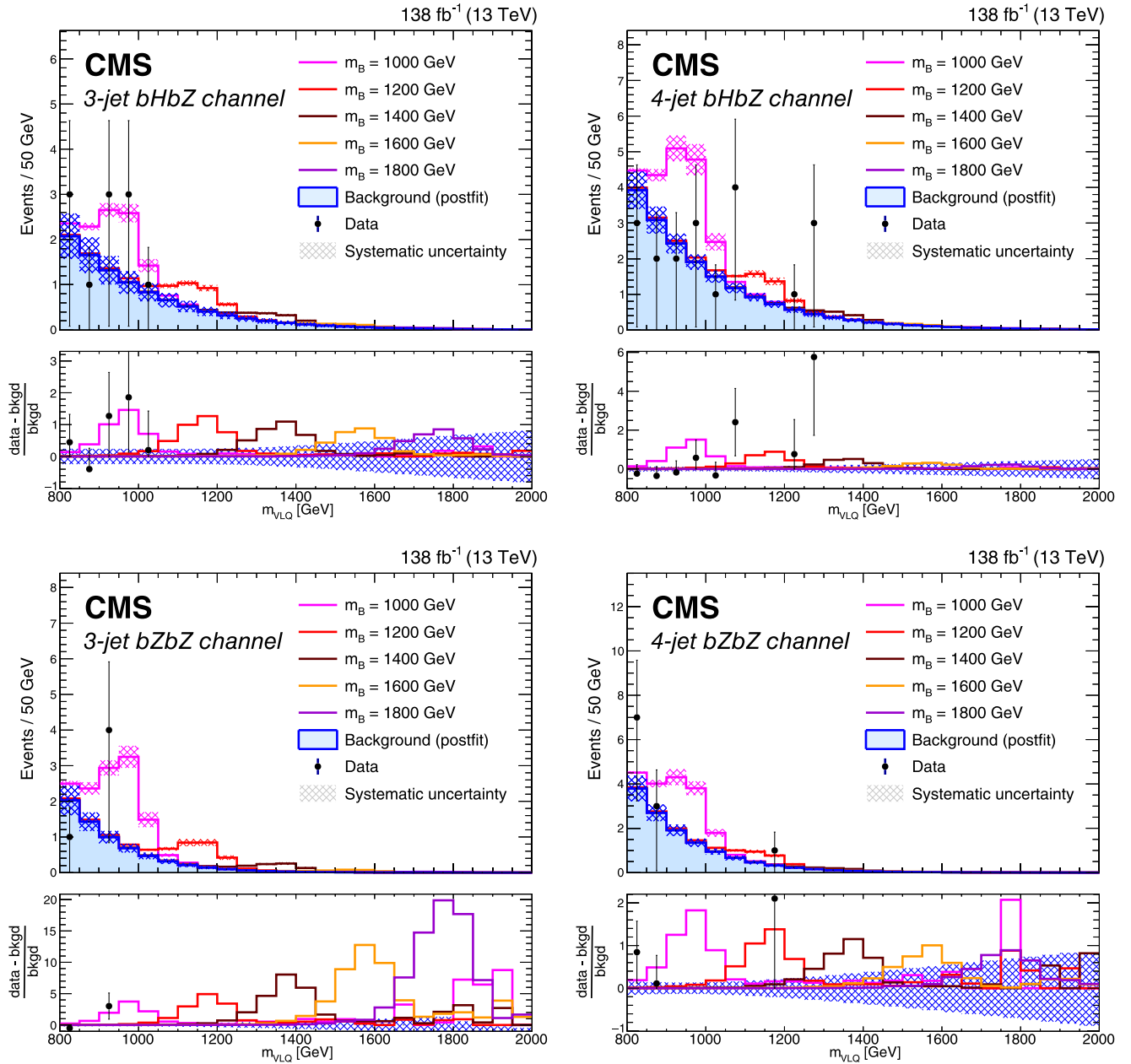


FIG. 17. Distributions of reconstructed VLQ mass for expected postfit background (blue histogram), signal plus background (colored lines), and observed data (black points) for events in the leptonic category. The channels shown are three-jet $bHbZ$ (upper left), four-jet $bHbZ$ (upper right), three-jet $bZbZ$ (lower left), and four-jet $bZbZ$ (lower right). Five signal masses are shown: 1000 (magenta), 1200 (red), 1400 (maroon), 1600 (orange), and 1800 GeV (purple). The signal distributions are normalized to the number of events estimated from the expected VLQ production cross section. The assumed branching fractions are $\mathcal{B}(B \rightarrow bH) = \mathcal{B}(B \rightarrow bZ) = 50\%$, $\mathcal{B}(B \rightarrow tW) = 0\%$. The background distribution is independent of the signal branching fractions. The hatched regions indicate the total systematic uncertainties in the background estimate.

(Georgia); BMBF, DFG, and HGF (Germany); GSRI (Greece); NKFIH (Hungary); DAE and DST (India); IPM (Iran); SFI (Ireland); INFN (Italy); MSIP and NRF (Republic of Korea); MES (Latvia); LMTLT (Lithuania); MOE and UM (Malaysia); BUAP, CINVESTAV, CONACYT, LNS, SEP, and UASLP-FAI (Mexico); MOS (Montenegro); MBIE (New Zealand); PAEC

(Pakistan); MES and NSC (Poland); FCT (Portugal); MESTD (Serbia); MCIN/AEI and PCTI (Spain); MOSTR (Sri Lanka); Swiss Funding Agencies (Switzerland); MST (Taipei); MHESI and NSTDA (Thailand); TUBITAK and TENMAK (Turkey); NASU (Ukraine); STFC (United Kingdom); DOE and NSF (USA). Individuals have received support from the

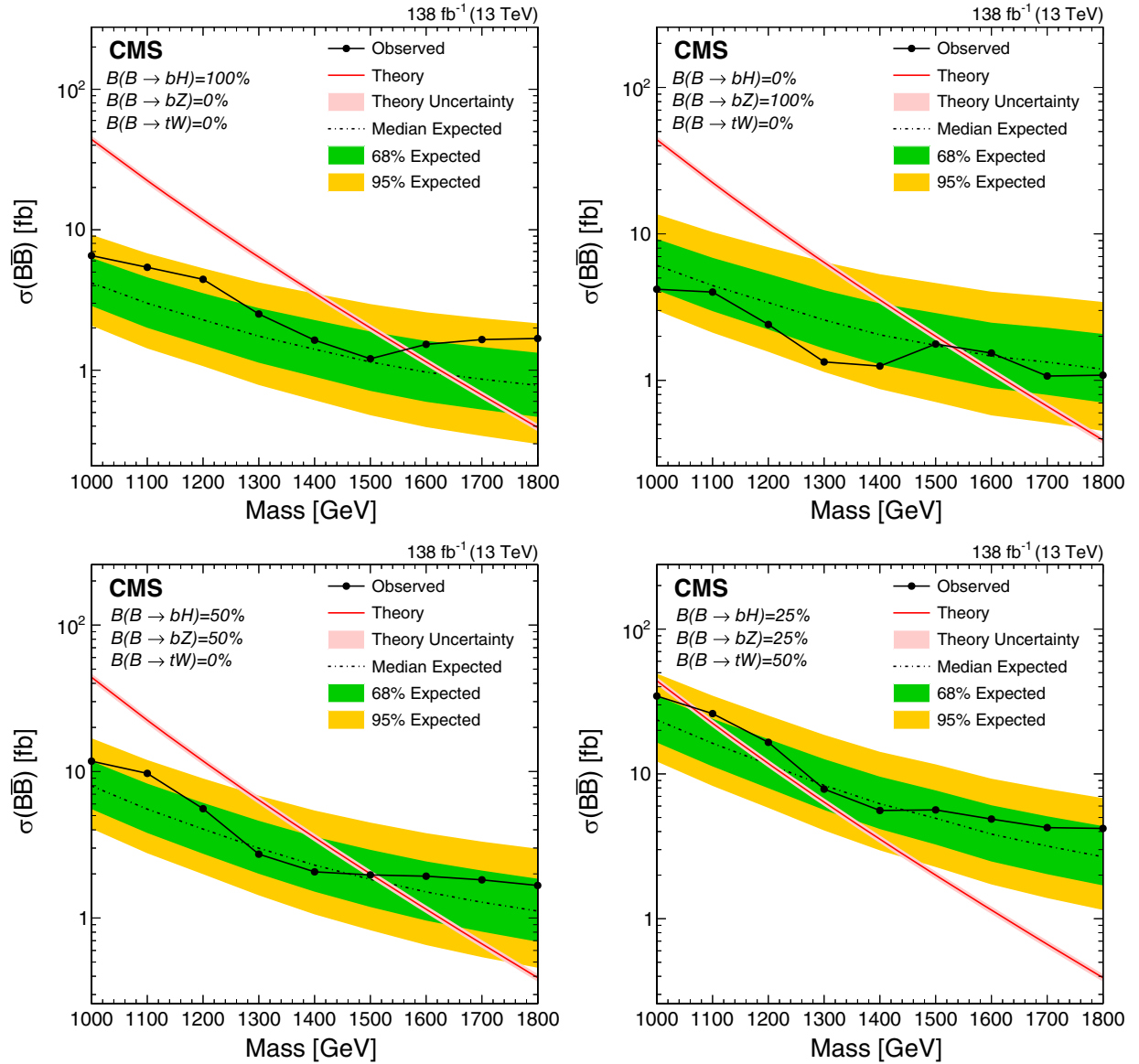


FIG. 18. Limit at 95% CL on the cross section for VLQ pair production for four different branching fraction hypotheses: $B(B \rightarrow bH) = 100\%$ (upper left), $B(B \rightarrow bZ) = 100\%$ (upper right), $B(B \rightarrow bH) = B(B \rightarrow bZ) = 50\%$, corresponding to the TB doublet model with no Tt mixing and also to the large VLQ mass XTB triplet model (lower left), and $B(B \rightarrow bH) = B(B \rightarrow bZ) = 25\%$, $B(B \rightarrow tW) = 50\%$, corresponding to the large VLQ mass TBY triplet model (lower right). The expected limit is shown as the dashed line, with the 68% and 95% uncertainties shown by the green (inner) and yellow (outer) bands, respectively. The theoretical cross section and its uncertainty are shown by the red line and light red band.

Marie-Curie programme and the European Research Council and Horizon 2020 Grant, Contracts No. 675440, No. 724704, No. 752730, No. 758316, No. 765710, No. 824093, No. 101115353, and COST Action CA16108 (European Union); the Leventis Foundation; the Alfred P. Sloan Foundation; the Alexander von Humboldt Foundation; the Science Committee, Project No. 22rl-037 (Armenia); the Belgian Federal Science Policy Office; the Fonds pour la Formation à la Recherche dans l'Industrie et dans l'Agriculture (FRIA-Belgium); the Agentschap voor Innovatie door Wetenschap

en Technologie (IWT-Belgium); the F.R.S.-FNRS and FWO (Belgium) under the “Excellence of Science—EOS”—be.h Project No. 30820817; the Beijing Municipal Science & Technology Commission, No. Z191100007219010 and Fundamental Research Funds for the Central Universities (China); the Ministry of Education, Youth and Sports (MEYS) of the Czech Republic; the Shota Rustaveli National Science Foundation, Grant No. FR-22-985 (Georgia); the Deutsche Forschungsgemeinschaft (DFG), under Germany’s Excellence Strategy—EXC 2121 “Quantum

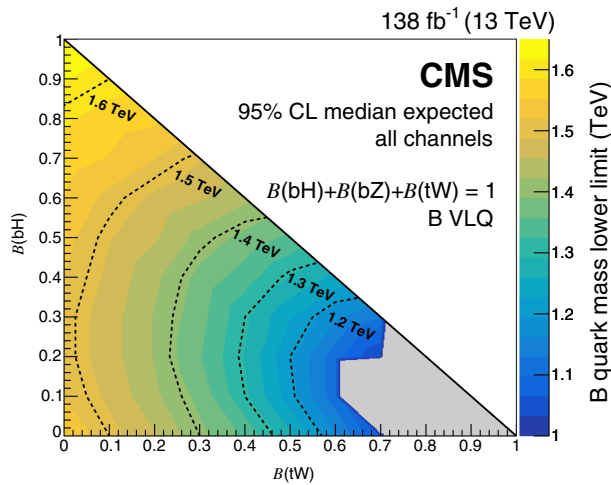


FIG. 19. Median expected exclusion limits on the VLQ mass at 95% CL as a function of the branching fractions $\mathcal{B}(B \rightarrow bH)$ and $\mathcal{B}(B \rightarrow tW)$, with $\mathcal{B}(B \rightarrow tW) = 1 - \mathcal{B}(B \rightarrow bH) - \mathcal{B}(B \rightarrow bZ)$. The gray area corresponds to the region where the exclusion limit is less than 1000 GeV.

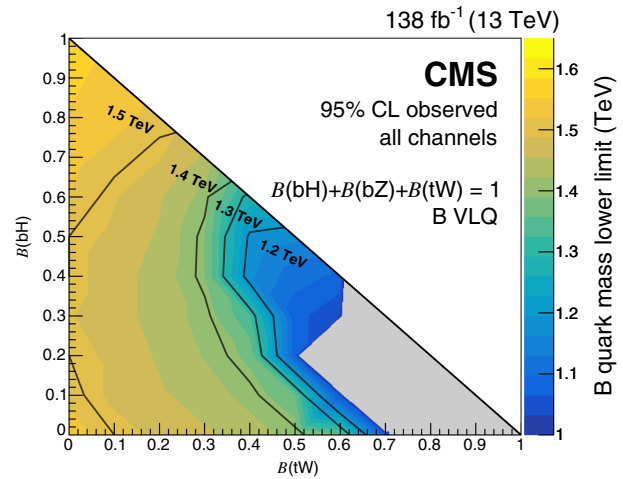


FIG. 20. Observed exclusion limits on the VLQ mass at 95% CL as a function of the branching fractions $\mathcal{B}(B \rightarrow bH)$ and $\mathcal{B}(B \rightarrow tW)$, with $\mathcal{B}(B \rightarrow tW) = 1 - \mathcal{B}(B \rightarrow bH) - \mathcal{B}(B \rightarrow bZ)$. The gray area corresponds to the region where the exclusion limit is less than 1000 GeV.

Universe”—390833306, and under Project No. 400140256—GRK2497; the Hellenic Foundation for Research and Innovation (HFRI), Project No. 2288 (Greece); the Hungarian Academy of Sciences, the New National Excellence Program—ÚNKP, the NKFIH Research Grants No. K 124845, No. K 124850, No. K 128713, No. K 128786, No. K 129058, No. K 131991, No. K 133046, No. K 138136, No. K 143460, No. K 143477, No. 2020-2.2.1-ED-2021-00181, and No. TKP2021-NKTA-64 (Hungary); the Council of Science and Industrial Research, India; ICSC—National Research Center for High Performance Computing, Big Data and Quantum Computing, funded by the EU NexGeneration program (Italy); the Latvian Council of Science; the Ministry of Education and Science, Project No. 2022/WK/14, and the National Science Center, Contracts No. Opus 2021/41/B/ST2/01369 and No. 2021/43/B/

ST2/01552 (Poland); the Fundação para a Ciência e a Tecnologia, Grant No. CEECIND/01334/2018 (Portugal); the National Priorities Research Program by Qatar National Research Fund; MCIN/AEI/10.13039/501100011033, ERDF “a way of making Europe,” and the Programa Estatal de Fomento de la Investigación Científica y Técnica de Excelencia María de Maeztu, Grant No. MDM-2017-0765 and Programa Severo Ochoa del Principado de Asturias (Spain); the Chulalongkorn Academic into Its 2nd Century Project Advancement Project, and the National Science, Research and Innovation Fund via the Program Management Unit for Human Resources & Institutional Development, Research and Innovation, Grant No. B37G660013 (Thailand); the Kavli Foundation; the Nvidia Corporation; the SuperMicro Corporation; the Welch Foundation, Contract No. C-1845; and the Weston Havens Foundation (USA).

- [1] G. 't Hooft, Naturalness, chiral symmetry, and spontaneous chiral symmetry breaking, *NATO Sci. Ser. B* **59**, 135 (1980).
- [2] ATLAS Collaboration, Observation of a new particle in the search for the standard model Higgs boson with the ATLAS detector at the LHC, *Phys. Lett. B* **716**, 1 (2012).
- [3] CMS Collaboration, Observation of a new boson at a mass of 125 GeV with the CMS experiment at the LHC, *Phys. Lett. B* **716**, 30 (2012).
- [4] CMS Collaboration, Observation of a new boson with mass near 125 GeV in pp collisions at $\sqrt{s} = 7$ and 8 TeV, *J. High Energy Phys.* **06** (2013) 081.

- [5] CMS Collaboration, A measurement of the Higgs boson mass in the diphoton decay channel, *Phys. Lett. B* **805**, 135425 (2020).
- [6] H. Georgi and A. Pais, Calculability and naturalness in gauge theories, *Phys. Rev. D* **10**, 539 (1974).
- [7] J. Wess and B. Zumino, A Lagrangian model invariant under supergauge transformations, *Phys. Lett.* **49B**, 52 (1974).
- [8] P. Fayet and S. Ferrara, Supersymmetry, *Phys. Rep.* **32**, 249 (1977).
- [9] D. B. Kaplan, H. Georgi, and S. Dimopoulos, Composite Higgs scalars, *Phys. Lett. B* **136**, 187 (1984).

- [10] K. Agashe, R. Contino, and A. Pomarol, The minimal composite Higgs model, *Nucl. Phys.* **B719**, 165 (2005).
- [11] N. Arkani-Hamed, A. G. Cohen, and H. Georgi, Electroweak symmetry breaking from dimensional deconstruction, *Phys. Lett. B* **513**, 232 (2001).
- [12] N. Arkani-Hamed, A. G. Cohen, E. Katz, and A. E. Nelson, The lightest Higgs, *J. High Energy Phys.* **07** (2002) 034.
- [13] M. Schmaltz, Physics beyond the standard model (theory): Introducing the little Higgs, *Nucl. Phys. B, Proc. Suppl.* **117**, 40 (2003).
- [14] F. del Aguila and M. J. Bowick, The possibility of new fermions with $\Delta I = 0$ mass, *Nucl. Phys.* **B224**, 107 (1983).
- [15] ATLAS Collaboration, Combined measurements of Higgs boson production and decay using up to 80 fb^{-1} of proton-proton collision data at $\sqrt{s} = 13 \text{ TeV}$ collected with the ATLAS experiment, *Phys. Rev. D* **101**, 012002 (2020).
- [16] CMS Collaboration, Measurement and interpretation of differential cross sections for Higgs boson production at $\sqrt{s} = 13 \text{ TeV}$, *Phys. Lett. B* **792**, 369 (2019).
- [17] J. A. Aguilar-Saavedra, R. Benbrik, S. Heinemeyer, and M. Pérez-Victoria, Handbook of vectorlike quarks: Mixing and single production, *Phys. Rev. D* **88**, 094010 (2013).
- [18] A. Atre, M. Carena, T. Han, and J. Santiago, Heavy quarks above the top at the Tevatron, *Phys. Rev. D* **79**, 054018 (2009).
- [19] A. Atre, G. Azuelos, M. Carena, T. Han, E. Ozcan, J. Santiago, and G. Unel, Model-independent searches for new quarks at the LHC, *J. High Energy Phys.* **08** (2011) 080.
- [20] F. del Aguila, M. Pérez-Victoria, and J. Santiago, Observable contributions of new exotic quarks to quark mixing, *J. High Energy Phys.* **09** (2000) 011.
- [21] J. A. Aguilar-Saavedra, Mixing with vector-like quarks: Constraints and expectations, *EPJ Web Conf.* **60**, 16012 (2013).
- [22] CMS Collaboration, A search for bottom-type, vector-like quark pair production in a fully hadronic final state in proton-proton collisions at $\sqrt{s} = 13 \text{ TeV}$, *Phys. Rev. D* **102**, 112004 (2020).
- [23] ATLAS Collaboration, Combination of the searches for pair-produced vector-like partners of the third-generation quarks at $\sqrt{s} = 13 \text{ TeV}$ with the ATLAS detector, *Phys. Rev. Lett.* **121**, 211801 (2018).
- [24] ATLAS Collaboration, Search for pair-production of vectorlike quarks in pp collision events at $\sqrt{s} = 13 \text{ TeV}$ with at least one leptonically decaying Z boson and a third-generation quark with the ATLAS detector, *Phys. Lett. B* **843**, 138019 (2023).
- [25] CMS Collaboration, Precision luminosity measurement in proton-proton collisions at $\sqrt{s} = 13 \text{ TeV}$ in 2015 and 2016 at CMS, *Eur. Phys. J. C* **81**, 800 (2021).
- [26] CMS Collaboration, CMS luminosity measurement for the 2017 data-taking period at $\sqrt{s} = 13 \text{ TeV}$, CMS Physics Analysis Summary Report No. CMS-PAS-LUM-17-004, 2018, <https://cds.cern.ch/record/2621960>.
- [27] CMS Collaboration, CMS luminosity measurement for the 2018 data-taking period at $\sqrt{s} = 13 \text{ TeV}$, CMS Physics Analysis Summary Report No. CMS-PAS-LUM-18-002, 2019, <https://cds.cern.ch/record/2676164>.
- [28] CMS Collaboration, Electron and photon reconstruction and identification with the CMS experiment at the CERN LHC, *J. Instrum.* **16**, P05014 (2021).
- [29] CMS Collaboration, ECAL 2016 refined calibration and Run2 summary plots, CMS Detector Performance Summary Report No. CMS-DP-2020-021, 2020, <https://cds.cern.ch/record/2717925>.
- [30] CMS Collaboration, Performance of the CMS muon detector and muon reconstruction with proton-proton collisions at $\sqrt{s} = 13 \text{ TeV}$, *J. Instrum.* **13**, P06015 (2018).
- [31] CMS Collaboration, Performance of the CMS Level-1 trigger in proton-proton collisions at $\sqrt{s} = 13 \text{ TeV}$, *J. Instrum.* **15**, P10017 (2020).
- [32] CMS Collaboration, The CMS trigger system, *J. Instrum.* **12**, P01020 (2017).
- [33] CMS Collaboration, The CMS experiment at the CERN LHC, *J. Instrum.* **3**, S08004 (2008).
- [34] J. Alwall, R. Frederix, S. Frixione, V. Hirschi, F. Maltoni, O. Mattelaer, H. S. Shao, T. Stelzer, P. Torrielli, and M. Zaro, The automated computation of tree-level and next-to-leading order differential cross sections, and their matching to parton shower simulations, *J. High Energy Phys.* **07** (2014) 079.
- [35] R. D. Ball *et al.* (NNPDF Collaboration), Parton distributions for the LHC Run II, *J. High Energy Phys.* **04** (2015) 040.
- [36] R. D. Ball *et al.* (NNPDF Collaboration), Parton distributions from high-precision collider data, *Eur. Phys. J. C* **77**, 663 (2017).
- [37] T. Sjöstrand, S. Ask, J. R. Christiansen, R. Corke, N. Desai, P. Ilten, S. Mrenna, S. Prestel, C. O. Rasmussen, and P. Z. Skands, An introduction to PYTHIA 8.2, *Comput. Phys. Commun.* **191**, 159 (2015).
- [38] CMS Collaboration, Event generator tunes obtained from underlying event and multiparton scattering measurements, *Eur. Phys. J. C* **76**, 155 (2016).
- [39] CMS Collaboration, Extraction and validation of a new set of CMS PYTHIA8 tunes from underlying-event measurements, *Eur. Phys. J. C* **80**, 4 (2020).
- [40] M. Czakon, P. Fiedler, and A. Mitov, Total top-quark pair-production cross section at hadron colliders through $O(\alpha_s^4)$, *Phys. Rev. Lett.* **110**, 252004 (2013).
- [41] M. Czakon and A. Mitov, Top++: A program for the calculation of the top-pair cross-section at hadron colliders, *Comput. Phys. Commun.* **185**, 2930 (2014).
- [42] M. Cacciari, M. Czakon, M. Mangano, A. Mitov, and P. Nason, Top-pair production at hadron colliders with next-to-next-to-leading logarithmic soft-gluon resummation, *Phys. Lett. B* **710**, 612 (2012).
- [43] M. R. Whalley, D. Bourilkov, and R. C. Group, The Les Houches accord PDFs (LHAPDF) and LHAGLUE, in *HERA and the LHC: A Workshop on the Implications of HERA for LHC Physics. Proceedings, Part B* (2005), p. 575, [arXiv:hep-ph/0508110](https://arxiv.org/abs/hep-ph/0508110).
- [44] D. Bourilkov, R. C. Group, and M. R. Whalley, LHAPDF: PDF use from the Tevatron to the LHC, in *TeV4LHC Workshop—4th Meeting Batavia, Illinois, 2005* (2006), [arXiv:hep-ph/0605240](https://arxiv.org/abs/hep-ph/0605240).

- [45] CMS Collaboration, Search for vector-like T and B quark pairs in final states with leptons at $\sqrt{s} = 13$ TeV, *J. High Energy Phys.* **08** (2018) 177.
- [46] R. Frederix and S. Frixione, Merging meets matching in MC@NLO, *J. High Energy Phys.* **12** (2012) 061.
- [47] J. Alwall *et al.*, Comparative study of various algorithms for the merging of parton showers and matrix elements in hadronic collisions, *Eur. Phys. J. C* **53**, 473 (2008).
- [48] CMS Collaboration, Measurement of the inelastic proton-proton cross section at $\sqrt{s} = 13$ TeV, *J. High Energy Phys.* **07** (2018) 161.
- [49] S. Agostinelli *et al.* (GEANT4 Collaboration), GEANT4—a simulation toolkit, *Nucl. Instrum. Methods Phys. Res., Sect. A* **506**, 250 (2003).
- [50] J. Allison *et al.*, Geant4 developments and applications, *IEEE Trans. Nucl. Sci.* **53**, 270 (2006).
- [51] CMS Collaboration, Jet energy scale and resolution in the CMS experiment in pp collisions at 8 TeV, *J. Instrum.* **12**, P02014 (2017).
- [52] CMS Collaboration, Performance of the DeepJet b tagging algorithm using 41.9/fb of data from proton-proton collisions at 13 TeV with Phase I CMS detector, CMS Detector Performance Summary Report No. CMS-DP-2018-058, 2018, <http://cds.cern.ch/record/2646773>.
- [53] CMS Collaboration, Identification of heavy-flavour jets with the CMS detector in pp collisions at 13 TeV, *J. Instrum.* **13**, P05011 (2018).
- [54] CMS Collaboration, Particle-flow reconstruction and global event description with the CMS detector, *J. Instrum.* **12**, P10003 (2017).
- [55] CMS Collaboration, Technical proposal for the Phase-II upgrade of the Compact Muon Solenoid, CMS Technical Proposal Reports No. CERN-LHCC-2015-010, No. CMS-TDR-15-02, 2015, <http://cds.cern.ch/record/2020886>.
- [56] M. Cacciari, G. P. Salam, and G. Soyez, The anti- k_T jet clustering algorithm, *J. High Energy Phys.* **04** (2008) 063.
- [57] M. Cacciari, G. P. Salam, and G. Soyez, FastJet user manual, *Eur. Phys. J. C* **72**, 1896 (2012).
- [58] CMS Collaboration, Pileup mitigation at CMS in 13 TeV data, *J. Instrum.* **15**, P09018 (2020).
- [59] D. Bertolini, P. Harris, M. Low, and N. Tran, Pileup per particle identification, *J. High Energy Phys.* **10** (2014) 059.
- [60] Y. L. Dokshitzer, G. D. Leder, S. Moretti, and B. R. Webber, Better jet clustering algorithms, *J. High Energy Phys.* **08** (1997) 001.
- [61] M. Wobisch and T. Wengler, Hadronization corrections to jet cross-sections in deep inelastic scattering, in *Proceedings of the Workshop on Monte Carlo Generators for HERA Physics, Hamburg, Germany* (1998), p. 270, [arXiv:hep-ph/9907280](https://arxiv.org/abs/hep-ph/9907280).
- [62] M. Dasgupta, A. Fregoso, S. Marzani, and G. P. Salam, Towards an understanding of jet substructure, *J. High Energy Phys.* **09** (2013) 029.
- [63] J. M. Butterworth, A. R. Davison, M. Rubin, and G. P. Salam, Jet substructure as a new Higgs search channel at the LHC, *Phys. Rev. Lett.* **100**, 242001 (2008).
- [64] A. J. Larkoski, S. Marzani, G. Soyez, and J. Thaler, Soft drop, *J. High Energy Phys.* **05** (2014) 146.
- [65] E. Bols, J. Kieseler, M. Verzetti, M. Stoye, and A. Stakia, Jet flavour classification using DeepJet, *J. Instrum.* **15**, P12012 (2020).
- [66] CMS Collaboration, Performance of the CMS muon trigger system in proton-proton collisions at $\sqrt{s} = 13$ TeV, *J. Instrum.* **16**, P07001 (2021).
- [67] CMS Collaboration, Search for pair production of vectorlike quarks in the fully hadronic final state, *Phys. Rev. D* **100**, 072001 (2019).
- [68] ATLAS Collaboration, Search for pair production of heavy vector-like quarks decaying into hadronic final states in pp collisions at $\sqrt{s} = 13$ TeV with the ATLAS detector, *Phys. Rev. D* **98**, 092005 (2018).
- [69] J. Butterworth *et al.*, PDF4LHC recommendations for LHC Run II, *J. Phys. G* **43**, 023001 (2016).
- [70] S. Catani, D. de Florian, M. Grazzini, and P. Nason, Soft gluon resummation for Higgs boson production at hadron colliders, *J. High Energy Phys.* **07** (2003) 028.
- [71] CMS Collaboration, The CMS statistical analysis and combination tool: COMBINE, [arXiv:2404.06614](https://arxiv.org/abs/2404.06614) [Comput. Software Big Sci. (to be published)].
- [72] HEPData record for this analysis, [10.17182/hepdata.145997](https://doi.org/10.17182/hepdata.145997) (2023).
- [73] T. Junk, Confidence level computation for combining searches with small statistics, *Nucl. Instrum. Methods Phys. Res., Sect. A* **434**, 435 (1999).
- [74] A. L. Read, Presentation of search results: The CL_s technique, *J. Phys. G* **28**, 2693 (2002).
- [75] G. Cowan, K. Cranmer, E. Gross, and O. Vitells, Asymptotic formulae for likelihood-based tests of new physics, *Eur. Phys. J. C* **71**, 1554 (2011); **73**, 2501(E) (2013).

A. Hayrapetyan,¹ A. Tumasyan^{1,b} W. Adam² J. W. Andrejkovic,² T. Bergauer² S. Chatterjee² K. Damanakis² M. Dragicevic² P. S. Hussain² M. Jeitler^{2,c} N. Krammer² A. Li² D. Liko² I. Mikulec² J. Schieck^{2,c} R. Schöfbeck² D. Schwarz² M. Sonawane² S. Templ² W. Waltenberger² C.-E. Wulz^{2,c} M. R. Darwish^{4,d} T. Janssen⁴ P. Van Mechelen⁴ E. S. Bols⁵ J. D’Hondt⁵ S. Dansana⁵ A. De Moor⁵ M. Delcourt⁵ H. El Faham⁵ S. Lowette⁵ I. Makarenko⁵ D. Müller⁵ A. R. Sahasransu⁵ S. Tavernier⁵ M. Tytgat^{5,e} G. P. Van Onsem⁵ S. Van Putte⁵ D. Vannerom⁵ B. Clerbaux⁶ A. K. Das,⁶ G. De Lentdecker⁶ L. Favart⁶ D. Hohov⁶ J. Jaramillo⁶ A. Khalilzadeh,⁶ K. Lee⁶ M. Mahdavihorrani⁶ A. Malara⁶ S. Paredes⁶ L. Pétre⁶ N. Postiau,⁶ L. Thomas⁶ M. Vanden Bemden⁶ C. Vander Velde⁶ P. Vanlaer⁶ M. De Coen⁷ D. Dobur⁷ Y. Hong⁷ J. Knolle⁷ L. Lambrecht⁷ G. Mestdach,⁷ K. Mota Amarilo⁷ C. Rendón,⁷ A. Samalan,⁷ K. Skovpen⁷

N. Van Den Bossche⁷, J. van der Linden⁷, L. Wezenbeek⁷, A. Benecke⁸, A. Bethani⁸, G. Bruno⁸, C. Caputo⁸, C. Delaere⁸, I. S. Donertas⁸, A. Giammanco⁸, K. Jaffel⁸, Sa. Jain⁸, V. Lemaître⁸, J. Lidrych⁸, P. Mastrapasqua⁸, K. Mondal⁸, T. T. Tran⁸, S. Wertz⁸, G. A. Alves⁹, E. Coelho⁹, C. Hensel⁹, T. Menezes De Oliveira⁹, A. Moraes⁹, P. Rebello Teles⁹, M. Soeiro⁹, W. L. Aldá Júnior¹⁰, M. Alves Gallo Pereira¹⁰, M. Barroso Ferreira Filho¹⁰, H. Brandao Malbouisson¹⁰, W. Carvalho¹⁰, J. Chinellato^{10,f}, E. M. Da Costa¹⁰, G. G. Da Silveira^{10,g}, D. De Jesus Damiao¹⁰, S. Fonseca De Souza¹⁰, R. Gomes De Souza¹⁰, J. Martins^{10,h}, C. Mora Herrera¹⁰, L. Mundim¹⁰, H. Nogima¹⁰, A. Santoro¹⁰, A. Sznajder¹⁰, M. Thiel¹⁰, A. Vilela Pereira¹⁰, C. A. Bernardes^{11,g}, L. Calligaris¹¹, T. R. Fernandez Perez Tomei¹¹, E. M. Gregores¹¹, P. G. Mercadante¹¹, S. F. Novaes¹¹, B. Orzari¹¹, Sandra S. Padula¹¹, A. Aleksandrov¹², G. Antchev¹², R. Hadjiiska¹², P. Iaydjiev¹², M. Misheva¹², M. Shopova¹², G. Sultanov¹², A. Dimitrov¹³, L. Litov¹³, B. Pavlov¹³, P. Petkov¹³, A. Petrov¹³, E. Shumka¹³, S. Keshri¹⁴, S. Thakur¹⁴, T. Cheng¹⁵, Q. Guo¹⁵, T. Javaid¹⁵, L. Yuan¹⁵, Z. Hu¹⁶, J. Liu¹⁶, K. Yi^{16,i,j}, G. M. Chen^{17,k}, H. S. Chen^{17,k}, M. Chen^{17,k}, F. Lemmi¹⁷, C. H. Jiang¹⁷, A. Kapoor^{17,l}, H. Liao¹⁷, Z.-A. Liu^{17,m}, R. Sharma^{17,n}, J. N. Song^{17,m}, J. Tao¹⁷, C. Wang^{17,k}, J. Wang¹⁷, Z. Wang^{17,k}, H. Zhang¹⁷, A. Agapitos¹⁸, Y. Ban¹⁸, A. Levin¹⁸, C. Li¹⁸, Q. Li¹⁸, Y. Mao¹⁸, S. J. Qian¹⁸, X. Sun¹⁸, D. Wang¹⁸, H. Yang¹⁸, L. Zhang¹⁸, C. Zhou¹⁸, Z. You¹⁹, N. Lu²⁰, G. Bauer^{21,o}, X. Gao^{22,p}, D. Leggat²², H. Okawa²², Z. Lin²³, C. Lu²³, M. Xiao²³, C. Avila²⁴, D. A. Barbosa Trujillo²⁴, A. Cabrera²⁴, C. Florez²⁴, J. Fraga²⁴, J. A. Reyes Vega²⁴, J. Mejia Guisao²⁵, F. Ramirez²⁵, M. Rodriguez²⁵, J. D. Ruiz Alvarez²⁵, D. Giljanovic²⁶, N. Godinovic²⁶, D. Lelas²⁶, A. Sculac²⁶, M. Kovac²⁷, T. Sculac^{27,q}, P. Bargassa²⁸, V. Brigljevic²⁸, B. K. Chitroda²⁸, D. Ferencek²⁸, S. Mishra²⁸, A. Starodumov^{28,r}, T. Susa²⁸, A. Attikis²⁹, K. Christoforou²⁹, S. Konstantinou²⁹, J. Mousa²⁹, C. Nicolaou²⁹, F. Ptochos²⁹, P. A. Razis²⁹, H. Rykaczewski²⁹, H. Saka²⁹, A. Stepennov²⁹, M. Finger³⁰, M. Finger Jr.³⁰, A. Kveton³⁰, E. Ayala³¹, E. Carrera Jarrin³², Y. Assran^{33,s,t}, S. Elgammal^{33,t}, M. A. Mahmoud³⁴, Y. Mohammed³⁴, K. Ehataht³⁵, M. Kadastik³⁵, T. Lange³⁵, S. Nandan³⁵, C. Nielsen³⁵, J. Pata³⁵, M. Raidal³⁵, L. Tani³⁵, C. Veelken³⁵, H. Kirschenmann³⁶, K. Osterberg³⁶, M. Voutilainen³⁶, S. Bharthuar³⁷, E. Brücken³⁷, F. Garcia³⁷, K. T. S. Kallonen³⁷, R. Kinnunen³⁷, T. Lampén³⁷, K. Lassila-Perini³⁷, S. Lehti³⁷, T. Lindén³⁷, L. Martikainen³⁷, M. Myllymäki³⁷, M. m. Rantanen³⁷, H. Siikonen³⁷, E. Tuominen³⁷, J. Tuominiemi³⁷, P. Luukka³⁸, H. Petrow³⁸, M. Besancon³⁹, F. Couderc³⁹, M. Dejardin³⁹, D. Denegri³⁹, J. L. Faure³⁹, F. Ferri³⁹, S. Ganjour³⁹, P. Gras³⁹, G. Hamel de Monchenault³⁹, V. Lohezic³⁹, J. Malcles³⁹, J. Rander³⁹, A. Rosowsky³⁹, M. Ö. Sahin³⁹, A. Savoy-Navarro^{39,u}, P. Simkina³⁹, M. Titov³⁹, M. Tornago³⁹, C. Baldenegro Barrera⁴⁰, F. Beaudette⁴⁰, A. Buchot Perraguin⁴⁰, P. Busson⁴⁰, A. Cappati⁴⁰, C. Charlot⁴⁰, F. Damas⁴⁰, O. Davignon⁴⁰, A. De Wit⁴⁰, B. A. Fontana Santos Alves⁴⁰, S. Ghosh⁴⁰, A. Gilbert⁴⁰, R. Granier de Cassagnac⁴⁰, A. Hakimi⁴⁰, B. Harikrishnan⁴⁰, L. Kalipoliti⁴⁰, G. Liu⁴⁰, J. Motta⁴⁰, M. Nguyen⁴⁰, C. Ochando⁴⁰, L. Portales⁴⁰, R. Salerno⁴⁰, J. B. Sauvan⁴⁰, Y. Sirois⁴⁰, A. Tarabini⁴⁰, E. Vernazza⁴⁰, A. Zabi⁴⁰, A. Zghiche⁴⁰, J.-L. Agram^{41,v}, J. Andrea⁴¹, D. Appar⁴¹, D. Bloch⁴¹, J.-M. Brom⁴¹, E. C. Chabert⁴¹, C. Collard⁴¹, S. Falke⁴¹, U. Goerlach⁴¹, C. Grimault⁴¹, R. Haeberle⁴¹, A.-C. Le Bihan⁴¹, M. Meena⁴¹, G. Saha⁴¹, M. A. Sessini⁴¹, P. Van Hove⁴¹, S. Beauceron⁴², B. Blancon⁴², G. Boudoul⁴², N. Chanon⁴², J. Choi⁴², D. Contardo⁴², P. Depasse⁴², C. Dozen^{42,w}, H. El Mamouni⁴², J. Fay⁴², S. Gascon⁴², M. Gouzevitch⁴², C. Greenberg⁴², G. Grenier⁴², B. Ille⁴², I. B. Laktineh⁴², M. Lethuillier⁴², L. Mirabito⁴², S. Perries⁴², A. Purohit⁴², M. Vander Donckt⁴², P. Verdier⁴², J. Xiao⁴², G. Adamov⁴³, I. Lomidze⁴³, Z. Tsamalaidze^{43,r}, V. Botta⁴⁴, L. Feld⁴⁴, K. Klein⁴⁴, M. Lipinski⁴⁴, D. Meuser⁴⁴, A. Pauls⁴⁴, N. Röwert⁴⁴, M. Teroerde⁴⁴, S. Diekmann⁴⁵, A. Dodonova⁴⁵, N. Eich⁴⁵, D. Eliseev⁴⁵, F. Engelke⁴⁵, J. Erdmann⁴⁵, M. Erdmann⁴⁵, P. Fackeldey⁴⁵, B. Fischer⁴⁵, T. Hebbeker⁴⁵, K. Hoepfner⁴⁵, F. Ivone⁴⁵, A. Jung⁴⁵, M. y. Lee⁴⁵, L. Mastrolorenzo⁴⁵, F. Mausolf⁴⁵, M. Merschmeyer⁴⁵, A. Meyer⁴⁵, S. Mukherjee⁴⁵, D. Noll⁴⁵, A. Novak⁴⁵, F. Nowotny⁴⁵, A. Pozdnyakov⁴⁵, Y. Rath⁴⁵, W. Redjeb⁴⁵, F. Rehm⁴⁵, H. Reithler⁴⁵, U. Sarkar⁴⁵, V. Sarkisovi⁴⁵, A. Schmidt⁴⁵, A. Sharma⁴⁵, J. L. Spah⁴⁵, A. Stein⁴⁵, F. Torres Da Silva De Araujo^{45,x}, L. Vigilante⁴⁵, S. Wiedenbeck⁴⁵, S. Zaleski⁴⁵, C. Dziwok⁴⁶, G. Flügge⁴⁶, W. Haj Ahmad^{46,y}, T. Kress⁴⁶, A. Nowack⁴⁶, O. Pooth⁴⁶, A. Stahl⁴⁶, T. Ziemons⁴⁶, A. Zotz⁴⁶, H. Aarup Petersen⁴⁷, M. Aldaya Martin⁴⁷, J. Alimena⁴⁷, S. Amoroso⁴⁷, Y. An⁴⁷, S. Baxter⁴⁷, M. Bayatmakou⁴⁷, H. Becerril Gonzalez⁴⁷, O. Behnke⁴⁷, A. Belvedere⁴⁷, S. Bhattacharya⁴⁷, F. Blekman^{47,z}, K. Borras^{47,aa}, A. Campbell⁴⁷, A. Cardini⁴⁷, C. Cheng⁴⁷, F. Colombina⁴⁷, S. Consuegra Rodríguez⁴⁷, G. Correia Silva⁴⁷, M. De Silva⁴⁷, G. Eckerlin⁴⁷, D. Eckstein⁴⁷, L. I. Estevez Banos⁴⁷

O. Filatov⁴⁷, E. Gallo^{47,z}, A. Geiser⁴⁷, A. Giraldi⁴⁷, G. Greau⁴⁷, V. Guglielmi⁴⁷, M. Guthoff⁴⁷, A. Hinzmann⁴⁷, A. Jafari^{47,bb}, L. Jepe⁴⁷, N. Z. Jomhari⁴⁷, B. Kaech⁴⁷, M. Kasemann⁴⁷, C. Kleinwort⁴⁷, R. Kogler⁴⁷, M. Komm⁴⁷, D. Krücker⁴⁷, W. Lange⁴⁷, D. Leyva Pernia⁴⁷, K. Lipka^{47,cc}, W. Lohmann^{47,dd}, R. Mankel⁴⁷, I.-A. Melzer-Pellmann⁴⁷, M. Mendizabal Morentin⁴⁷, A. B. Meyer⁴⁷, G. Milella⁴⁷, A. Mussgiller⁴⁷, L. P. Nair⁴⁷, A. Nürnberg⁴⁷, Y. Otari⁴⁷, J. Park⁴⁷, D. Pérez Adán⁴⁷, E. Ranken⁴⁷, A. Raspereza⁴⁷, B. Ribeiro Lopes⁴⁷, J. Rübenach⁴⁷, A. Saggio⁴⁷, M. Scham^{47,ee,aa}, S. Schnake^{47,aa}, P. Schütze⁴⁷, C. Schwanenberger^{47,z}, D. Selivanova⁴⁷, K. Sharke⁴⁷, M. Shchedrolosiev⁴⁷, R. E. Sosa Ricardo⁴⁷, D. Stafford⁴⁷, F. Vazzoler⁴⁷, A. Ventura Barroso⁴⁷, R. Walsh⁴⁷, Q. Wang⁴⁷, Y. Wen⁴⁷, K. Wichmann⁴⁷, L. Wiens^{47,aa}, C. Wissing⁴⁷, Y. Yang⁴⁷, A. Zimmermann Castro Santos⁴⁷, A. Albrecht⁴⁸, S. Albrecht⁴⁸, M. Antonello⁴⁸, S. Bein⁴⁸, L. Benato⁴⁸, M. Bonanomi⁴⁸, P. Connor⁴⁸, M. Eich⁴⁸, K. El Morabit⁴⁸, Y. Fischer⁴⁸, A. Fröhlich⁴⁸, C. Garbers⁴⁸, E. Garutti⁴⁸, A. Grohsjean⁴⁸, M. Hajheidari⁴⁸, J. Haller⁴⁸, H. R. Jabusch⁴⁸, G. Kasieczka⁴⁸, P. Keicher⁴⁸, R. Klanner⁴⁸, W. Korcari⁴⁸, T. Kramer⁴⁸, V. Kutzner⁴⁸, F. Labe⁴⁸, J. Lange⁴⁸, A. Lobanov⁴⁸, C. Matthies⁴⁸, A. Mehta⁴⁸, L. Moureaux⁴⁸, M. Mrowietz⁴⁸, A. Nigamova⁴⁸, Y. Nissan⁴⁸, A. Paasch⁴⁸, K. J. Pena Rodriguez⁴⁸, T. Quadfasel⁴⁸, B. Raciti⁴⁸, M. Rieger⁴⁸, D. Savoie⁴⁸, J. Schindler⁴⁸, P. Schleper⁴⁸, M. Schröder⁴⁸, J. Schwandt⁴⁸, M. Sommerhalder⁴⁸, H. Stadie⁴⁸, G. Steinbrück⁴⁸, A. Tews⁴⁸, M. Wolf⁴⁸, S. Brommer⁴⁹, M. Burkart⁴⁹, E. Butz⁴⁹, T. Chwalek⁴⁹, A. Dierlamm⁴⁹, A. Droll⁴⁹, N. Faltermann⁴⁹, M. Giffels⁴⁹, A. Gottmann⁴⁹, F. Hartmann^{49,ff}, R. Hofsaess⁴⁹, M. Horzela⁴⁹, U. Husemann⁴⁹, J. Kieseler⁴⁹, M. Klute⁴⁹, R. Koppenhöfer⁴⁹, J. M. Lawhorn⁴⁹, M. Link⁴⁹, A. Lintuluoto⁴⁹, S. Maier⁴⁹, S. Mitra⁴⁹, M. Mormile⁴⁹, Th. Müller⁴⁹, M. Neukum⁴⁹, M. Oh⁴⁹, M. Presilla⁴⁹, G. Quast⁴⁹, K. Rabbertz⁴⁹, B. Regnery⁴⁹, N. Shadskiy⁴⁹, I. Shvetsov⁴⁹, H. J. Simonis⁴⁹, M. Toms⁴⁹, N. Trevisani⁴⁹, R. Ulrich⁴⁹, R. F. Von Cube⁴⁹, M. Wassmer⁴⁹, S. Wieland⁴⁹, F. Wittig⁴⁹, R. Wolf⁴⁹, X. Zuo⁴⁹, G. Anagnostou⁵⁰, G. Daskalakis⁵⁰, A. Kyriakis⁵⁰, A. Papadopoulos^{50,ff}, A. Stakia⁵⁰, P. Kontaxakis⁵¹, G. Melachroinos⁵¹, A. Panagiotou⁵¹, I. Papavergou⁵¹, I. Paraskevas⁵¹, N. Saoulidou⁵¹, K. Theofilatos⁵¹, E. Tziaferi⁵¹, K. Vellidis⁵¹, I. Zisopoulos⁵¹, G. Bakas⁵², T. Chatzistavrou⁵², G. Karapostoli⁵², K. Kousouris⁵², I. Papakrivopoulos⁵², E. Siamarkou⁵², G. Tsipolitis⁵², A. Zacharopoulou⁵², K. Adamidis⁵³, I. Bestintzanos⁵³, I. Evangelou⁵³, C. Foudas⁵³, P. Gianneios⁵³, C. Kamtsikis⁵³, P. Katsoulis⁵³, P. Kokkas⁵³, P. G. Kosmoglou Kioseoglou⁵³, N. Manthos⁵³, I. Papadopoulos⁵³, J. Strologas⁵³, M. Bartók^{54,gg}, C. Hajdu⁵⁴, D. Horvath^{54,hh,ii}, F. Sikler⁵⁴, V. Veszpremi⁵⁴, M. Csanád⁵⁵, K. Farkas⁵⁵, M. M. A. Gadallah^{55,ij}, Á. Kadlecik⁵⁵, P. Major⁵⁵, K. Mandal⁵⁵, G. Pásztor⁵⁵, A. J. Rádl^{55,kk}, G. I. Veres⁵⁵, P. Raics⁵⁶, B. Ujvari⁵⁶, G. Zilizi⁵⁶, G. Bencze⁵⁷, S. Czellar⁵⁷, J. Molnar⁵⁷, Z. Szillasi⁵⁷, T. Csorgo^{58,kk}, F. Nemes^{58,kk}, T. Novak⁵⁸, J. Babbar⁵⁹, S. Bansal⁵⁹, S. B. Beri⁵⁹, V. Bhatnagar⁵⁹, G. Chaudhary⁵⁹, S. Chauhan⁵⁹, N. Dhingra^{59,ll}, A. Kaur⁵⁹, A. Kaur⁵⁹, H. Kaur⁵⁹, M. Kaur⁵⁹, S. Kumar⁵⁹, K. Sandeep⁵⁹, T. Sheokand⁵⁹, J. B. Singh⁵⁹, A. Singla⁵⁹, A. Ahmed⁶⁰, A. Bhardwaj⁶⁰, A. Chhetri⁶⁰, B. C. Choudhary⁶⁰, A. Kumar⁶⁰, A. Kumar⁶⁰, M. Naimuddin⁶⁰, K. Ranjan⁶⁰, S. Saumya⁶⁰, S. Baradia⁶¹, S. Barman^{61,mm}, S. Bhattacharya⁶¹, S. Dutta⁶¹, S. Dutta⁶¹, P. Palit⁶¹, S. Sarkar⁶¹, M. M. Ameen⁶², P. K. Behera⁶², S. C. Behera⁶², S. Chatterjee⁶², P. Jana⁶², P. Kalbhor⁶², J. R. Komaragiri^{62,nn}, D. Kumar^{62,nn}, L. Panwar^{62,nn}, P. R. Pujahari⁶², N. R. Saha⁶², A. Sharma⁶², A. K. Sikdar⁶², S. Verma⁶², S. Dugad⁶³, M. Kumar⁶³, G. B. Mohanty⁶³, P. Suryadevara⁶³, A. Bala⁶⁴, S. Banerjee⁶⁴, R. M. Chatterjee⁶⁴, R. K. Dewanjee^{64,oo}, M. Guchait⁶⁴, Sh. Jain⁶⁴, S. Karmakar⁶⁴, S. Kumar⁶⁴, G. Majumder⁶⁴, K. Mazumdar⁶⁴, S. Parolia⁶⁴, A. Thachayath⁶⁴, S. Bahinipati^{65,pp}, C. Kar⁶⁵, D. Maity^{65,qq}, P. Mal⁶⁵, T. Mishra⁶⁵, V. K. Muraleedharan Nair Bindhu^{65,qq}, K. Naskar^{65,qq}, A. Nayak^{65,qq}, P. Sadangi⁶⁵, P. Saha⁶⁵, S. K. Swain⁶⁵, S. Varghese^{65,qq}, D. Vats^{65,qq}, S. Acharya^{66,rr}, A. Alpana⁶⁶, S. Dube⁶⁶, B. Gumber^{66,rr}, B. Kansal⁶⁶, A. Laha⁶⁶, B. Sahu^{66,rr}, S. Sharma⁶⁶, H. Bakshiansohi^{67,ss}, E. Khazaie^{67,tt}, M. Zeinali^{67,uu}, S. Chenarani^{68,vv}, S. M. Etesami⁶⁸, M. Khakzad⁶⁸, M. Mohammadi Najafabadi⁶⁸, M. Grunewald⁶⁹, M. Abbrescia^{70a,70b}, R. Aly^{70a,70c,ww}, A. Colaleo^{70a,70b}, D. Creanza^{70a,70c}, B. D'Anzi^{70a,70b}, N. De Filippis^{70a,70c}, M. De Palma^{70a,70b}, A. Di Florio^{70a,70c}, W. Elmetenawee^{70a,70b,ww}, L. Fiore^{70a}, G. Iaselli^{70a,70c}, M. Louka^{70a,70b}, G. Maggi^{70a,70c}, M. Maggi^{70a}, I. Margjeka^{70a,70b}, V. Mastrapasqua^{70a,70b}, S. My^{70a,70b}, S. Nuzzo^{70a,70b}, A. Pellicchia^{70a,70b}, A. Pompili^{70a,70b}, G. Pugliese^{70a,70c}, R. Radogna^{70a}, G. Ramirez-Sanchez^{70a,70c}, D. Ramos^{70a}, A. Ranieri^{70a}, L. Silvestris^{70a}, F. M. Simone^{70a,70b}, Ü. Sözbilir^{70a}, A. Stamerra^{70a}, R. Venditti^{70a}, P. Verwilligen^{70a}, A. Zaza^{70a,70b}, G. Abbiendi^{71a}, C. Battilana^{71a,71b}, L. Borgonovi^{71a}, R. Campanini^{71a,71b}, P. Capiluppi^{71a,71b}, A. Castro^{71a,71b}, F. R. Cavallo^{71a}, M. Cuffiani^{71a,71b}, G. M. Dallavalle^{71a}, T. Diotallevi^{71a,71b}, F. Fabbri^{71a}

A. Fanfani^{71a,71b} D. Fasanella^{71a,71b} P. Giacomelli^{71a} L. Giommi^{71a,71b} C. Grandi^{71a} L. Guiducci^{71a,71b}
 S. Lo Meo^{71a,xx} L. Lunerti^{71a,71b} S. Marcellini^{71a} G. Masetti^{71a} F. L. Navarra^{71a,71b} A. Perrotta^{71a}
 F. Primavera^{71a,71b} A. M. Rossi^{71a,71b} T. Rovelli^{71a,71b} G. P. Siroli^{71a,71b} S. Costa^{72a,72b,yy} A. Di Mattia^{72a}
 R. Potenza^{72a,72b} A. Tricomi^{72a,72b,yy} C. Tuve^{72a,72b} P. Assiouras^{73a} G. Barbagli^{73a} G. Bardelli^{73a,73b}
 B. Camaiani^{73a,73b} A. Cassese^{73a} R. Ceccarelli^{73a} V. Ciulli^{73a,73b} C. Civinini^{73a} R. D'Alessandro^{73a,73b}
 E. Focardi^{73a,73b} T. Kello^{73a} G. Latino^{73a,73b} P. Lenzi^{73a,73b} M. Lizzo^{73a} M. Meschini^{73a} S. Paoletti^{73a}
 A. Papanastassiou^{73a,73b} G. Sguazzoni^{73a} L. Viliani^{73a} L. Benussi⁷⁴ S. Bianco⁷⁴ S. Meola^{74,zz} D. Piccolo⁷⁴
 P. Chatagnon^{75a} F. Ferro^{75a} E. Robutti^{75a} S. Tosi^{75a,75b} A. Benaglia^{76a} G. Boldrini^{76a,76b} F. Brivio^{76a}
 F. Cetorelli^{76a} F. De Guio^{76a,76b} M. E. Dinardo^{76a,76b} P. Dini^{76a} S. Gennai^{76a} R. Gerosa^{76a,76b} A. Ghezzi^{76a,76b}
 P. Govoni^{76a,76b} L. Guzzi^{76a} M. T. Lucchini^{76a,76b} M. Malberti^{76a} S. Malvezzi^{76a} A. Massironi^{76a}
 D. Menasce^{76a} L. Moroni^{76a} M. Paganoni^{76a,76b} D. Pedrini^{76a} B. S. Pinolini^{76a} S. Ragazzi^{76a,76b}
 T. Tabarelli de Fatis^{76a,76b} D. Zuolo^{76a} S. Buontempo^{77a} A. Cagnotta^{77a,77b} F. Carnevali^{77a,77b} N. Cavallo^{77a,77c}
 A. De Iorio^{77a,77b} F. Fabozzi^{77a,77c} A. O. M. Iorio^{77a,77b} L. Lista^{77a,77b,aaa} P. Paolucci^{77a,ff} B. Rossi^{77a}
 C. Sciacca^{77a,77b} R. Ardino^{78a} P. Azzi^{78a} N. Bacchetta^{78a,bbb} M. Benettoni^{78a} D. Bisello^{78a,78b} P. Bortignon^{78a}
 A. Bragagnolo^{78a,78b} R. Carlin^{78a,78b} P. Checchia^{78a} T. Dorigo^{78a} F. Gasparini^{78a,78b} U. Gasparini^{78a,78b}
 E. Lusiani^{78a} M. Margoni^{78a,78b} F. Marini^{78a} A. T. Meneguzzo^{78a,78b} M. Migliorini^{78a,78b} J. Pazzini^{78a,78b}
 P. Ronchese^{78a,78b} R. Rossin^{78a,78b} F. Simonetto^{78a,78b} G. Strong^{78a} M. Tosi^{78a,78b} A. Triossi^{78a,78b}
 S. Ventura^{78a} H. Yarar^{78a,78b} M. Zanetti^{78a,78b} P. Zotto^{78a,78b} A. Zucchetta^{78a,78b} S. Abu Zeid^{79a,ccc}
 C. Aimè^{79a,79b} A. Braghieri^{79a} S. Calzaferri^{79a} D. Fiorina^{79a} P. Montagna^{79a,79b} V. Re^{79a} C. Riccardi^{79a,79b}
 P. Salvini^{79a} I. Vai^{79a,79b} P. Vitulo^{79a,79b} S. Ajmal^{80a,80b} P. Asenov^{80a,ddd} G. M. Bilei^{80a} D. Ciangottini^{80a,80b}
 L. Fanò^{80a,80b} M. Magherini^{80a,80b} G. Mantovani^{80a,80b} V. Mariani^{80a,80b} M. Menichelli^{80a} F. Moscatelli^{80a,ddd}
 A. Rossi^{80a,80b} A. Santocchia^{80a,80b} D. Spiga^{80a} T. Tedeschi^{80a,80b} P. Azzurri^{81a} G. Bagliesi^{81a}
 R. Bhattacharya^{81a} L. Bianchini^{81a,81b} T. Boccali^{81a} E. Bossini^{81a} D. Bruschini^{81a,81c} R. Castaldi^{81a}
 M. A. Ciocci^{81a,81b} M. Cipriani^{81a,81b} V. D'Amante^{81a,81d} R. Dell'Orso^{81a} S. Donato^{81a} A. Giassi^{81a}
 F. Ligabue^{81a,81c} D. Matos Figueiredo^{81a} A. Messineo^{81a,81b} M. Musich^{81a,81b} F. Palla^{81a} A. Rizzi^{81a,81b}
 G. Rolandi^{81a,81c} S. Roy Chowdhury^{81a} T. Sarkar^{81a} A. Scribano^{81a} P. Spagnolo^{81a} R. Tenchini^{81a}
 G. Tonelli^{81a,81b} N. Turini^{81a,81d} A. Venturi^{81a} P. G. Verdini^{81a} P. Barria^{82a} M. Campana^{82a,82b} F. Cavallari^{82a}
 L. Cunqueiro Mendez^{82a,82b} D. Del Re^{82a,82b} E. Di Marco^{82a} M. Diemoz^{82a} F. Errico^{82a,82b} E. Longo^{82a,82b}
 P. Meridiani^{82a} J. Mijuskovic^{82a,82b} G. Organtini^{82a,82b} F. Pandolfi^{82a} R. Paramatti^{82a,82b} C. Quaranta^{82a,82b}
 S. Rahatlou^{82a,82b} C. Rovelli^{82a} F. Santanastasio^{82a,82b} L. Soffi^{82a} N. Amapane^{83a,83b} R. Arcidiacono^{83a,83c}
 S. Argiro^{83a,83b} M. Arneodo^{83a,83c} N. Bartosik^{83a} R. Bellan^{83a,83b} A. Bellora^{83a,83b} C. Biino^{83a} N. Cartiglia^{83a}
 M. Costa^{83a,83b} R. Covarelli^{83a,83b} N. Demaria^{83a} L. Finco^{83a} M. Grippo^{83a,83b} B. Kiani^{83a,83b} F. Legger^{83a}
 F. Luongo^{83a,83b} C. Mariotti^{83a} S. Maselli^{83a} A. Mecca^{83a,83b} E. Migliore^{83a,83b} M. Monteno^{83a}
 R. Mulargia^{83a} M. M. Obertino^{83a,83b} G. Ortona^{83a} L. Pacher^{83a,83b} N. Pastrone^{83a} M. Pelliccioni^{83a}
 M. Ruspa^{83a,83c} F. Siviero^{83a,83b} V. Sola^{83a,83b} A. Solano^{83a,83b} A. Staiano^{83a} C. Tarricone^{83a,83b} D. Trocino^{83a}
 G. Umoret^{83a,83b} E. Vlasov^{83a,83b} S. Belforte^{84a} V. Candelise^{84a,84b} M. Casarsa^{84a} F. Cossutti^{84a}
 K. De Leo^{84a,84b} G. Della Ricca^{84a,84b} S. Dogra⁸⁵ J. Hong⁸⁵ C. Huh⁸⁵ B. Kim⁸⁵ D. H. Kim⁸⁵ J. Kim⁸⁵
 H. Lee⁸⁵ S. W. Lee⁸⁵ C. S. Moon⁸⁵ Y. D. Oh⁸⁵ M. S. Ryu⁸⁵ S. Sekmen⁸⁵ Y. C. Yang⁸⁵ M. S. Kim⁸⁶
 G. Bak⁸⁷ P. Gwak⁸⁷ H. Kim⁸⁷ D. H. Moon⁸⁷ E. Asilar⁸⁸ D. Kim⁸⁸ T. J. Kim⁸⁸ J. A. Merlin⁸⁸ S. Choi⁸⁹
 S. Han⁸⁹ B. Hong⁸⁹ K. Lee⁸⁹ K. S. Lee⁸⁹ S. Lee⁸⁹ J. Park⁸⁹ S. K. Park⁸⁹ J. Yoo⁸⁹ J. Goh⁹⁰ S. Yang⁹⁰
 H. S. Kim⁹¹ Y. Kim⁹¹ S. Lee⁹¹ J. Almond⁹² J. H. Bhyun⁹² J. Choi⁹² W. Jun⁹² J. Kim⁹² S. Ko⁹² H. Kwon⁹²
 H. Lee⁹² J. Lee⁹² J. Lee⁹² B. H. Oh⁹² S. B. Oh⁹² H. Seo⁹² U. K. Yang⁹² I. Yoon⁹² W. Jang⁹³ D. Y. Kang⁹³
 Y. Kang⁹³ S. Kim⁹³ B. Ko⁹³ J. S. H. Lee⁹³ Y. Lee⁹³ I. C. Park⁹³ Y. Roh⁹³ I. J. Watson⁹³ S. Ha⁹⁴
 H. D. Yoo⁹⁴ M. Choi⁹⁵ M. R. Kim⁹⁵ H. Lee⁹⁵ Y. Lee⁹⁵ I. Yu⁹⁵ T. Beyrouthy⁹⁶ Y. Maghrbi⁹⁶ K. Dreimanis⁹⁷
 A. Gaile⁹⁷ G. Pikurs⁹⁷ A. Potrebko⁹⁷ M. Seidel⁹⁷ V. Veckalns^{97,eee} N. R. Strautnieks⁹⁸ M. Ambrozias⁹⁹
 A. Juodagalvis⁹⁹ A. Rinkevicius⁹⁹ G. Tamulaitis⁹⁹ N. Bin Norjoharuddeen¹⁰⁰ I. Yusuff^{100,fff} Z. Zolkapli¹⁰⁰
 J. F. Benitez¹⁰¹ A. Castaneda Hernandez¹⁰¹ H. A. Encinas Acosta¹⁰¹ L. G. Gallegos Maríñez¹⁰¹ M. León Coello¹⁰¹
 J. A. Murillo Quijada¹⁰¹ A. Sehrawat¹⁰¹ L. Valencia Palomo¹⁰¹ G. Ayala¹⁰² H. Castilla-Valdez¹⁰²
 E. De La Cruz-Burelo¹⁰² I. Heredia-De La Cruz^{102,ggg} R. Lopez-Fernandez¹⁰² C. A. Mondragon Herrera¹⁰²

A. Sánchez Hernández¹⁰² C. Oropeza Barrera¹⁰³ M. Ramírez García¹⁰³ I. Bautista¹⁰⁴ I. Pedraza¹⁰⁴
 H. A. Salazar Ibarguen¹⁰⁴ C. Uribe Estrada¹⁰⁴ I. Bubanja¹⁰⁵ N. Raicevic¹⁰⁵ P. H. Butler¹⁰⁶ A. Ahmad¹⁰⁷
 M. I. Asghar¹⁰⁷ A. Awais¹⁰⁷ M. I. M. Awan¹⁰⁷ H. R. Hoorani¹⁰⁷ W. A. Khan¹⁰⁷ V. Avati¹⁰⁸ L. Grzanka¹⁰⁸
 M. Malawski¹⁰⁸ H. Bialkowska¹⁰⁹ M. Bluj¹⁰⁹ B. Boimska¹⁰⁹ M. Górski¹⁰⁹ M. Kazana¹⁰⁹ M. Szleper¹⁰⁹
 P. Zalewski¹⁰⁹ K. Bunkowski¹¹⁰ K. Doroba¹¹⁰ A. Kalinowski¹¹⁰ M. Konecki¹¹⁰ J. Krolikowski¹¹⁰
 A. Muhammad¹¹⁰ K. Pozniak¹¹¹ W. Zabolotny¹¹¹ M. Araujo¹¹² D. Bastos¹¹² C. Beirão Da Cruz E Silva¹¹²
 A. Boletti¹¹² M. Bozzo¹¹² T. Camposi¹¹² G. Da Molin¹¹² P. Faccioli¹¹² M. Gallinaro¹¹² J. Hollar¹¹²
 N. Leonardo¹¹² T. Niknejad¹¹² A. Petrilli¹¹² M. Pisano¹¹² J. Seixas¹¹² J. Varela¹¹² J. W. Wulff¹¹² P. Adzic¹²⁵
 P. Milenovic¹²⁵ M. Dordevic¹²⁶ J. Milosevic¹²⁶ V. Rekovic¹²⁶ M. Aguilar-Benitez¹²⁷ J. Alcaraz Maestre¹²⁷
 Cristina F. Bedoya¹²⁷ M. Cepeda¹²⁷ M. Cerrada¹²⁷ N. Colino¹²⁷ B. De La Cruz¹²⁷ A. Delgado Peris¹²⁷
 A. Escalante Del Valle¹²⁷ D. Fernández Del Val¹²⁷ J. P. Fernández Ramos¹²⁷ J. Flix¹²⁷ M. C. Fouz¹²⁷
 O. Gonzalez Lopez¹²⁷ S. Goy Lopez¹²⁷ J. M. Hernandez¹²⁷ M. I. Josa¹²⁷ D. Moran¹²⁷ C. M. Morcillo Perez¹²⁷
 Á. Navarro Tobar¹²⁷ C. Perez Dengra¹²⁷ A. Pérez-Calero Yzquierdo¹²⁷ J. Puerta Pelayo¹²⁷ I. Redondo¹²⁷
 D. D. Redondo Ferrero¹²⁷ L. Romero¹²⁷ S. Sánchez Navas¹²⁷ L. Urda Gómez¹²⁷ J. Vázquez Escobar¹²⁷
 C. Willmott¹²⁷ J. F. de Trocóniz¹²⁸ B. Alvarez Gonzalez¹²⁹ J. Cuevas¹²⁹ J. Fernandez Menendez¹²⁹
 S. Folgueras¹²⁹ I. Gonzalez Caballero¹²⁹ J. R. González Fernández¹²⁹ E. Palencia Cortezon¹²⁹
 C. Ramón Álvarez¹²⁹ V. Rodríguez Bouza¹²⁹ A. Soto Rodríguez¹²⁹ A. Trapote¹²⁹ C. Vico Villalba¹²⁹
 P. Vischia¹²⁹ S. Bhowmik¹³⁰ S. Blanco Fernández¹³⁰ J. A. Brochero Cifuentes¹³⁰ I. J. Cabrillo¹³⁰
 A. Calderon¹³⁰ J. Duarte Campderros¹³⁰ M. Fernandez¹³⁰ G. Gomez¹³⁰ C. Lasaosa García¹³⁰
 C. Martinez Rivero¹³⁰ P. Martinez Ruiz del Arbol¹³⁰ F. Matorras¹³⁰ P. Matorras Cuevas¹³⁰
 E. Navarrete Ramos¹³⁰ J. Piedra Gomez¹³⁰ L. Scodellaro¹³⁰ I. Vila¹³⁰ J. M. Vizan Garcia¹³⁰
 M. K. Jayananda¹³¹ B. Kailasapathy^{131,hhh} D. U. J. Sonnadara¹³¹ D. D. C. Wickramaratna¹³¹
 W. G. D. Dharmaratna^{132,iii} K. Liyanage¹³² N. Perera¹³² N. Wickramage¹³² D. Abbaneo¹³³ C. Amendola¹³³
 E. Auffray¹³³ G. Auzinger¹³³ J. Baechler¹³³ D. Barney¹³³ A. Bermúdez Martínez¹³³ M. Bianco¹³³ B. Bilin¹³³
 A. A. Bin Anuar¹³³ A. Bocci¹³³ C. Botta¹³³ E. Brondolin¹³³ C. Caillol¹³³ G. Cerminara¹³³
 N. Chernyavskaya¹³³ D. d'Enterria¹³³ A. Dabrowski¹³³ A. David¹³³ A. De Roeck¹³³ M. M. Defranchis¹³³
 M. Deile¹³³ M. Dobson¹³³ L. Forthomme¹³³ G. Franzoni¹³³ W. Funk¹³³ S. Giani¹³³ D. Gigi¹³³ K. Gill¹³³
 F. Glege¹³³ L. Gouskos¹³³ M. Haranko¹³³ J. Hegeman¹³³ B. Huber¹³³ V. Innocente¹³³ T. James¹³³
 P. Janot¹³³ S. Laurila¹³³ P. Lecoq¹³³ E. Leutgeb¹³³ C. Lourenço¹³³ B. Maier¹³³ L. Malgeri¹³³
 M. Mannelli¹³³ A. C. Marini¹³³ M. Matthewman¹³³ F. Meijers¹³³ S. Mersi¹³³ E. Meschi¹³³ V. Milosevic¹³³
 F. Monti¹³³ F. Moortgat¹³³ M. Mulders¹³³ I. Neutelings¹³³ S. Orfanelli¹³³ F. Pantaleo¹³³ G. Petrucciani¹³³
 A. Pfeiffer¹³³ M. Pierini¹³³ D. Piparo¹³³ H. Qu¹³³ D. Rabady¹³³ G. Reales Gutiérrez¹³³ M. Rovere¹³³
 H. Sakulin¹³³ S. Scarfi¹³³ C. Schwick¹³³ M. Selvaggi¹³³ A. Sharma¹³³ K. Shchelina¹³³ P. Silva¹³³
 P. Sphicas^{133,jjj} A. G. Stahl Leitner¹³³ A. Steen¹³³ S. Summers¹³³ D. Treille¹³³ P. Tropea¹³³ A. Tsiros¹³³
 D. Walter¹³³ J. Wanczyk^{133,kkk} J. Wang¹³³ S. Wuchterl¹³³ P. Zehetner¹³³ P. Zexl¹³³ W. D. Zeuner¹³³
 T. Bevilacqua^{134,lll} L. Caminada^{134,lll} A. Ebrahimi¹³⁴ W. Erdmann¹³⁴ R. Horisberger¹³⁴ Q. Ingram¹³⁴
 H. C. Kaestli¹³⁴ D. Kotlinski¹³⁴ C. Lange¹³⁴ M. Missiroli^{134,lll} L. Noehte^{134,lll} T. Rohe¹³⁴ T. K. Aarrestad¹³⁵
 K. Androsov^{135,kkk} M. Backhaus¹³⁵ A. Calandri¹³⁵ C. Cazzaniga¹³⁵ K. Datta¹³⁵ A. De Cosa¹³⁵
 G. Dissertori¹³⁵ M. Dittmar¹³⁵ M. Donegà¹³⁵ F. Eble¹³⁵ M. Galli¹³⁵ K. Gedia¹³⁵ F. Glessgen¹³⁵ C. Grab¹³⁵
 D. Hits¹³⁵ W. Lustermann¹³⁵ A.-M. Lyon¹³⁵ R. A. Manzoni¹³⁵ M. Marchegiani¹³⁵ L. Marchese¹³⁵
 C. Martin Perez¹³⁵ A. Mascellani^{135,kkk} F. Nessi-Tedaldi¹³⁵ F. Pauss¹³⁵ V. Perovic¹³⁵ S. Pigazzini¹³⁵
 C. Reissel¹³⁵ T. Reitenspiess¹³⁵ B. Ristic¹³⁵ F. Riti¹³⁵ D. Ruini¹³⁵ R. Seidita¹³⁵ J. Steggemann^{135,kkk}
 D. Valsecchi¹³⁵ R. Wallny¹³⁵ C. Amsler^{136,mmm} P. Bärtzsch¹³⁶ D. Brzhechko¹³⁶ M. F. Canelli¹³⁶ K. Cormier¹³⁶
 J. K. Heikkilä¹³⁶ M. Huwiler¹³⁶ W. Jin¹³⁶ A. Jofrehei¹³⁶ B. Kilminster¹³⁶ S. Leontsinis¹³⁶ S. P. Liechi¹³⁶
 A. Macchiolo¹³⁶ P. Meiring¹³⁶ U. Molinatti¹³⁶ A. Reimers¹³⁶ P. Robmann¹³⁶ S. Sanchez Cruz¹³⁶ M. Senger¹³⁶
 Y. Takahashi¹³⁶ R. Tramontano¹³⁶ C. Adloff^{137,nnn} D. Bhowmik¹³⁷ C. M. Kuo¹³⁷ W. Lin¹³⁷ P. K. Rout¹³⁷
 P. C. Tiwari^{137,nn} S. S. Yu¹³⁷ L. Ceard¹³⁸ Y. Chao¹³⁸ K. F. Chen¹³⁸ P. s. Chen¹³⁸ Z. g. Chen¹³⁸ W.-S. Hou¹³⁸
 T. h. Hsu¹³⁸ Y. w. Kao¹³⁸ R. Khurana¹³⁸ G. Kole¹³⁸ Y. y. Li¹³⁸ R.-S. Lu¹³⁸ E. Paganis¹³⁸ X. f. Su¹³⁸
 J. Thomas-Wilsker¹³⁸ L. s. Tsai¹³⁸ H. y. Wu¹³⁸ E. Yazgan¹³⁸ C. Asawatangtrakuldee¹³⁹ N. Srimanobhas¹³⁹

V. Wachirapusanand¹³⁹ D. Agyel¹⁴⁰ F. Boran¹⁴⁰ Z. S. Demiroglu¹⁴⁰ F. Dolek¹⁴⁰ I. Dumanoglu^{140,ooo}
E. Eskut¹⁴⁰ Y. Guler^{140,ppp} E. Gurpinar Guler^{140,ppp} C. Isik¹⁴⁰ O. Kara¹⁴⁰ A. Kayis Topaksu¹⁴⁰ U. Kiminsu¹⁴⁰
G. Onengut¹⁴⁰ K. Ozdemir^{140,qqq} A. Polatoz¹⁴⁰ B. Tali^{140,rrr} U. G. Tok¹⁴⁰ S. Turkcapar¹⁴⁰ E. Uslan¹⁴⁰
I. S. Zorbakir¹⁴⁰ M. Yalvac^{141,sss} B. Akgun¹⁴² I. O. Atakisi¹⁴² E. Gülmez¹⁴² M. Kaya^{142,ttt} O. Kaya^{142,uuu}
S. Tekten^{142,vvv} A. Cakir¹⁴³ K. Cankocak^{143,ooo,www} Y. Komurcu¹⁴³ S. Sen^{143,xxx} O. Aydilek¹⁴⁴ S. Cerci^{144,rrr}
V. Epshteyn¹⁴⁴ B. Hacisahinoglu¹⁴⁴ I. Hos^{144,yyy} B. Kaynak¹⁴⁴ S. Ozkorucuklu¹⁴⁴ O. Potok¹⁴⁴ H. Sert¹⁴⁴
C. Simsek¹⁴⁴ C. Zorbilmez¹⁴⁴ B. Isildak^{145,zzz} D. Sunar Cerci^{145,rrr} A. Boyaryntsev¹⁴⁶ B. Grynyov¹⁴⁶
L. Levchuk¹⁴⁷ D. Anthony¹⁴⁸ J. J. Brooke¹⁴⁸ A. Bundock¹⁴⁸ F. Bury¹⁴⁸ E. Clement¹⁴⁸ D. Cussans¹⁴⁸
H. Flacher¹⁴⁸ M. Glowacki¹⁴⁸ J. Goldstein¹⁴⁸ H. F. Heath¹⁴⁸ L. Kreczko¹⁴⁸ S. Paramesvaran¹⁴⁸
S. Seif El Nasr-Storey¹⁴⁸ V. J. Smith¹⁴⁸ N. Stylianou^{148,aaaa} K. Walkingshaw Pass¹⁴⁸ R. White¹⁴⁸ A. H. Ball¹⁴⁹
K. W. Bell¹⁴⁹ A. Belyaev^{149,bbbb} C. Brew¹⁴⁹ R. M. Brown¹⁴⁹ D. J. A. Cockerill¹⁴⁹ C. Cooke¹⁴⁹ K. V. Ellis¹⁴⁹
K. Harder¹⁴⁹ S. Harper¹⁴⁹ M.-L. Holmberg^{149,cccc} J. Linacre¹⁴⁹ K. Manolopoulos¹⁴⁹ D. M. Newbold¹⁴⁹
E. Olaiya¹⁴⁹ D. Petyt¹⁴⁹ T. Reis¹⁴⁹ G. Salvi¹⁴⁹ T. Schuh¹⁴⁹ C. H. Shepherd-Themistocleous¹⁴⁹ I. R. Tomalin¹⁴⁹
T. Williams¹⁴⁹ R. Bainbridge¹⁵⁰ P. Bloch¹⁵⁰ C. E. Brown¹⁵⁰ O. Buchmuller¹⁵⁰ V. Cacchio¹⁵⁰
C. A. Carrillo Montoya¹⁵⁰ G. S. Chahal^{150,ddd} D. Colling¹⁵⁰ J. S. Dancu¹⁵⁰ I. Das¹⁵⁰ P. Dauncey¹⁵⁰
G. Davies¹⁵⁰ J. Davies¹⁵⁰ M. Della Negra¹⁵⁰ S. Fayer¹⁵⁰ G. Fedi¹⁵⁰ G. Hall¹⁵⁰ M. H. Hassanshahi¹⁵⁰
A. Howard¹⁵⁰ G. Iles¹⁵⁰ M. Knight¹⁵⁰ J. Langford¹⁵⁰ J. León Holgado¹⁵⁰ L. Lyons¹⁵⁰ A.-M. Magnan¹⁵⁰
S. Malik¹⁵⁰ M. Mieskolainen¹⁵⁰ J. Nash^{150,eeee} M. Pesaresi¹⁵⁰ B. C. Radburn-Smith¹⁵⁰ A. Richards¹⁵⁰
A. Rose¹⁵⁰ K. Sava¹⁵⁰ C. Seez¹⁵⁰ R. Shukla¹⁵⁰ A. Tapper¹⁵⁰ K. Uchida¹⁵⁰ G. P. Uttley¹⁵⁰ L. H. Vage¹⁵⁰
T. Virdee^{150,fff} M. Vojinovic¹⁵⁰ N. Wardle¹⁵⁰ D. Winterbottom¹⁵⁰ K. Coldham¹⁵¹ J. E. Cole¹⁵¹ A. Khan¹⁵¹
P. Kyberd¹⁵¹ I. D. Reid¹⁵¹ S. Abdullin¹⁵² A. Brinkerhoff¹⁵² B. Caraway¹⁵² J. Dittmann¹⁵² K. Hatakeyama¹⁵²
J. Hiltbrand¹⁵² B. McMaster¹⁵² M. Saunders¹⁵² S. Sawant¹⁵² C. Sutantawibul¹⁵² J. Wilson¹⁵² R. Bartek¹⁵³
A. Dominguez¹⁵³ C. Huerta Escamilla¹⁵³ A. E. Simsek¹⁵³ R. Uniyal¹⁵³ A. M. Vargas Hernandez¹⁵³ B. Bam¹⁵⁴
R. Chudasama¹⁵⁴ S. I. Cooper¹⁵⁴ S. V. Gleyzer¹⁵⁴ C. U. Perez¹⁵⁴ P. Rumerio^{154,ffff} E. Usai¹⁵⁴ R. Yi¹⁵⁴
A. Akpinar¹⁵⁵ D. Arcaro¹⁵⁵ C. Cosby¹⁵⁵ Z. Demiragli¹⁵⁵ C. Erice¹⁵⁵ C. Fangmeier¹⁵⁵
C. Fernandez Madrazo¹⁵⁵ E. Fontanesi¹⁵⁵ D. Gastler¹⁵⁵ F. Golf¹⁵⁵ S. Jeon¹⁵⁵ I. Reed¹⁵⁵ J. Rohlf¹⁵⁵
K. Salyer¹⁵⁵ D. Sperka¹⁵⁵ D. Spitzbart¹⁵⁵ I. Suarez¹⁵⁵ A. Tsatsos¹⁵⁵ S. Yuan¹⁵⁵ A. G. Zecchinelli¹⁵⁵
G. Benelli¹⁵⁶ X. Coubez^{156,aa} D. Cutts¹⁵⁶ M. Hadley¹⁵⁶ U. Heintz¹⁵⁶ J. M. Hogan^{156,gggg} T. Kwon¹⁵⁶
G. Landsberg¹⁵⁶ K. T. Lau¹⁵⁶ D. Li¹⁵⁶ J. Luo¹⁵⁶ S. Mondal¹⁵⁶ M. Narain^{156,a} N. Pervan¹⁵⁶ S. Sagir^{156,hhhh}
F. Simpson¹⁵⁶ M. Stamenkovic¹⁵⁶ W. Y. Wong¹⁵⁶ X. Yan¹⁵⁶ W. Zhang¹⁵⁶ S. Abbott¹⁵⁷ J. Bonilla¹⁵⁷
C. Brainerd¹⁵⁷ R. Breedon¹⁵⁷ M. Calderon De La Barca Sanchez¹⁵⁷ M. Chertok¹⁵⁷ M. Citron¹⁵⁷ J. Conway¹⁵⁷
P. T. Cox¹⁵⁷ R. Erbacher¹⁵⁷ F. Jensen¹⁵⁷ O. Kukral¹⁵⁷ G. Mocellin¹⁵⁷ M. Mulhearn¹⁵⁷ D. Pellett¹⁵⁷
W. Wei¹⁵⁷ Y. Yao¹⁵⁷ F. Zhang¹⁵⁷ M. Bachtis¹⁵⁸ R. Cousins¹⁵⁸ A. Datta¹⁵⁸ G. Flores Avila¹⁵⁸ J. Hauser¹⁵⁸
M. Ignatenko¹⁵⁸ M. A. Iqbal¹⁵⁸ T. Lam¹⁵⁸ E. Manca¹⁵⁸ A. Nunez Del Prado¹⁵⁸ D. Saltzberg¹⁵⁸ V. Valuev¹⁵⁸
R. Clare¹⁵⁹ J. W. Gary¹⁵⁹ M. Gordon¹⁵⁹ G. Hanson¹⁵⁹ W. Si¹⁵⁹ S. Wimpenny^{159,a} J. G. Branson¹⁶⁰
S. Cittolin¹⁶⁰ S. Cooperstein¹⁶⁰ D. Diaz¹⁶⁰ J. Duarte¹⁶⁰ L. Giannini¹⁶⁰ J. Guiang¹⁶⁰ R. Kansal¹⁶⁰
V. Krutelyov¹⁶⁰ R. Lee¹⁶⁰ J. Letts¹⁶⁰ M. Masciovecchio¹⁶⁰ F. Mokhtar¹⁶⁰ S. Mukherjee¹⁶⁰ M. Pieri¹⁶⁰
M. Quinnan¹⁶⁰ B. V. Sathia Narayanan¹⁶⁰ V. Sharma¹⁶⁰ M. Tadel¹⁶⁰ E. Vourliotis¹⁶⁰ F. Würthwein¹⁶⁰
Y. Xiang¹⁶⁰ A. Yagil¹⁶⁰ A. Barzdukas¹⁶¹ L. Brennan¹⁶¹ C. Campagnari¹⁶¹ A. Dorsett¹⁶¹ J. Incandela¹⁶¹
J. Kim¹⁶¹ A. J. Li¹⁶¹ P. Masterson¹⁶¹ H. Mei¹⁶¹ J. Richman¹⁶¹ U. Sarica¹⁶¹ R. Schmitz¹⁶¹ F. Setti¹⁶¹
J. Shephlock¹⁶¹ D. Stuart¹⁶¹ T. Á. Vámi¹⁶¹ S. Wang¹⁶¹ A. Bornheim¹⁶² O. Cerri¹⁶² A. Latorre¹⁶² J. Mao¹⁶²
H. B. Newman¹⁶² M. Spiropulu¹⁶² J. R. Vlimant¹⁶² C. Wang¹⁶² S. Xie¹⁶² R. Y. Zhu¹⁶² J. Alison¹⁶³
S. An¹⁶³ M. B. Andrews¹⁶³ P. Bryant¹⁶³ M. Cremonesi¹⁶³ V. Dutta¹⁶³ T. Ferguson¹⁶³ A. Harilal¹⁶³ C. Liu¹⁶³
T. Mudholkar¹⁶³ S. Murthy¹⁶³ M. Paulini¹⁶³ A. Roberts¹⁶³ A. Sanchez¹⁶³ W. Terrill¹⁶³ J. P. Cumalat¹⁶⁴
W. T. Ford¹⁶⁴ A. Hassani¹⁶⁴ G. Karathanasis¹⁶⁴ E. MacDonald¹⁶⁴ N. Manganelli¹⁶⁴ A. Perloff¹⁶⁴ C. Savard¹⁶⁴
N. Schonbeck¹⁶⁴ K. Stenson¹⁶⁴ K. A. Ulmer¹⁶⁴ S. R. Wagner¹⁶⁴ N. Zipper¹⁶⁴ J. Alexander¹⁶⁵
S. Bright-Thonney¹⁶⁵ X. Chen¹⁶⁵ D. J. Cranshaw¹⁶⁵ J. Fan¹⁶⁵ X. Fan¹⁶⁵ D. Gadkari¹⁶⁵ S. Hogan¹⁶⁵
P. Kotamnives¹⁶⁵ J. Monroy¹⁶⁵ M. Oshiro¹⁶⁵ J. R. Patterson¹⁶⁵ J. Reichert¹⁶⁵ M. Reid¹⁶⁵ A. Ryd¹⁶⁵
J. Thom¹⁶⁵ P. Wittich¹⁶⁵ R. Zou¹⁶⁵ M. Albrow¹⁶⁶ M. Alyari¹⁶⁶ O. Amram¹⁶⁶ G. Apollinari¹⁶⁶

- A. Apresyan¹⁶⁶, L. A. T. Bauerdick¹⁶⁶, D. Berry¹⁶⁶, J. Berryhill¹⁶⁶, P. C. Bhat¹⁶⁶, K. Burkett¹⁶⁶, J. N. Butler¹⁶⁶, A. Canepa¹⁶⁶, G. B. Cerati¹⁶⁶, H. W. K. Cheung¹⁶⁶, F. Chlebana¹⁶⁶, G. Cummings¹⁶⁶, J. Dickinson¹⁶⁶, I. Dutta¹⁶⁶, V. D. Elvira¹⁶⁶, Y. Feng¹⁶⁶, J. Freeman¹⁶⁶, A. Gandrakota¹⁶⁶, Z. Gece¹⁶⁶, L. Gray¹⁶⁶, D. Green¹⁶⁶, A. Grummer¹⁶⁶, S. Grünendahl¹⁶⁶, D. Guerrero¹⁶⁶, O. Gutsche¹⁶⁶, R. M. Harris¹⁶⁶, R. Heller¹⁶⁶, T. C. Herwig¹⁶⁶, J. Hirschauer¹⁶⁶, L. Horyn¹⁶⁶, B. Jayatilaka¹⁶⁶, S. Jindariani¹⁶⁶, M. Johnson¹⁶⁶, U. Joshi¹⁶⁶, T. Klijnsma¹⁶⁶, B. Klima¹⁶⁶, K. H. M. Kwok¹⁶⁶, S. Lammel¹⁶⁶, D. Lincoln¹⁶⁶, R. Lipton¹⁶⁶, T. Liu¹⁶⁶, C. Madrid¹⁶⁶, K. Maeshima¹⁶⁶, C. Mantilla¹⁶⁶, D. Mason¹⁶⁶, P. McBride¹⁶⁶, P. Merkel¹⁶⁶, S. Mrenna¹⁶⁶, S. Nahn¹⁶⁶, J. Ngadiuba¹⁶⁶, D. Noonan¹⁶⁶, V. Papadimitriou¹⁶⁶, N. Pastika¹⁶⁶, K. Pedro¹⁶⁶, C. Pena^{166,iii}, F. Ravera¹⁶⁶, A. Reinsvold Hall^{166,iiii}, L. Ristori¹⁶⁶, E. Sexton-Kennedy¹⁶⁶, N. Smith¹⁶⁶, A. Soha¹⁶⁶, L. Spiegel¹⁶⁶, S. Stoynev¹⁶⁶, J. Strait¹⁶⁶, L. Taylor¹⁶⁶, S. Tkaczyk¹⁶⁶, N. V. Tran¹⁶⁶, L. Uplegger¹⁶⁶, E. W. Vaandering¹⁶⁶, I. Zoi¹⁶⁶, C. Aruta¹⁶⁷, P. Avery¹⁶⁷, D. Bourilkov¹⁶⁷, L. Cadamuro¹⁶⁷, P. Chang¹⁶⁷, V. Cherepanov¹⁶⁷, R. D. Field¹⁶⁷, E. Koenig¹⁶⁷, M. Kolosova¹⁶⁷, J. Konigsberg¹⁶⁷, A. Korytov¹⁶⁷, K. H. Lo¹⁶⁷, K. Matchev¹⁶⁷, N. Menendez¹⁶⁷, G. Mitselmakher¹⁶⁷, K. Mohrman¹⁶⁷, A. Muthirakalayil Madhu¹⁶⁷, N. Rawal¹⁶⁷, D. Rosenzweig¹⁶⁷, S. Rosenzweig¹⁶⁷, K. Shi¹⁶⁷, J. Wang¹⁶⁷, T. Adams¹⁶⁸, A. Al Kadhim¹⁶⁸, A. Askew¹⁶⁸, N. Bower¹⁶⁸, R. Habibullah¹⁶⁸, V. Hagopian¹⁶⁸, R. Hashmi¹⁶⁸, R. S. Kim¹⁶⁸, S. Kim¹⁶⁸, T. Kolberg¹⁶⁸, G. Martinez¹⁶⁸, H. Prosper¹⁶⁸, P. R. Prova¹⁶⁸, M. Wulansatiti¹⁶⁸, R. Yohay¹⁶⁸, J. Zhang¹⁶⁸, B. Alsufyani¹⁶⁹, M. M. Baarmand¹⁶⁹, S. Butalla¹⁶⁹, T. Elkafrawy^{169,ccc}, M. Hohmann¹⁶⁹, R. Kumar Verma¹⁶⁹, M. Rahmani¹⁶⁹, E. Yanes¹⁶⁹, M. R. Adams¹⁷⁰, A. Baty¹⁷⁰, C. Bennett¹⁷⁰, R. Cavanaugh¹⁷⁰, R. Escobar Franco¹⁷⁰, O. Evdokimov¹⁷⁰, C. E. Gerber¹⁷⁰, D. J. Hofman¹⁷⁰, J. h. Lee¹⁷⁰, D. S. Lemos¹⁷⁰, A. H. Merrit¹⁷⁰, C. Mills¹⁷⁰, S. Nanda¹⁷⁰, G. Oh¹⁷⁰, B. Ozek¹⁷⁰, D. Pilipovic¹⁷⁰, R. Pradhan¹⁷⁰, T. Roy¹⁷⁰, S. Rudrabhatla¹⁷⁰, M. B. Tonjes¹⁷⁰, N. Varelas¹⁷⁰, Z. Ye¹⁷⁰, J. Yoo¹⁷⁰, M. Alhousseini¹⁷¹, D. Blend¹⁷¹, K. Dilsiz^{171,kkkk}, L. Emediato¹⁷¹, G. Karaman¹⁷¹, O. K. Köseyan¹⁷¹, J.-P. Merlo¹⁷¹, A. Mestvirishvili^{171,llll}, J. Nachtman¹⁷¹, O. Neogi¹⁷¹, H. Ogul^{171,mmmm}, Y. Onel¹⁷¹, A. Penzo¹⁷¹, C. Snyder¹⁷¹, E. Tiras^{171,nnnn}, B. Blumenfeld¹⁷², L. Corcodilos¹⁷², J. Davis¹⁷², A. V. Gritsan¹⁷², L. Kang¹⁷², S. Kyriacou¹⁷², P. Maksimovic¹⁷², M. Roguljic¹⁷², J. Roskes¹⁷², S. Sekhar¹⁷², M. Swartz¹⁷², A. Abreu¹⁷³, L. F. Alcerro Alcerro¹⁷³, J. Anguiano¹⁷³, P. Baringer¹⁷³, A. Bean¹⁷³, Z. Flowers¹⁷³, D. Grove¹⁷³, J. King¹⁷³, G. Krintiras¹⁷³, M. Lazarovits¹⁷³, C. Le Mahieu¹⁷³, C. Lindsey¹⁷³, J. Marquez¹⁷³, N. Minafra¹⁷³, M. Murray¹⁷³, M. Nickel¹⁷³, M. Pitt¹⁷³, S. Popescu^{173,oooo}, C. Rogan¹⁷³, C. Royon¹⁷³, R. Salvatico¹⁷³, S. Sanders¹⁷³, C. Smith¹⁷³, Q. Wang¹⁷³, G. Wilson¹⁷³, B. Allmond¹⁷⁴, A. Ivanov¹⁷⁴, K. Kaadze¹⁷⁴, A. Kalogeropoulos¹⁷⁴, D. Kim¹⁷⁴, Y. Maravin¹⁷⁴, K. Nam¹⁷⁴, J. Natoli¹⁷⁴, D. Roy¹⁷⁴, G. Sorrentino¹⁷⁴, F. Rebassoo¹⁷⁵, D. Wright¹⁷⁵, A. Baden¹⁷⁶, A. Belloni¹⁷⁶, Y. M. Chen¹⁷⁶, S. C. Eno¹⁷⁶, N. J. Hadley¹⁷⁶, S. Jabeen¹⁷⁶, R. G. Kellogg¹⁷⁶, T. Koeth¹⁷⁶, Y. Lai¹⁷⁶, S. Lascio¹⁷⁶, A. C. Mignerey¹⁷⁶, S. Nabili¹⁷⁶, C. Palmer¹⁷⁶, C. Papageorgakis¹⁷⁶, M. M. Paranjpe¹⁷⁶, L. Wang¹⁷⁶, J. Bendavid¹⁷⁷, W. Busza¹⁷⁷, I. A. Cali¹⁷⁷, M. D'Alfonso¹⁷⁷, J. Eysermans¹⁷⁷, C. Freer¹⁷⁷, G. Gomez-Ceballos¹⁷⁷, M. Goncharov¹⁷⁷, G. Grosso¹⁷⁷, P. Harris¹⁷⁷, D. Hoang¹⁷⁷, D. Kovalskyi¹⁷⁷, J. Krupa¹⁷⁷, L. Lavezzo¹⁷⁷, Y.-J. Lee¹⁷⁷, K. Long¹⁷⁷, C. Mironov¹⁷⁷, N. Paladino¹⁷⁷, C. Paus¹⁷⁷, D. Rankin¹⁷⁷, C. Roland¹⁷⁷, G. Roland¹⁷⁷, S. Rothman¹⁷⁷, G. S. F. Stephans¹⁷⁷, Z. Wang¹⁷⁷, B. Wyslouch¹⁷⁷, T. J. Yang¹⁷⁷, B. Crossman¹⁷⁸, B. M. Joshi¹⁷⁸, C. Kapsiak¹⁷⁸, M. Krohn¹⁷⁸, D. Mahon¹⁷⁸, J. Mans¹⁷⁸, B. Marzocchi¹⁷⁸, S. Pandey¹⁷⁸, M. Revering¹⁷⁸, R. Rusack¹⁷⁸, R. Saradhy¹⁷⁸, N. Schroeder¹⁷⁸, N. Strobbe¹⁷⁸, M. A. Wadud¹⁷⁸, L. M. Cremaldi¹⁷⁹, K. Bloom¹⁸⁰, D. R. Claes¹⁸⁰, G. Haza¹⁸⁰, J. Hossain¹⁸⁰, C. Joo¹⁸⁰, I. Kravchenko¹⁸⁰, J. E. Siado¹⁸⁰, W. Tabb¹⁸⁰, A. Vagnerini¹⁸⁰, A. Wightman¹⁸⁰, F. Yan¹⁸⁰, D. Yu¹⁸⁰, H. Bandyopadhyay¹⁸¹, L. Hay¹⁸¹, I. Iashvili¹⁸¹, A. Kharchilava¹⁸¹, M. Morris¹⁸¹, D. Nguyen¹⁸¹, S. Rappoccio¹⁸¹, H. Rejeb Sfar¹⁸¹, A. Williams¹⁸¹, G. Alverson¹⁸², E. Barberis¹⁸², J. Dervan¹⁸², Y. Haddad¹⁸², Y. Han¹⁸², A. Krishna¹⁸², J. Li¹⁸², M. Lu¹⁸², G. Madigan¹⁸², R. Mccarthy¹⁸², D. M. Morse¹⁸², V. Nguyen¹⁸², T. Orimoto¹⁸², A. Parker¹⁸², L. Skinnari¹⁸², A. Tishelman-Charny¹⁸², B. Wang¹⁸², D. Wood¹⁸², S. Bhattacharya¹⁸³, J. Bueghly¹⁸³, Z. Chen¹⁸³, S. Dittmer¹⁸³, K. A. Hahn¹⁸³, Y. Liu¹⁸³, Y. Miao¹⁸³, D. G. Monk¹⁸³, M. H. Schmitt¹⁸³, A. Talierecio¹⁸³, M. Velasco¹⁸³, G. Agarwal¹⁸⁴, R. Band¹⁸⁴, R. Bucci¹⁸⁴, S. Castells¹⁸⁴, A. Das¹⁸⁴, R. Goldouzian¹⁸⁴, M. Hildreth¹⁸⁴, K. W. Ho¹⁸⁴, K. Hurtado Anampa¹⁸⁴, T. Ivanov¹⁸⁴, C. Jessop¹⁸⁴, K. Lannon¹⁸⁴, J. Lawrence¹⁸⁴, N. Loukas¹⁸⁴, L. Lutton¹⁸⁴, J. Mariano¹⁸⁴, N. Marinelli¹⁸⁴, I. Mcalister¹⁸⁴, T. McCauley¹⁸⁴, C. Mcgrady¹⁸⁴, C. Moore¹⁸⁴, Y. Musienko^{184,r}, H. Nelson¹⁸⁴, M. Osherson¹⁸⁴, A. Piccinelli¹⁸⁴, R. Ruchti¹⁸⁴, A. Townsend¹⁸⁴, Y. Wan¹⁸⁴

M. Wayne¹⁸⁴, H. Yockey¹⁸⁴, M. Zarucki¹⁸⁴, L. Zygalá¹⁸⁴, A. Basnet¹⁸⁵, B. Bylsma¹⁸⁵, M. Carrigan¹⁸⁵,
L. S. Durkin¹⁸⁵, C. Hill¹⁸⁵, M. Joyce¹⁸⁵, M. Nunez Ornelas¹⁸⁵, K. Wei¹⁸⁵, B. L. Winer¹⁸⁵, B. R. Yates¹⁸⁵,
F. M. Addesa¹⁸⁶, H. Bouchamaoui¹⁸⁶, P. Das¹⁸⁶, G. Dezoort¹⁸⁶, P. Elmer¹⁸⁶, A. Frankenthal¹⁸⁶, B. Greenberg¹⁸⁶,
N. Haubrich¹⁸⁶, G. Kopp¹⁸⁶, S. Kwan¹⁸⁶, D. Lange¹⁸⁶, A. Loeliger¹⁸⁶, D. Marlow¹⁸⁶, I. Ojalvo¹⁸⁶, J. Olsen¹⁸⁶,
A. Shevelev¹⁸⁶, D. Stickland¹⁸⁶, C. Tully¹⁸⁶, S. Malik¹⁸⁷, A. S. Bakshi¹⁸⁸, V. E. Barnes¹⁸⁸, S. Chandra¹⁸⁸,
R. Chawla¹⁸⁸, S. Das¹⁸⁸, A. Gu¹⁸⁸, L. Gutay¹⁸⁸, M. Jones¹⁸⁸, A. W. Jung¹⁸⁸, D. Kondratyev¹⁸⁸, A. M. Koshy¹⁸⁸,
M. Liu¹⁸⁸, G. Negro¹⁸⁸, N. Neumeister¹⁸⁸, G. Paspalaki¹⁸⁸, S. Piperov¹⁸⁸, V. Scheurer¹⁸⁸, J. F. Schulte¹⁸⁸,
M. Stojanovic¹⁸⁸, J. Thieman¹⁸⁸, A. K. Viridi¹⁸⁸, F. Wang¹⁸⁸, W. Xie¹⁸⁸, J. Dolen¹⁸⁹, N. Parashar¹⁸⁹,
A. Pathak¹⁸⁹, D. Acosta¹⁹⁰, T. Carnahan¹⁹⁰, K. M. Ecklund¹⁹⁰, P. J. Fernández Manteca¹⁹⁰, S. Freed¹⁹⁰,
P. Gardner¹⁹⁰, F. J. M. Geurts¹⁹⁰, W. Li¹⁹⁰, O. Miguel Colin¹⁹⁰, B. P. Padley¹⁹⁰, R. Redjimi¹⁹⁰, J. Rotter¹⁹⁰,
E. Yigitbasi¹⁹⁰, Y. Zhang¹⁹⁰, A. Bodek¹⁹¹, P. de Barbaro¹⁹¹, R. Demina¹⁹¹, J. L. Dulemba¹⁹¹,
A. Garcia-Bellido¹⁹¹, O. Hindrichs¹⁹¹, A. Khukhunaishvili¹⁹¹, N. Parmar¹⁹¹, P. Parygin^{191,r}, E. Popova^{191,r},
R. Taus¹⁹¹, K. Goulianos¹⁹², B. Chiarito¹⁹³, J. P. Chou¹⁹³, Y. Gershtein¹⁹³, E. Halkiadakis¹⁹³, A. Hart¹⁹³,
M. Heindl¹⁹³, D. Jaroslowski¹⁹³, O. Karacheban^{193,dd}, I. Laflotte¹⁹³, A. Lath¹⁹³, R. Montalvo¹⁹³, K. Nash¹⁹³,
P. Pajarillo¹⁹³, H. Routray¹⁹³, S. Salur¹⁹³, S. Schnetzer¹⁹³, S. Somalwar¹⁹³, R. Stone¹⁹³, S. A. Thayil¹⁹³,
S. Thomas¹⁹³, J. Vora¹⁹³, H. Wang¹⁹³, H. Acharya¹⁹⁴, D. Ally¹⁹⁴, A. G. Delannoy¹⁹⁴, S. Fiorendi¹⁹⁴,
S. Higginbotham¹⁹⁴, T. Holmes¹⁹⁴, A. R. Kanuganti¹⁹⁴, N. Karunarathna¹⁹⁴, L. Lee¹⁹⁴, E. Nibigira¹⁹⁴,
S. Spanier¹⁹⁴, D. Aebi¹⁹⁵, M. Ahmad¹⁹⁵, O. Bouhali^{195,pppp}, R. Eusebi¹⁹⁵, J. Gilmore¹⁹⁵, T. Huang¹⁹⁵,
T. Kamon^{195,qqqq}, H. Kim¹⁹⁵, S. Luo¹⁹⁵, R. Mueller¹⁹⁵, D. Overton¹⁹⁵, D. Rathjens¹⁹⁵, A. Safonov¹⁹⁵,
N. Akchurin¹⁹⁶, J. Damgov¹⁹⁶, V. Hegde¹⁹⁶, A. Hussain¹⁹⁶, Y. Kazhykarim¹⁹⁶, K. Lamichhane¹⁹⁶, S. W. Lee¹⁹⁶,
A. Mankel¹⁹⁶, T. Peltola¹⁹⁶, I. Volobouev¹⁹⁶, A. Whitbeck¹⁹⁶, E. Appelt¹⁹⁷, Y. Chen¹⁹⁷, S. Greene¹⁹⁷,
A. Gurrola¹⁹⁷, W. Johns¹⁹⁷, R. Kunnawalkam Elayavalli¹⁹⁷, A. Melo¹⁹⁷, F. Romeo¹⁹⁷, P. Sheldon¹⁹⁷, S. Tuo¹⁹⁷,
J. Velkovska¹⁹⁷, J. Viinikainen¹⁹⁷, B. Cardwell¹⁹⁸, B. Cox¹⁹⁸, J. Hakala¹⁹⁸, R. Hirosky¹⁹⁸, A. Ledovskoy¹⁹⁸,
C. Neu¹⁹⁸, C. E. Perez Lara¹⁹⁸, P. E. Karchin¹⁹⁹, A. Aravind²⁰⁰, S. Banerjee²⁰⁰, K. Black²⁰⁰, T. Bose²⁰⁰,
S. Dasu²⁰⁰, I. De Bruyn²⁰⁰, P. Everaerts²⁰⁰, C. Galloni²⁰⁰, H. He²⁰⁰, M. Herndon²⁰⁰, A. Herve²⁰⁰,
C. K. Koraka²⁰⁰, A. Lanaro²⁰⁰, R. Loveless²⁰⁰, J. Madhusudanan Sreekala²⁰⁰, A. Mallampalli²⁰⁰,
A. Mohammadi²⁰⁰, S. Mondal²⁰⁰, G. Parida²⁰⁰, D. Pinna²⁰⁰, A. Savin²⁰⁰, V. Shang²⁰⁰, V. Sharma²⁰⁰, W. H. Smith²⁰⁰,
D. Teague²⁰⁰, H. F. Tsoi²⁰⁰, W. Vetens²⁰⁰, A. Warden²⁰⁰, S. Afanasiev²⁰¹, V. Andreev²⁰¹, Yu. Andreev²⁰¹,
T. Aushev²⁰¹, M. Azarkin²⁰¹, A. Babaev²⁰¹, A. Belyaev²⁰¹, V. Blinov^{201,r}, E. Boos²⁰¹, V. Borshch²⁰¹,
D. Budkouski²⁰¹, V. Bunichev²⁰¹, V. Chekhovsky²⁰¹, R. Chistov^{201,r}, M. Danilov^{201,r}, A. Dermenev²⁰¹,
T. Dimova^{201,r}, D. Druzhkin^{201,rrr}, M. Dubinin^{201,iiii}, L. Dudko²⁰¹, A. Ershov²⁰¹, G. Gavrillov²⁰¹, V. Gavrillov²⁰¹,
S. Gninenko²⁰¹, V. Golovtsov²⁰¹, N. Golubev²⁰¹, I. Golutvin²⁰¹, I. Gorbunov²⁰¹, A. Gribushin²⁰¹, Y. Ivanov²⁰¹,
V. Kachanov²⁰¹, V. Karjavine²⁰¹, A. Karneyeu²⁰¹, V. Kim^{201,r}, M. Kirakosyan²⁰¹, D. Kirpichnikov²⁰¹,
M. Kirsanov²⁰¹, V. Klyukhin²⁰¹, O. Kodolova^{201,ssss}, V. Korenkov²⁰¹, A. Kozyrev^{201,r}, N. Krasnikov²⁰¹,
A. Lanev²⁰¹, P. Levchenko^{201,tttt}, N. Lychkovskaya²⁰¹, V. Makarenko²⁰¹, A. Malakhov²⁰¹, V. Matveev^{201,r},
V. Murzin²⁰¹, A. Nikitenko^{201,uuuu,ssss}, S. Obraztsov²⁰¹, V. Oreshkin²⁰¹, V. Palichik²⁰¹, V. Perelygin²⁰¹,
S. Petrushanko²⁰¹, S. Polikarpov^{201,r}, V. Popov²⁰¹, O. Radchenko^{201,r}, M. Savina²⁰¹, V. Savrin²⁰¹, V. Shalaev²⁰¹,
S. Shmatov²⁰¹, S. Shulha²⁰¹, Y. Skovpen^{201,r}, S. Slabospitskii²⁰¹, V. Smirnov²⁰¹, A. Snigirev²⁰¹, D. Sosnov²⁰¹,
V. Sulimov²⁰¹, E. Tcherniaev²⁰¹, A. Terkulov²⁰¹, O. Teryaev²⁰¹, I. Tlisova²⁰¹, A. Toropin²⁰¹,
L. Uvarov²⁰¹, A. Uzunian²⁰¹, A. Vorobyev^{201,a}, N. Voytishin²⁰¹, B. S. Yuldashev^{201,vvvv}, A. Zarubin²⁰¹,
I. Zhizhin²⁰¹ and A. Zhokin²⁰¹

(CMS Collaboration)

¹*Yerevan Physics Institute, Yerevan, Armenia*²*Institut für Hochenergiephysik, Vienna, Austria*⁴*Universiteit Antwerpen, Antwerpen, Belgium*⁵*Vrije Universiteit Brussel, Brussel, Belgium*⁶*Université Libre de Bruxelles, Bruxelles, Belgium*⁷*Ghent University, Ghent, Belgium*

- ⁸*Université Catholique de Louvain, Louvain-la-Neuve, Belgium*
⁹*Centro Brasileiro de Pesquisas Físicas, Rio de Janeiro, Brazil*
¹⁰*Universidade do Estado do Rio de Janeiro, Rio de Janeiro, Brazil*
¹¹*Universidade Estadual Paulista, Universidade Federal do ABC, São Paulo, Brazil*
¹²*Institute for Nuclear Research and Nuclear Energy, Bulgarian Academy of Sciences, Sofia, Bulgaria*
¹³*University of Sofia, Sofia, Bulgaria*
¹⁴*Instituto De Alta Investigación, Universidad de Tarapacá, Casilla 7 D, Arica, Chile*
¹⁵*Beihang University, Beijing, China*
¹⁶*Department of Physics, Tsinghua University, Beijing, China*
¹⁷*Institute of High Energy Physics, Beijing, China*
¹⁸*State Key Laboratory of Nuclear Physics and Technology, Peking University, Beijing, China*
¹⁹*Sun Yat-Sen University, Guangzhou, China*
²⁰*University of Science and Technology of China, Hefei, China*
²¹*Nanjing Normal University, Nanjing, China*
²²*Institute of Modern Physics and Key Laboratory of Nuclear Physics and Ion-beam Application (MOE)-Fudan University, Shanghai, China*
²³*Zhejiang University, Hangzhou, Zhejiang, China*
²⁴*Universidad de Los Andes, Bogota, Colombia*
²⁵*Universidad de Antioquia, Medellin, Colombia*
²⁶*University of Split, Faculty of Electrical Engineering, Mechanical Engineering and Naval Architecture, Split, Croatia*
²⁷*University of Split, Faculty of Science, Split, Croatia*
²⁸*Institute Rudjer Boskovic, Zagreb, Croatia*
²⁹*University of Cyprus, Nicosia, Cyprus*
³⁰*Charles University, Prague, Czech Republic*
³¹*Escuela Politecnica Nacional, Quito, Ecuador*
³²*Universidad San Francisco de Quito, Quito, Ecuador*
³³*Academy of Scientific Research and Technology of the Arab Republic of Egypt, Egyptian Network of High Energy Physics, Cairo, Egypt*
³⁴*Center for High Energy Physics (CHEP-FU), Fayoum University, El-Fayoum, Egypt*
³⁵*National Institute of Chemical Physics and Biophysics, Tallinn, Estonia*
³⁶*Department of Physics, University of Helsinki, Helsinki, Finland*
³⁷*Helsinki Institute of Physics, Helsinki, Finland*
³⁸*Lappeenranta-Lahti University of Technology, Lappeenranta, Finland*
³⁹*IRFU, CEA, Université Paris-Saclay, Gif-sur-Yvette, France*
⁴⁰*Laboratoire Leprince-Ringuet, CNRS/IN2P3, Ecole Polytechnique, Institut Polytechnique de Paris, Palaiseau, France*
⁴¹*Université de Strasbourg, CNRS, IPHC UMR 7178, Strasbourg, France*
⁴²*Institut de Physique des 2 Infinis de Lyon (IP2I), Villeurbanne, France*
⁴³*Georgian Technical University, Tbilisi, Georgia*
⁴⁴*RWTH Aachen University, I. Physikalisches Institut, Aachen, Germany*
⁴⁵*RWTH Aachen University, III. Physikalisches Institut A, Aachen, Germany*
⁴⁶*RWTH Aachen University, III. Physikalisches Institut B, Aachen, Germany*
⁴⁷*Deutsches Elektronen-Synchrotron, Hamburg, Germany*
⁴⁸*University of Hamburg, Hamburg, Germany*
⁴⁹*Karlsruher Institut fuer Technologie, Karlsruhe, Germany*
⁵⁰*Institute of Nuclear and Particle Physics (INPP), NCSR Demokritos, Aghia Paraskevi, Greece*
⁵¹*National and Kapodistrian University of Athens, Athens, Greece*
⁵²*National Technical University of Athens, Athens, Greece*
⁵³*University of Ioánnina, Ioánnina, Greece*
⁵⁴*HUN-REN Wigner Research Centre for Physics, Budapest, Hungary*
⁵⁵*MTA-ELTE Lendület CMS Particle and Nuclear Physics Group, Eötvös Loránd University, Budapest, Hungary*
⁵⁶*Faculty of Informatics, University of Debrecen, Debrecen, Hungary*
⁵⁷*Institute of Nuclear Research ATOMKI, Debrecen, Hungary*
⁵⁸*Karoly Robert Campus, MATE Institute of Technology, Gyongyos, Hungary*
⁵⁹*Panjab University, Chandigarh, India*
⁶⁰*University of Delhi, Delhi, India*
⁶¹*Saha Institute of Nuclear Physics, HBNI, Kolkata, India*
⁶²*Indian Institute of Technology Madras, Madras, India*

- ⁶³*Tata Institute of Fundamental Research-A, Mumbai, India*
⁶⁴*Tata Institute of Fundamental Research-B, Mumbai, India*
⁶⁵*National Institute of Science Education and Research,
 An OCC of Homi Bhabha National Institute, Bhubaneswar, Odisha, India*
⁶⁶*Indian Institute of Science Education and Research (IISER), Pune, India*
⁶⁷*Isfahan University of Technology, Isfahan, Iran*
⁶⁸*Institute for Research in Fundamental Sciences (IPM), Tehran, Iran*
⁶⁹*University College Dublin, Dublin, Ireland*
⁷⁰*INFN Sezione di Bari, Università di Bari, Politecnico di Bari, Bari, Italy*
^{70a}*INFN Sezione di Bari, Bari, Italy*
^{70b}*Università di Bari , Bari, Italy*
^{70c}*Politecnico di Bari, Bari, Italy*
⁷¹*INFN Sezione di Bologna, Università di Bologna, Bologna, Italy*
^{71a}*INFN Sezione di Bologna, Bologna, Italy*
^{71b}*Università di Bologna , Bologna, Italy*
⁷²*INFN Sezione di Catania, Università di Catania, Catania, Italy*
^{72a}*INFN Sezione di Catania, Catania, Italy*
^{72b}*Università di Catania , Catania, Italy*
⁷³*INFN Sezione di Firenze, Università di Firenze, Firenze, Italy*
^{73a}*INFN Sezione di Firenze, Firenze, Italy*
^{73b}*Università di Firenze , Firenze, Italy*
⁷⁴*INFN Laboratori Nazionali di Frascati, Frascati, Italy*
⁷⁵*INFN Sezione di Genova, Università di Genova, Genova, Italy*
^{75a}*INFN Sezione di Genova, Genova, Italy*
^{75b}*Università di Genova , Genova, Italy*
⁷⁶*INFN Sezione di Milano-Bicocca, Università di Milano-Bicocca, Milano, Italy*
^{76a}*INFN Sezione di Milano-Bicocca, Milano, Italy*
^{76b}*Università di Milano-Bicocca , Milano, Italy*
⁷⁷*INFN Sezione di Napoli, Università di Napoli 'Federico II', Napoli, Italy, Università della Basilicata,
 Potenza, Italy, Scuola Superiore Meridionale (SSM), Napoli, Italy*
^{77a}*INFN Sezione di Napoli, Napoli, Italy*
^{77b}*Università di Napoli 'Federico II', Napoli, Italy*
^{77c}*Università della Basilicata , Potenza, Italy*
^{77d}*Scuola Superiore Meridionale (SSM), Napoli, Italy*
⁷⁸*INFN Sezione di Padova, Università di Padova, Padova, Italy, Università di Trento, Trento, Italy*
^{78a}*INFN Sezione di Padova, Padova, Italy*
^{78b}*Università di Padova, Padova, Italy*
^{78c}*Università di Trento, Trento, Italy*
⁷⁹*INFN Sezione di Pavia, Università di Pavia, Pavia, Italy*
^{79a}*INFN Sezione di Pavia, Pavia, Italy*
^{79b}*Università di Pavia , Pavia, Italy*
⁸⁰*INFN Sezione di Perugia, Università di Perugia, Perugia, Italy*
^{80a}*INFN Sezione di Perugia, Perugia, Italy*
^{80b}*Università di Perugia, Perugia, Italy*
⁸¹*INFN Sezione di Pisa, Università di Pisa, Scuola Normale Superiore di Pisa, Pisa Italy,
 Università di Siena, Siena, Italy*
^{81a}*INFN Sezione di Pisa, Pisa, Italy*
^{81b}*Università di Pisa , Pisa, Italy*
^{81c}*Scuola Normale Superiore di Pisa, Pisa, Italy*
^{81d}*Università di Siena, Siena, Italy*
⁸²*INFN Sezione di Roma, Sapienza Università di Roma, Roma, Italy*
^{82a}*INFN Sezione di Roma, Roma, Italy*
^{82b}*Sapienza Università di Roma, Roma, Italy*
⁸³*INFN Sezione di Torino, Università di Torino,
 Torino, Italy, Università del Piemonte Orientale, Novara, Italy*
^{83a}*INFN Sezione di Torino, Torino, Italy*
^{83b}*Università di Torino , Torino, Italy*
^{83c}*Università del Piemonte Orientale , Novara, Italy*
⁸⁴*INFN Sezione di Trieste, Università di Trieste, Trieste, Italy*
^{84a}*INFN Sezione di Trieste, Trieste, Italy*

- ^{84b}*Università di Trieste , Trieste, Italy*
- ⁸⁵*Kyungpook National University, Daegu, Korea*
- ⁸⁶*Department of Mathematics and Physics-GWNU, Gangneung, Korea*
- ⁸⁷*Chonnam National University, Institute for Universe and Elementary Particles, Kwangju, Korea*
- ⁸⁸*Hanyang University, Seoul, Korea*
- ⁸⁹*Korea University, Seoul, Korea*
- ⁹⁰*Kyung Hee University, Department of Physics, Seoul, Korea*
- ⁹¹*Sejong University, Seoul, Korea*
- ⁹²*Seoul National University, Seoul, Korea*
- ⁹³*University of Seoul, Seoul, Korea*
- ⁹⁴*Yonsei University, Department of Physics, Seoul, Korea*
- ⁹⁵*Sungkyunkwan University, Suwon, Korea*
- ⁹⁶*College of Engineering and Technology, American University of the Middle East (AUM),
Dasman, Kuwait*
- ⁹⁷*Riga Technical University, Riga, Latvia*
- ⁹⁸*University of Latvia (LU), Riga, Latvia*
- ⁹⁹*Vilnius University, Vilnius, Lithuania*
- ¹⁰⁰*National Centre for Particle Physics, Universiti Malaya, Kuala Lumpur, Malaysia*
- ¹⁰¹*Universidad de Sonora (UNISON), Hermosillo, Mexico*
- ¹⁰²*Centro de Investigacion y de Estudios Avanzados del IPN, Mexico City, Mexico*
- ¹⁰³*Universidad Iberoamericana, Mexico City, Mexico*
- ¹⁰⁴*Benemerita Universidad Autonoma de Puebla, Puebla, Mexico*
- ¹⁰⁵*University of Montenegro, Podgorica, Montenegro*
- ¹⁰⁶*University of Canterbury, Christchurch, New Zealand*
- ¹⁰⁷*National Centre for Physics, Quaid-I-Azam University, Islamabad, Pakistan*
- ¹⁰⁸*AGH University of Krakow, Faculty of Computer Science,
Electronics and Telecommunications, Krakow, Poland*
- ¹⁰⁹*National Centre for Nuclear Research, Swierk, Poland*
- ¹¹⁰*Institute of Experimental Physics, Faculty of Physics, University of Warsaw, Warsaw, Poland*
- ¹¹¹*Warsaw University of Technology, Warsaw, Poland*
- ¹¹²*Laboratório de Instrumentação e Física Experimental de Partículas, Lisboa, Portugal*
- ¹²⁵*Faculty of Physics, University of Belgrade, Belgrade, Serbia*
- ¹²⁶*VINCA Institute of Nuclear Sciences, University of Belgrade, Belgrade, Serbia*
- ¹²⁷*Centro de Investigaciones Energéticas Medioambientales y Tecnológicas (CIEMAT), Madrid, Spain*
- ¹²⁸*Universidad Autónoma de Madrid, Madrid, Spain*
- ¹²⁹*Universidad de Oviedo, Instituto Universitario de Ciencias y Tecnologías
Espaciales de Asturias (ICTEA), Oviedo, Spain*
- ¹³⁰*Instituto de Física de Cantabria (IFCA), CSIC-Universidad de Cantabria, Santander, Spain*
- ¹³¹*University of Colombo, Colombo, Sri Lanka*
- ¹³²*University of Ruhuna, Department of Physics, Matara, Sri Lanka*
- ¹³³*CERN, European Organization for Nuclear Research, Geneva, Switzerland*
- ¹³⁴*Paul Scherrer Institut, Villigen, Switzerland*
- ¹³⁵*ETH Zurich-Institute for Particle Physics and Astrophysics (IPA), Zurich, Switzerland*
- ¹³⁶*Universität Zürich, Zurich, Switzerland*
- ¹³⁷*National Central University, Chung-Li, Taiwan*
- ¹³⁸*National Taiwan University (NTU), Taipei, Taiwan*
- ¹³⁹*High Energy Physics Research Unit, Department of Physics, Faculty of Science,
Chulalongkorn University, Bangkok, Thailand*
- ¹⁴⁰*Çukurova University, Physics Department, Science and Art Faculty, Adana, Turkey*
- ¹⁴¹*Middle East Technical University, Physics Department, Ankara, Turkey*
- ¹⁴²*Bogazici University, Istanbul, Turkey*
- ¹⁴³*Istanbul Technical University, Istanbul, Turkey*
- ¹⁴⁴*Istanbul University, Istanbul, Turkey*
- ¹⁴⁵*Yildiz Technical University, Istanbul, Turkey*
- ¹⁴⁶*Institute for Scintillation Materials of National Academy of Science of Ukraine, Kharkiv, Ukraine*
- ¹⁴⁷*National Science Centre, Kharkiv Institute of Physics and Technology, Kharkiv, Ukraine*
- ¹⁴⁸*University of Bristol, Bristol, United Kingdom*
- ¹⁴⁹*Rutherford Appleton Laboratory, Didcot, United Kingdom*
- ¹⁵⁰*Imperial College, London, United Kingdom*
- ¹⁵¹*Brunel University, Uxbridge, United Kingdom*

- ¹⁵²Baylor University, Waco, Texas, USA
¹⁵³Catholic University of America, Washington, DC, USA
¹⁵⁴The University of Alabama, Tuscaloosa, Alabama, USA
¹⁵⁵Boston University, Boston, Massachusetts, USA
¹⁵⁶Brown University, Providence, Rhode Island, USA
¹⁵⁷University of California, Davis, Davis, California, USA
¹⁵⁸University of California, Los Angeles, California, USA
¹⁵⁹University of California, Riverside, Riverside, California, USA
¹⁶⁰University of California, San Diego, La Jolla, California, USA
¹⁶¹University of California, Santa Barbara-Department of Physics, Santa Barbara, California, USA
¹⁶²California Institute of Technology, Pasadena, California, USA
¹⁶³Carnegie Mellon University, Pittsburgh, Pennsylvania, USA
¹⁶⁴University of Colorado Boulder, Boulder, Colorado, USA
¹⁶⁵Cornell University, Ithaca, New York, USA
¹⁶⁶Fermi National Accelerator Laboratory, Batavia, Illinois, USA
¹⁶⁷University of Florida, Gainesville, Florida, USA
¹⁶⁸Florida State University, Tallahassee, Florida, USA
¹⁶⁹Florida Institute of Technology, Melbourne, Florida, USA
¹⁷⁰University of Illinois Chicago, Chicago, USA, Chicago, USA
¹⁷¹The University of Iowa, Iowa City, Iowa, USA
¹⁷²Johns Hopkins University, Baltimore, Maryland, USA
¹⁷³The University of Kansas, Lawrence, Kansas, USA
¹⁷⁴Kansas State University, Manhattan, Kansas, USA
¹⁷⁵Lawrence Livermore National Laboratory, Livermore, California, USA
¹⁷⁶University of Maryland, College Park, Maryland, USA
¹⁷⁷Massachusetts Institute of Technology, Cambridge, Massachusetts, USA
¹⁷⁸University of Minnesota, Minneapolis, Minnesota, USA
¹⁷⁹University of Mississippi, Oxford, Mississippi, USA
¹⁸⁰University of Nebraska-Lincoln, Lincoln, Nebraska, USA
¹⁸¹State University of New York at Buffalo, Buffalo, New York, USA
¹⁸²Northeastern University, Boston, Massachusetts, USA
¹⁸³Northwestern University, Evanston, Illinois, USA
¹⁸⁴University of Notre Dame, Notre Dame, Indiana, USA
¹⁸⁵The Ohio State University, Columbus, Ohio, USA
¹⁸⁶Princeton University, Princeton, New Jersey, USA
¹⁸⁷University of Puerto Rico, Mayaguez, Puerto Rico, USA
¹⁸⁸Purdue University, West Lafayette, Indiana, USA
¹⁸⁹Purdue University Northwest, Hammond, Indiana, USA
¹⁹⁰Rice University, Houston, Texas, USA
¹⁹¹University of Rochester, Rochester, New York, USA
¹⁹²The Rockefeller University, New York, New York, USA
¹⁹³Rutgers, The State University of New Jersey, Piscataway, New Jersey, USA
¹⁹⁴University of Tennessee, Knoxville, Tennessee, USA
¹⁹⁵Texas A&M University, College Station, Texas, USA
¹⁹⁶Texas Tech University, Lubbock, Texas, USA
¹⁹⁷Vanderbilt University, Nashville, Tennessee, USA
¹⁹⁸University of Virginia, Charlottesville, Virginia, USA
¹⁹⁹Wayne State University, Detroit, Michigan, USA
²⁰⁰University of Wisconsin-Madison, Madison, Wisconsin, USA
²⁰¹An institute or international laboratory covered by a cooperation agreement with CERN

^aDeceased.^bAlso at Yerevan State University, Yerevan, Armenia.^cAlso at TU Wien, Vienna, Austria.^dAlso at Institute of Basic and Applied Sciences, Faculty of Engineering, Arab Academy for Science, Technology and Maritime Transport, Alexandria, Egypt.^eAlso at Ghent University, Ghent, Belgium.^fAlso at Universidade Estadual de Campinas, Campinas, Brazil.^gAlso at Federal University of Rio Grande do Sul, Porto Alegre, Brazil.^hAlso at UFMS, Nova Andradina, Brazil.

- ⁱ Also at Nanjing Normal University, Nanjing, China.
- ^j Also at The University of Iowa, Iowa City, Iowa, USA.
- ^k Also at University of Chinese Academy of Sciences, Beijing, China.
- ^l Also at China Center of Advanced Science and Technology, Beijing, China.
- ^m Also at University of Chinese Academy of Sciences, Beijing, China.
- ⁿ Also at China Spallation Neutron Source, Guangdong, China.
- ^o Also at Henan Normal University, Xinxiang, China.
- ^p Also at Université Libre de Bruxelles, Bruxelles, Belgium.
- ^q Also at University of Latvia (LU), Riga, Latvia.
- ^r Also at Another institute or international laboratory covered by a cooperation agreement with CERN.
- ^s Also at Suez University, Suez, Egypt.
- ^t Also at British University in Egypt, Cairo, Egypt.
- ^u Also at Purdue University, West Lafayette, Indiana, USA.
- ^v Also at Université de Haute Alsace, Mulhouse, France.
- ^w Also at Department of Physics, Tsinghua University, Beijing, China.
- ^x Also at The University of the State of Amazonas, Manaus, Brazil.
- ^y Also at Erzincan Binali Yildirim University, Erzincan, Turkey.
- ^z Also at University of Hamburg, Hamburg, Germany.
- ^{aa} Also at RWTH Aachen University, III. Physikalisches Institut A, Aachen, Germany.
- ^{bb} Also at Isfahan University of Technology, Isfahan, Iran.
- ^{cc} Also at Bergische University Wuppertal (BUW), Wuppertal, Germany.
- ^{dd} Also at Brandenburg University of Technology, Cottbus, Germany.
- ^{ee} Also at Forschungszentrum Jülich, Juelich, Germany.
- ^{ff} Also at CERN, European Organization for Nuclear Research, Geneva, Switzerland.
- ^{gg} Also at Institute of Physics, University of Debrecen, Debrecen, Hungary.
- ^{hh} Also at Institute of Nuclear Research ATOMKI, Debrecen, Hungary.
- ⁱⁱ Also at Universitatea Babeş-Bolyai—Facultatea de Fizică, Cluj-Napoca, Romania.
- ^{jj} Also at Physics Department, Faculty of Science, Assiut University, Assiut, Egypt.
- ^{kk} Also at HUN-REN Wigner Research Centre for Physics, Budapest, Hungary.
- ^{ll} Also at Punjab Agricultural University, Ludhiana, India.
- ^{mm} Also at University of Visva-Bharati, Santiniketan, India.
- ⁿⁿ Also at Indian Institute of Science (IISc), Bangalore, India.
- ^{oo} Also at Birla Institute of Technology, Mesra, Mesra, India.
- ^{pp} Also at IIT Bhubaneswar, Bhubaneswar, India.
- ^{qq} Also at Institute of Physics, Bhubaneswar, India.
- ^{rr} Also at University of Hyderabad, Hyderabad, India.
- ^{ss} Also at Deutsches Elektronen-Synchrotron, Hamburg, Germany.
- ^{tt} Also at Department of Physics, Isfahan University of Technology, Isfahan, Iran.
- ^{uu} Also at Sharif University of Technology, Tehran, Iran.
- ^{vv} Also at Department of Physics, University of Science and Technology of Mazandaran, Behshahr, Iran.
- ^{ww} Also at Helwan University, Cairo, Egypt.
- ^{xx} Also at Italian National Agency for New Technologies, Energy and Sustainable Economic Development, Bologna, Italy.
- ^{yy} Also at Centro Siciliano di Fisica Nucleare e di Struttura Della Materia, Catania, Italy.
- ^{zz} Also at Università degli Studi Guglielmo Marconi, Roma, Italy.
- ^{aaa} Also at Scuola Superiore Meridionale, Università di Napoli 'Federico II', Napoli, Italy.
- ^{bbb} Also at Fermi National Accelerator Laboratory, Batavia, Illinois, USA.
- ^{ccc} Also at Ain Shams University, Cairo, Egypt.
- ^{ddd} Also at Consiglio Nazionale delle Ricerche—Istituto Officina dei Materiali, Perugia, Italy.
- ^{eee} Also at Riga Technical University, Riga, Latvia.
- ^{fff} Also at Department of Applied Physics, Faculty of Science and Technology, Universiti Kebangsaan Malaysia, Bangi, Malaysia.
- ^{ggg} Also at Consejo Nacional de Ciencia y Tecnología, Mexico City, Mexico.
- ^{hhh} Also at Trincomalee Campus, Eastern University, Sri Lanka, Nilaveli, Sri Lanka.
- ⁱⁱⁱ Also at Saegis Campus, Nugegoda, Sri Lanka.
- ^{jjj} Also at National and Kapodistrian University of Athens, Athens, Greece.
- ^{kkk} Also at Ecole Polytechnique Fédérale Lausanne, Lausanne, Switzerland.
- ^{lll} Also at Universität Zürich, Zurich, Switzerland.
- ^{mmm} Also at Stefan Meyer Institute for Subatomic Physics, Vienna, Austria.
- ⁿⁿⁿ Also at Laboratoire d'Annecy-le-Vieux de Physique des Particules, IN2P3-CNRS, Annecy-le-Vieux, France.
- ^{ooo} Also at Near East University, Research Center of Experimental Health Science, Mersin, Turkey.
- ^{ppp} Also at Konya Technical University, Konya, Turkey.

- ^{qqq}Also at Izmir Bakircay University, Izmir, Turkey.
- ^{rrr}Also at Adiyaman University, Adiyaman, Turkey.
- ^{sss}Also at Bozok Universitetesi Rektörlüğü, Yozgat, Turkey.
- ^{ttt}Also at Marmara University, Istanbul, Turkey.
- ^{uuu}Also at Milli Savunma University, Istanbul, Turkey.
- ^{vvv}Also at Kafkas University, Kars, Turkey.
- ^{www}Also at Istanbul Okan University, Istanbul, Turkey.
- ^{xxx}Also at Hacettepe University, Ankara, Turkey.
- ^{yyy}Also at Istanbul University—Cerrahpasa, Faculty of Engineering, Istanbul, Turkey.
- ^{zzz}Also at Yildiz Technical University, Istanbul, Turkey.
- ^{aaa}Also at Vrije Universiteit Brussel, Brussel, Belgium.
- ^{bbb}Also at School of Physics and Astronomy, University of Southampton, Southampton, United Kingdom.
- ^{ccc}Also at University of Bristol, Bristol, United Kingdom.
- ^{ddd}Also at IPPP Durham University, Durham, United Kingdom.
- ^{eee}Also at Monash University, Faculty of Science, Clayton, Australia.
- ^{fff}Also at Università di Torino, Torino, Italy.
- ^{ggg}Also at Bethel University, St. Paul, Minnesota, USA.
- ^{hhh}Also at Karamanoğlu Mehmetbey University, Karaman, Turkey.
- ⁱⁱⁱAlso at California Institute of Technology, Pasadena, California, USA.
- ^{jjj}Also at United States Naval Academy, Annapolis, Maryland, USA.
- ^{kkk}Also at Bingol University, Bingol, Turkey.
- ^{lll}Also at Georgian Technical University, Tbilisi, Georgia.
- ^{mmm}Also at Sinop University, Sinop, Turkey.
- ⁿⁿⁿAlso at Erciyes University, Kayseri, Turkey.
- ^{ooo}Also at Horia Hulubei National Institute of Physics and Nuclear Engineering (IFIN-HH), Bucharest, Romania.
- ^{ppp}Also at Texas A&M University at Qatar, Doha, Qatar.
- ^{qqq}Also at Kyungpook National University, Daegu, Korea.
- ^{rrr}Also at Universiteit Antwerpen, Antwerpen, Belgium.
- ^{sss}Also at Yerevan Physics Institute, Yerevan, Armenia.
- ^{ttt}Also at Northeastern University, Boston, Massachusetts, USA.
- ^{uuu}Also at Imperial College, London, United Kingdom.
- ^{vvv}Also at Institute of Nuclear Physics of the Uzbekistan Academy of Sciences, Tashkent, Uzbekistan.